博士論文

Sand Dune Erosion Mechanism During Tsunami Overwash

（津波の越流による砂堆侵食機構に関する研究）

K. M. Ahtesham Hossain Raju

ケー．エム．アテシャム　ホセイン　ラジュ

Department of Civil Engineering

The University of Tokyo

September 2016

Sand Dune Erosion Mechanism During Tsunami Overwash

K. M. Ahtesham Hossain Raju

A dissertation submitted to the Department of Civil Engineering,
in partial fulfillment of the requirements for the Degree of

Doctor of Philosophy

In the Field of Civil Engineering

Department of Civil Engineering
Graduate School of Engineering
The University of Tokyo

September 2016

Approved by the Members of the Examination Committee

Shinji Sato — **Professor**
Department of Civil Engineering — Supervisor
The University of Tokyo, Tokyo, Japan

Yoshimitsu Tajima — **Professor**
Department of Civil Engineering
The University of Tokyo, Tokyo, Japan

Junichi Koseki — **Professor**
Department of Civil Engineering
The University of Tokyo, Tokyo, Japan

Takenori Shimozono — **Associate Professor**
Department of Civil Engineering
The University of Tokyo, Tokyo, Japan

Taro Arikawa — **Professor**
Department of Civil and Environmental Engineering
Chuo University, Tokyo, Japan

DECLARATION

This is to certify that this thesis work has been done by the author and neither this thesis nor any part thereof has been submitted elsewhere for award of any degree or diploma.

K. M. Ahtesham Hossain Raju

TABLE OF CONTENTS

LIST OF FIGURES

LIST OF TABLES

LIST OF NOTATIONS

B_D	width of barrier throat during overwash
C_{bore}	overwash bore celerity
C_B	bore celerity
C_d	weir coefficient
C_s	sediment transport rate coefficient
$\overline{C_s}$	average volumetric sediment concentration
C_1	constant to determine intrinsic permeability
c	flux averaged volumetric sediment concentration
c_a	local near bed sediment concentration in volume
c_d	deposition coefficient
c_e	sediment erosion coefficient
D	deposition flux of sediment
D_*	non-dimensional particle size
d	sediment grain diameter
d_d	dune height
d_{10}	grain diameter for which 10% of the sediment by weight is smaller
d_{16}	grain diameter for which 16% of the sediment by weight is smaller
d_{25}	grain diameter for which 25% of the sediment by weight is smaller
d_{50}	median sediment size
d_{75}	grain diameter for which 75% of the sediment by weight is smaller
d_{84}	grain diameter for which 84% of the sediment by weight is smaller
d_{90}	grain diameter for which 90% of the sediment by weight is smaller
E	entrainment of sediment flux from bed layer
F_b	buoyancy force
F_D	drag force
F_L	lift force
F_p	pressure force
g	acceleration due to gravity
H_B	bore height

h	depth of water
h_b	depth of bore front at dune crest
h_{crest}	depth of flow over crest
h_w	depth of water flow upstream of dune
h'_w	depth of water flow upstream of overwashed dune
h_1	depth of water at downstream of dam-break gate
h_2	depth of water at upstream of dam-break gate
I_{ex}	exfiltration
I_{in}	infiltration
K	hydraulic conductivity
K_B	empirical coefficient for dune crest sediment transport
K_{B1}	sediment overwash coefficient
K_c	empirical sediment transport coefficient in swash zone
K_1, K_2, K_3	proportionality constant
k	intrinsic permeability
k_s	effective bed roughness (= $\alpha_1 d_{90}$)
m	discharge coefficient
n_1	empirical exponent
P_w	pore water pressure
p	porosity
q_s	sediment overwash rate
q_{sd}	cross-shore sediment overwash rate at dune crest
q_{sl}	cross-shore sediment transport rate in landward side of dune
q_{ss}	cross-shore sediment transport rate in swash zone
q_w	water overtopping rate
q_{wo}	water overtopping rate per wave per unit width
q_{WR} overwash	cross-shore sediment transport rate over beach crest for run-up
q_{WI} overwash	cross-shore sediment transport rate over beach crest for inundation

R	wave runup height
R_T	time ratio
R_{*c}	critical boundary Reynolds number
S	storm surge height
S_o	sorting coefficient of sediment grain
s_d	horizontal distance from dune crest
T	wave period
T_B	bore period
T_i	time scale for infiltration
T_o	overwash duration
T_s	swash period
T_{ws}	waterfront spreading time through dune cross section
t	time
t_o	submergence time
U_∞	free surface velocity (=$7u/6$)
u	depth averaged stream wise velocity
u_b	bore celerity
$\bar{u}_c$	critical depth averaged flow velocity
u_{oc}	fluid velocity near the bed under critical conditions
u_*	bed shear/friction velocity [=$\sqrt{(\tau/\rho)}$]
u_{*c}	critical shear/friction velocity [=$\sqrt{(\tau_c/\rho)}$]
V	volume of sand dune
V_{WR}	average volume of flow per overtopping (runup) wave
V_{WI}	average volume of flow per overtopping (inundation) wave
v	flow velocity
W_D	width of dune
w_o	fall velocity of sediment grain
x	stream wise coordinate
z	bed level
z_d	dune height above ground level

z'_d	overwashed dune height above ground level
z_{dw}	dune height above mean water level
z_{dw}	dune crest height above mean water level
z_o	elevation of dune foot above still water level
$\Re$	roundness of sediment grain
α	ratio of the near bed and depth-averaged sediment concentration
α_o	empirical value for non-equilibrium adaptation coefficient
α_1	empirical coefficient
α_2	empirical exponent
α_1	coefficient of bed roughness
β_l	local foreshore slope
β_e	equilibrium foreshore slope
γ	specific weight of water
γ_s	specific weight of sand
Δ	relative submerged density (= $\frac{\rho_s - \rho}{\rho}$)
ΔH	water surface elevation difference to generate bore (dam break wave)
ΔR	excess wave runup
Δz	difference between still water level and dune base
ε	coefficient related with flow and sediment condition (wet/dry) as well as bottom slope
η_{tide}	sea water level variation due to tide
θ	angle of the bed with horizontal
θ'	side slope of dune
λ	coefficient related with flow and sediment condition as well as bottom slope
μ	dynamic viscosity of water
μ'	coefficient of water spreading on back dune
ν	kinematic viscosity
ρ	density of water
ρ_s	density of sediment grain

σ_g	standard deviation
τ_b	bottom shear stress
τ_{be}	effective bottom shear stress
τ_c	critical shear stress
φ	angle of repose
φ''	deformed dune angle
Ψ	Shields parameter
Ψ_c	critical Shields stress

ACKNOWLEDGEMENT

The author expresses utmost sincere gratitude and respect to Professor Shinji Sato, supervisor during the doctoral program; for his cordial and constant supervision, valuable suggestions and keen interest throughout the study. His meticulous guidelines, constructive comments and enormous expertise helped the author for better understanding and progress of the study.

The author's sincere thanks go to Professor Yoshimitsu Tajima for his valuable comments, suggestions, caring and fruitful criticism throughout the study. The author is very much grateful to Associate Professor Takenori Shimozono, for his support and cooperation that helped to step forward. The author would like to express his gratitude to Professor Junichi Koseki for his valuable criticism and constructive suggestions. Sincere thanks to Professor Taro Arikawa, Chuo University, for his valuable comments and advice.

The author is particularly grateful to his class-room teacher, master's supervisor and advisor, Professor Abdul Matin, Bangladesh University of Engineering and Technology (BUET), Dhaka, who founded his research base with great care and motivated as well as inspired to undergo challenging works.

The author is profoundly obliged to his parents, wife and daughter, without whose constant support, encouragement and pleasant cooperation, the study would not have been completed in due course and therefore, carries his immense and deep heartfelt gratitude to them. The author also wishes to give thanks to his friends, lab-mates and foreign student office.

Finally, sincere indebtedness to Department of Civil Engineering, the University of Tokyo and Japan Government for awarding the MEXT scholarship envisioned for doctoral program at the University of Tokyo.

Above all, the author is grateful to the Almighty Allah Who Has given him the opportunity and ability to work hard with pleasure.

K. M. Ahtesham Hossain Raju

September, 2016.

ABSTRACT

Sand dune erosion mechanism is investigated in this study both by conducting laboratory experiments and numerical simulation. This is completely focusing on the erosion mechanism of subaerial sediments that constitute dune. Inundation overwash is reproduced in the laboratory by generating tsunami like wave. Laboratory experiments were conducted to investigate the mechanisms and parameters involved in dune sediment transport due to overwash. A total of 16 experimental runs have been conducted comprising of three types of sand on two different slopes for three bore condition. In each experiment, initial dune condition is set as: (i) dry and, (ii) wet. Up to the author's knowledge, this study considers this wet/dry condition for the first time.

Dune size and principal bore parameters are believed to be the essential factors in this transport process and simple analytical approach can reasonably represent this relationship. According to the analysis of the experimental results, it appears that air escaping behavior, incident bore parameters, bed slope, porosity, time scale, angle of repose have influence to generate difference in overwashed dune sediment transport for initially dry and wet condition as well as sediment types. Fine sand in wet condition exhibited highest erosion resistance. Coarse sand is dominated by porosity and the shorter time ratio for in/exfiltration.

Numerical modelling of hydrodynamics and dune morphology is performed based on the shallow water equations and energetics-based sand transport models. The model can predict the dune profile after the overwash by considering initial wet and dry condition. Effective shear stress is the key factor for sediment erosion. For fine sand, higher stress is required to simulate dry dune profile than wet dune. This shear stress increases proportionally to grain sizes.

The outcome of this study is expected to draw detailed picture of dune erosion mechanism, both externally and internally along with the sediment transport characteristics in initially wet and initially dry sediments of different grain sizes in sub aerial part.

CHAPTR ONE

INTRODUCTION

1.1 Introduction

Coastal dunes, either natural or man-made, act as a barrier against natural disaster like tsunami and storm surge. Nowadays dune overwash (over flowing of water resulting sediment transport) has drawn the attention of many investigators which imply its increasing significance in coastal communities and habitat. Field observations of the 2011 Tohoku Tsunami revealed that overwash of a dune increased the damage vulnerability of landward lying property and infrastructure as well as ecosystems, since overwash reduces dune height and increases flood or inundation possibility. Figure 1.1 illustrates a typical example of large dune deformation due to the 2011 Tohoku Tsunami observed at Nakoso, Fukushima Prefecture. The 2 km stretch of sand dune, apparently dry before the tsunami, was significantly eroded by the massive tsunami. Moreover the overwashed sediment is transported and deposited onshore of the dune and most often changes the adjacent morphology drastically. Donnelly et al. (2006) reported 1-2 m sediment deposition on Santa Rosa Island during Hurricane Ivan. Dune overwash process is also important for beach and dune design for storm protection (Donnelly et al. 2006). A number of studies have been conducted for dune erosion on the foreshore side. Among those notable works are of Kobayashi et al. (2009, 2010), Figlus et al. (2011) while limited investigations are available for dune overwash.

Figure 1.1 Significant dune erosion due to the 2011 Tohoku Tsunami

1.2 Background and Scope

Donnelly et al. (2006) have presented a critical review and extensive summary of literature on coastal overwash including field and laboratory studies, overwash modeling of washover volume and beach profile evolution. Kobayashi et al. (2010) examined wave overtopping and overflow on an impermeable smooth levee and developed a hydrodynamic model coupled with sediment transport (suspended and bed load) to predict levee erosion and dune overwash. Kobayashi et al. (2010) also compared this model with two small scale laboratory experiments with no or minor dune overwash by Kobayashi et al. (2009). They concluded that the dune erosion was mainly in offshore direction due to suspended sediment transport as complete overwash and landward sediment transport did not occurred.

Figlus et al. (2011) conducted laboratory tests with different initial dune geometry and identified three phases of dune overwash. An impermeable vertical wall was placed just at the end of back dune. Sediment that passed over the wall was collected in a sand trap and the overtopped water was collected in a tank. The experimental data were analyzed to observe the temporal variations of sand overwash, wave overtopping and dune profile evolution. These tests were used to modify and calibrate a numerical model for wave overtopping and dune overwash. However, in this study the spatial variation of onshore sediment transport was not possible to observe as the dune was truncated at the back dune end.

Laboratory study on solitary wave and bore overtopping a plane beach has been done by Baldock et al. (2012). New scaling was introduced for solitary wave overtopping volume but no unique scaling was found for overtopping solitary bore. However, dune or sediment was not incorporated in this investigation.

Fuchs and Hager (2015) investigated solitary impulse wave transformation to overland flow. They conducted physical experiments and focuses mainly on the transformation of this wave from inclined to horizontal portion. Therefore, it appears that overland flow of long waves are drawing attention of researchers nowadays and there are much scopes to deal with this topic, particularly when overland (subaerial) e.g. sand dune sediment transport due to long waves are concerned.

There are scopes to improve the prediction of overwash rates of dune by laboratory investigation as mentioned by Kobayashi et al. (2010). Donnelly et al. (2006) claimed the necessity of comprehensive laboratory data sets to make a model capable of simulating various washover morphologies that have been produced by different mechanisms (e.g. friction and percolation). Lack of data for wave overtopping and specially overwash of dune have been reported by Donnelly et al. (2006), Kobayashi et al. (2010), Figlus et al. (2011), Baldock et al. (2012). Very little work has considered measurement of dune washover volume and hence, literature on comparison of landward sediment transport is scare. However, the mechanism of overwash is still not fully understood, particularly, the influence of in situ air void within dune in this transport process. It appears from the general view that more sand will be transported in initially dry condition. It is not certain however that whether initially dry or initially wet sand has more mobility character while overwash takes place. The present study focuses on the landward sediment transport due to overwash of dune for initially dry sand and initially wet sand to investigate the influence of air void on the overwash process.

1.3 Objectives of the Study

The main objectives of this study have been setup as follows:

1. To investigate the nature/physics of dune erosion resulted from the tsunami overwash,
2. To investigate the influence of sediment grain size of dune as a coastal protection structure,
3. To investigate the landward sediment transport of dune composed of initially wet sand and initially dry sand quantitatively; to assess the influence of air void in this transport process, and
4. Numerical simulation to assess sediment transport and post overwash profile of sand dune.

1.4 Organization of the Thesis

This thesis has been organized under six chapters. Chapter one describes the background and objectives of the study. In Chapter two the review of literature related to the subject matter of the study has been described. In Chapter three, the laboratory set-up and experimentation formulation are presented chronologically. Chapter four illustrates the numerical simulation of the laboratory experiments. In Chapter five, the results of analyses and discussions are presented. Finally, the main conclusions of this study and recommendations for further study are presented in Chapter six.

CHAPTER TWO

LITERATURE REVIEW

2.1 Introduction

Coastal dune may undergo erosion due to wave action on the fore dune side and overflow (overwash) when the wave run up the dune crest during extreme situation like storm surge and more devastating case, the tsunami. Study on dune erosion due to wave is abundant whereas study on dune overwash is scare. Huge amount of sediment may be moved landward by the wave energy. The mode of this sediment transport needs to be investigated in order to quantify the rate and volume of dune material displacement. Moreover, deposition of this volume may go farther inland causing damage to land and property. Therefore, dune sediment deposition requires analysis on this aspect. This chapter describes the literature survey of aforementioned topics.

2.2 Previous Study: Sand-Dike Breach

Visser (1988) conducted laboratory experiments with sand-dike (d50=0.50 mm) to investigate breach growth and proposed a mathematical model to simulate temporal change of breach growth width and elevation. The breach was initiated manually and a constant upstream water level was maintained to provide continuous water flow. Visser et al. (1990) presented the result of the field experiment conducted to apply Visser (1988) model and found that the model can be suited only for first stage of breaching out of five stages.

Steetzel (1990) conducted laboratory study in order to predict dune erosion during extreme wave attack like storm surge; and presented a model capable of predicting profile evolution and sediment transport. It is to be noted that dune erosion means fore dune (sea side) erosion.

Steetzel and Visser (1992) investigated 2DV-breach growth of dike along the breach axis. They used three outer slopes and different sand sizes. The water level was raised 0.05 m above the crest and released in order to initiate breaching. It is mentioned that it is a difficult task to study breaching process due to the speedy nature of the processes

involved. They concluded that the effect of sand porosity is relatively small and coarser sand results higher erosion rate.

Visser (1994) proposed a mathematical model based on five step breach erosion process, to simulate the breach growth and discharge rate through the breach for a large scale experiments. Breach was initiated manually by creating a pilot channel at the dike crown. The model predicts the breach width from phase 1 to phase 4 and the agreement with the experimental data is good.

Loof et al. (1996) proposed an empirical relation to describe breach growth. The data employed were derived from the wave basin experiments, conducted to closely investigate the breach width growth. These experiments investigated the influence of dike height, width and level of foundation. It is evident from the experiments that dike erosion is rapid for a narrow or low crest than wider or higher crest. An additional wave attack resulted a larger breach width as expected.

2.3 Previous Study: Wave Overtopping and Overwash

Hancock and Kobayashi (1994) conducted laboratory experiments of wave overtopping over dunes and investigated water overtopping rate and sediment transport rate by applying existing formula. They found that scale and non-equilibrium effects are responsible for the discrepancy between measured and predicted beach slopes. The study concludes that a good correlation underlies between the sediment overwash rate and wave overtopping rate. Perhaps, they have taken the first initiative to investigate dune sediment transport due to overwash by irregular waves.

Kobayashi et al. (1996) investigated wave reflection, overtopping and overwash of dunes in small scale laboratory experiments. They established empirical relationships to predict the order of magnitude of the measured wave reflection coefficients and overtopping rates. The outcome of the study were expected to be included in the existing beach and dune erosion model to predict the post-storm dune profile, as they concluded.

Kobayashi et al. (2009) conducted small scale laboratory experiments to investigate berm and dune erosion by changing berm geometry. They proposed cross-shore and

alongshore sediment transport formulas, and incorporated them into a numerical model which is then applied to predict final beach and dune profile. However, dune overtopping did not occurred during the experiments rather they investigated fore-dune erosion i.e. erosion of dune on the sea side and the eroded sediment transport process to result the final beach as well as dune profile.

Kobayashi et al. (2010) carried out experiments on impermeable levee to examine overtopping and overflow of waves and formulated relations to predict water surface elevation and fluid velocity by applying numerical model based on continuity, momentum and wave action equations. The hydrodynamic model, coupled with sediment transport model, was applied to predict dune erosion and minor overwash. They emphasized on the measurement of wave overtopping and overwash rates to improve the model performance.

Figlus et al. (2011) conducted laboratory tests with different initial dune geometry and identified three phases of dune overwash. An impermeable vertical wall was placed just at the end of back dune. Sediment that passed over the wall was collected in a sand trap and the overtopped water was collected in a tank. The experimental data were analyzed to observe the temporal variations of sand overwash, wave overtopping and dune profile evolution. These tests were used to modify and calibrate a numerical model for wave overtopping and dune overwash. However, in this study the spatial variation of onshore sediment transport was not possible to observe as the dune was truncated at the back dune end. Figlus et al. (2012) conducted laboratory experiments and numerical modeling of wave induced ridge-runnel migration.

Gralher et al. (2012) and Kobayashi et al. (2013) presented laboratory study to investigate the performance of vegetation on sand dune erosion and overwash due to wave action. It was observed that wide vegetation on fore-dune and back dune revealed higher resistance against dune erosion, overtopping of water and consequently overwash of sediment than that of narrow vegetation; which is expected to happen. However, this study may be helpful in designing and modeling vegetated dune to reduce overwash.

Ayat and Kobayashi (2015) investigated the vegetation (cylindrical woody plant) density and its toppling effect in dune erosion and overwash by including drag force acting on cylinders into a numerical model. The model was calibrated and compared with the experiments of Gralher et al. (2012) to predict dune profile.

2.4 Previous Study: Coastal Overwash

Donnelly et al. (2006) presented a detailed overview of the state of knowledge on coastal overwash. An overwash may be due to excessive wave run-up and/or mean water level exceeding the beach or dune crest which may be named as run-up overwash and inundation overwash, respectively. As shown in Figure 2.1, run-up overwash may be again categorized as crest accumulation (no overtopping of water, $R+S \approx z_{dw}$) and crest lowering (eroded sediment deposited on back dune, $R+S > z_{dw}$). Inundation overwash may be categorized as minor inundation ($S \approx z_{dw}$) and complete inundation ($S > z_{dw}$) with significant sediment transportation and deposition on the shoreward side.

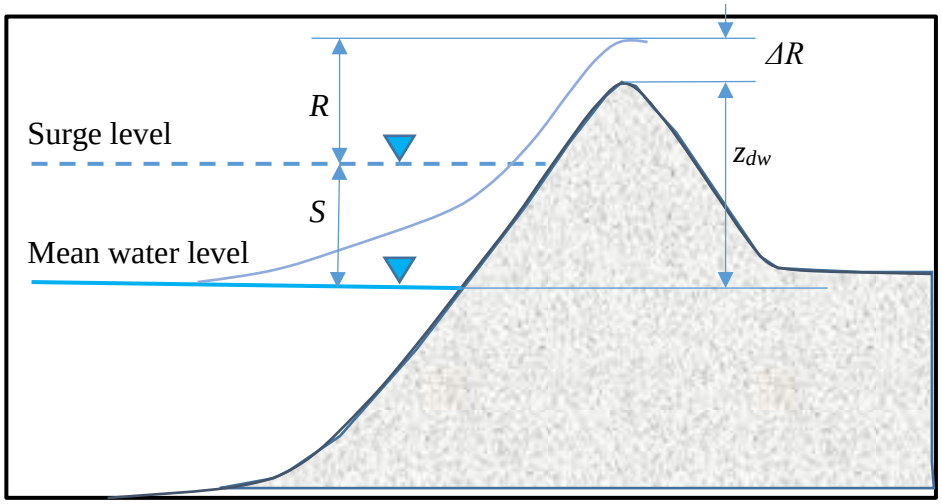

Figure 2.1 Definition sketch of overwash processes (adopted from Donnelly et al. 2006)

The deposition depth may be 1-2 m and transportation length of over hundreds of meters. Leatherman et al. (1977) conducted field study and reported 20 m^3 of sediment per meter of dune breach, on an average, was transported as overwash due to a northeaster on December 1, 1974 in Assateague Island, Maryland. Field studies on dune overwash are mostly performed on qualitative observation by researchers of

different areas like geology, geography, ecology, planning, engineering etc. On the other hand, laboratory study on overwash are very few.

Donnelly et al. (2006) mentioned that Williams (1978) was the first to conduct laboratory study focusing overwash. Objective of the study was to set predictive relationship between wave steepness, profile response and washover volume due to monochromatic wave run-up on barrier island coastline. Stauble (1979) conducted experiments to study the interaction of swash and sediment transport on backshore by creating single uprush bore. Normal backwash after run-up and backwash after overwash is investigated to observe sediment transport and the resulting morphological profile change.

Bradbury and Powell (1992) investigated profile response of shingle spit due to storm wave. They have conducted field work and physical model study in a 3-D wave basin under random wave condition for a wide range of beach geometry and suggested a dimensionless parametric framework to predict crest morphology of shingle barrier beaches.

Srinivas et al. (1992) conducted experiments for barrier island overwash due to wave run-up (insufficient to overwash), water level at and above crest level. It was observed that offshore bar formed for the regular wave motion but not for irregular waves.

2.5 Modeling Overwash

Holland et al. (1991) conducted field study to measure overwash bore celerity during overwash on a barrier. It was found that the celerity can be expressed as,

$$C_{bore} = 2.6\sqrt{g h_{crest}} \tag{2.1}$$

where, g = acceleration due to gravity, h_{crest} = flow depth over crest.

Hancock and Kobayashi (1994) defined average volumetric sediment concentration as

$$\overline{C_s} = \frac{q_s}{q_w} \tag{2.2}$$

where, q_s = sediment (without void) overwash rate, q_w = water overtopping rate. The range of $\overline{C_s}$ is 0.023~0.056. However, Kobayashi et al. (1996) found this value to be 0.0389.

Williams (1978) stated following relationship based on laboratory study to predict sediment transport rate,

$$q_s = \frac{K_1}{T}(\Delta R)^{\alpha 2} \tag{2.3}$$

where, K_1 = proportionality constant, T = wave period, ΔR = excess runup, α_2 = empirical exponent. He also proposed another expression for faster transport rate:

$$q_s = \frac{K_2}{T}(\Delta R)e^{-K_3 \Delta R} \tag{2.4}$$

where, K_2, K_3 = proportionality constant.

Tanaka et al. (2002) expressed overtopping water rate per wave per unit width as:

$$q_{wo} = \alpha_1(R + \eta_{tide} - H_c)^{n_1} \tag{2.5}$$

where, R = wave runup height, η_{tide}= sea water level variation due to tide, α_1 = 0.50 m/s, n_1 = 2.

Kraus and Wise (1993) improved SBEACH (Larson and Kraus, 1989) model by including runup overwash. Larson et al. (2004, 2005) enhanced SBEACH (Kraus and Wise, 1993) model by including sediment transport rate.

To determine sediment transport rate in swash zone, Larson et al. (2001, 2004) proposed the following formula,

$$q_{ss} = K_c \frac{u_b^3}{g}(tan\,\beta_l - \tan\beta_e)\frac{t_o}{T_s} \tag{2.6}$$

where, K_c = empirical transport coefficient, u_b = bore celerity, β_l = local foreshore slope, β_e = equilibrium foreshore slope, t_o = submergence time, T_s = swash period.

The sediment transport rate (q_{sd}) at dune crest is assumed proportional to the overwash volume as proposed by Hancock and Kobayashi (1994) and Kobayashi et al. (1996) as,

$$q_{sd} = K_B 2\sqrt{\frac{2g}{R}}(R - z_{dw})^2 \tag{2.7}$$

where, K_B = empirical coefficient, R = runup height, z_{dw} = dune crest elevation above mean water level.

On the other hand, sediment transport rate (q_{sl}) on back dune (landward) side is given by,

$$q_{sl} = \frac{q_{sd}}{1 - \frac{\mu' s_d}{B_D}} \tag{2.8}$$

where, μ' = spreading coefficient, s_d = horizontal distance from dune crest, B_D = width of throat during overwash.

Based on several simplified assumption, Larson et al. (2009) presented analytical model of dune erosion rate during overwash due to wave impact as follows,

$$\frac{dV}{dt} = -4C_s \frac{(R - z_o) z_d}{T} \tag{2.9}$$

where, V = dune volume, t = time, C_s = transport rate coefficient (2×10^{-4}), R = runup height above still water level, z_o = elevation of dune foot above still water level, z_d = dune height, T = wave or swash period.

Donnelly et al. (2009) developed numerical model of coastal overwash. For runup overwash, average volume of flow per overtopping wave (V_{WR}) is expressed as:

$$V_{WR} = \frac{2\sqrt{2g}}{C_u^2} (R - z_{dw})^{\frac{3}{2}} \sqrt{1 - \frac{z_{dw}}{R}} \tag{2.10}$$

where, C_u = bore celerity coefficient.

For inundation overwash, the expression becomes,

$$V_{WI} = \frac{2}{3} C_d \sqrt{2g} h_b^{\frac{3}{2}} \tag{2.11}$$

where, C_d = weir coefficient, h_b = depth of bore front at dune crest.

Donnelly et al. (2009) conducted laboratory study and established linear relationship between overtopping flow rate and sediment transport rate. The sediment transport rate for run-up overwash and inundation overwash is given respectively as,

$$q_{WR} = 2K_{B1} \sqrt{2g} (R - z_d)^{\frac{3}{2}} \sqrt{1 - \frac{z_d}{R}} \tag{2.12}$$

where, K_{B1} = sediment overwash coefficient.

$$q_{WI} = 2K_{B1} \sqrt{2g} h_b^{\frac{3}{2}} \tag{2.13}$$

2.6 Incipient sediment motion based on critical shear stress

The forces acting on a particle over which a fluid is flowing are the gravity forces of weight and buoyancy, hydrodynamic lift normal to the bed, and hydrodynamic drag parallel to the bed. The lift is often neglected without proper justification because both analytical and experimental studies have established its presence. Most treatments of forces on a particle on a bed consider only drag; lift does not appear explicitly. But, because the constants in the resulting theoretical equations are determined experimentally and because lift depends on the same variable as drag, the effect of lift regardless of its importance is automatically considered (Vanoni 1975).

The forces on a particle on the bed is depicted in Figure 2.2, in which θ = the slope angle of the bed; and ϕ = the angle of repose of the particle submerged in the fluid, and intergranular forces are ignored. The particle will be moved or entrained if the hydrodynamic forces overcome the resistance. When motion is impending, the bed shear stress attains the critical or competent value, τ_c, which is also termed the critical tractive force. Under critical conditions, also, the particle is about to move by rolling about its point of support.

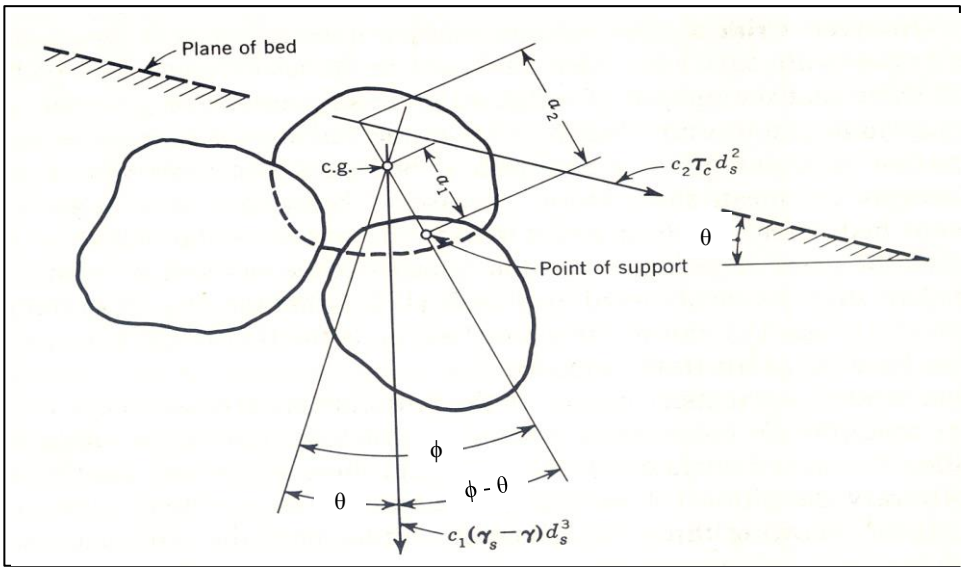

Figure 2.2 Forces on particle in flowing stream (Source: Vanoni 1975)

Major variables that affect the incipient motion include critical shear stress, τ_c; grain diameter, d; specific weight of sand, γ_s; specific weight of water, γ; density of water, ρ

and kinematic viscosity, v. From dimensional analysis they may be grouped into the following dimensionless parameters,

$$F\left[\frac{\tau_c}{(\gamma_s-\gamma)d}, \frac{\left(\frac{\tau_c}{\rho}\right)^{\frac{1}{2}} d}{\nu}\right] = 0 \tag{2.14}$$

$$or, \frac{\tau_c}{(\gamma_s-\gamma)d} = F\left(\frac{u_{*c}d}{\nu}\right) \tag{2.15}$$

Where $u_{*c}=\sqrt{(\tau_c/\rho)}$ is the critical friction velocity. The left-hand side of this equation is the dimensionless critical Shields stress, τ_{*c}. The right-hand side is called the critical boundary Reynolds number and is denoted by R_{*c}. Figure 2.3 shows the functional relationship of equation (2.15) established based on experimental data, obtained by Shields (1936) and other investigators, on flumes with a flat bed. It is generally referred to as the Shields diagram. Each data point corresponds to the condition of incipient motion.

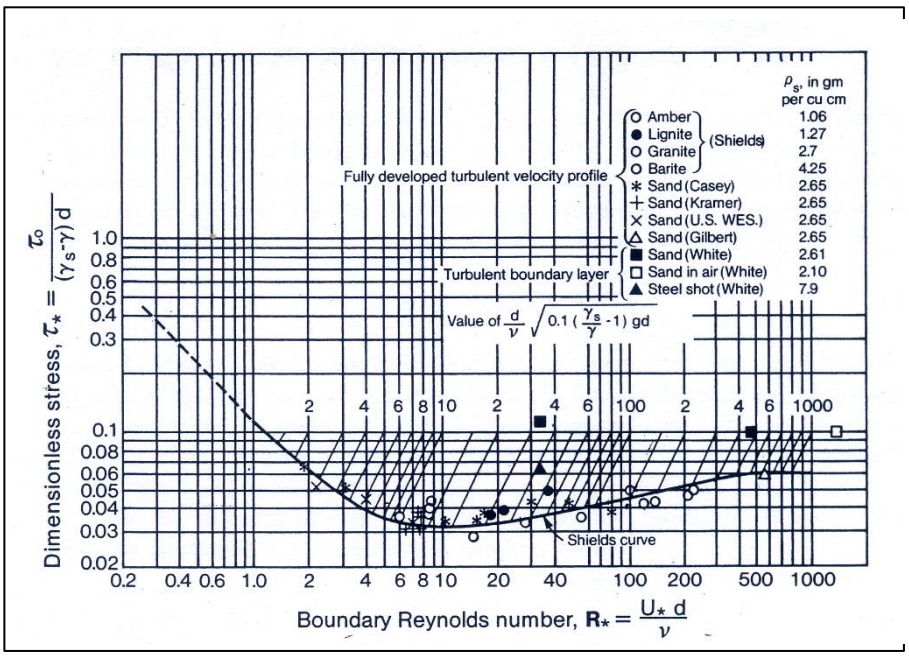

Figure 2.3 Shield's diagram for incipient motion (Source: Chang 1992)

2.7 Incipient sediment motion based on critical depth averaged velocity

The earliest studies were related to critical velocities of stones (Brahms, 1753 and Sternberg, 1875). They studied the critical near bed velocity and found that it was related to the particle diameter, as follows:

$u_{oc}^2 \sim d$

in which u_{oc} is the fluid velocity near the bed under critical conditions. Taking

$\tau_c \sim u_{oc}^2$

and substituting this also gives:

$u_{oc}^2 \sim d$

Cubing both sides of the relation gives:

$d^3 \sim u_{oc}^6$

which is the well-known sixth power law. Because the volume or weight of a particle is proportional to d^3, the law states that the weight of largest particle that a flow will move is proportional to the sixth power of the velocity in the neighborhood of the particle. Rubey (1948) found that this law applied only when d is large compared with the thickness of the laminar sub layer and the flow about the grain is turbulent.

It is better to use the critical depth averaged velocity, $\overline{u_c}$ than the near bed velocity, since it is not very well defined (van Rijn 1993). According to van Rijn (1993) Critical depth averaged velocity can be derived from the critical bed shear stress using the Chezy equation. Assuming hydraulic rough flow conditions $\left(\frac{u_* k_s}{\nu} > 70\right)$, the critical depth averaged flow velocity for a plane bed can be expressed as:

$$\bar{u}_c = 5.75\, u_{*c} log\left(\frac{12h}{k_s}\right) \tag{2.16}$$

Where $\overline{u_c}$ = critical depth averaged flow velocity; h = water depth; $k_s = \alpha_3 d_{90}$ = effective bed roughness of a flatbed; α_3 = coefficient ($\alpha_3 = 1$ for stones $d_{50} \geq 0.1$ m and $\alpha_3 = 3$ for sand and gravel material); $u_{*c} = \sqrt{\Psi_c \Delta g d_{50}}$ = critical bed shear velocity; and Ψ_c = critical Shields parameter.

2.8 Sediment Transport Formulae

The sediment entrainment, *E,* from bed layer is calculated using total-load formula of Engelund and Hansen (1967),

$$E = 0.05\frac{u^2}{h}\left\{\frac{\rho d}{(\rho_s-\rho)g}\right\}^{\frac{1}{2}}\left\{\frac{\tau_{be}}{(\rho_s-\rho)gd}\right\}^{\frac{3}{2}} \tag{2.17}$$

Where u = mean flow velocity; ρ = density of water; ρ_s = density of sediment grain; d = grain size and τ_{be} = effective bottom shear stress. To account for gravity effect due to bed slope, stream wise component of gravitational force is added to bottom shear stress by Wu (2004)'s method,

$$\tau_{be} = \tau_b + \lambda\tau_c\frac{sin\theta}{sin\varphi} \tag{2.18}$$

where τ_b = bottom shear stress; τ_c = critical shear stress; θ = bed angle with horizontal; φ = repose angle; λ = coefficient related with flow and sediment condition as well as bottom slope.

Sediment transport model proposed by Cao (1999) is applied to evaluate the performance of reproducing the laboratory study in numerical simulation. This model is also used by Cao et al. (2004) to compute dam-break wave induced sediment transport. The model is based on Shields parameter. It can be written as,

$$E = \frac{160}{R^{0.8}}\frac{(1-p)}{\Psi_c}\frac{(\Psi-\Psi_c)hU_\infty}{h} \tag{2.19}$$

where $R = \sqrt{sgd}\frac{d}{\nu}$, U_∞= free surface velocity (=*7u/6*), Ψ = Shields parameter, Ψ_c = critical Shields parameter for initiation of sediment movement.

2.9 Remarks

Abundant literature are available for dune erosion on the foreshore side while dune overwash study is scare. Dune overwash studies are mostly based on field level study.

Few of the laboratory studies consider overwash of dune that appears to be not the main goal rather the primary focus is given on foreshore dune erosion. Hence, measured data of dune sediment transport due to overwash is not sufficient enough to investigate/compare in detail of the experimental study as well as numerical simulation.

This study completely focuses on dune overwash due to tsunami overflow by conducting laboratory experiments and performing numerical simulation. The prime attention of the present study is given to dune sediment transport for two cases: (i) Initially Dry Dune (DD) and (ii) Initially Wet Dune (WD). The next chapter describes the experimental features of this study.

CHAPTER THREE

EXPERIMENTATION

3.1 Introduction

To increase the understanding of the dune erosion process caused by overwash of long waves like tsunami or storm surge, small scale laboratory study has been conducted in the Hydraulics Laboratory of the Department of Civil Engineering, The University of Tokyo. This chapter describes the wave flume set-up along with the devices used for measurements, fabrication and construction of dunes and the experimental features. Figure 3.1 shows the schematic diagram of the experimental set-up.

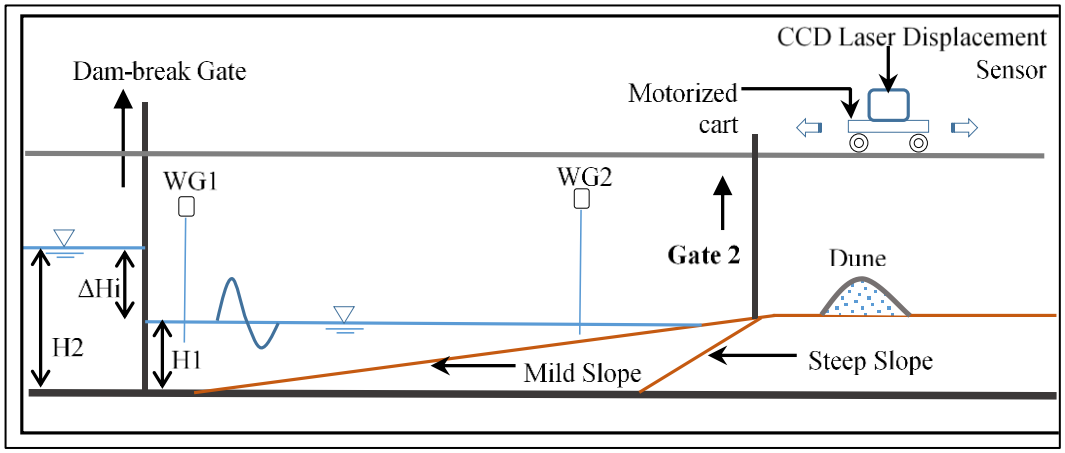

Figure 3.1 Schematic diagram of experimental set-up

3.2 Laboratory Setup

3.2.1 Wave Flume

Laboratory experiments were conducted in a 35 m long wave flume (Figure 3.2). The flume is equipped with a pressure driven dam-break gate (Figure 3.3) to generate a bore. The width and depth of the flume is 0.60 m and 0.80 m, respectively. Glass wall of flume helps to observe the dune erosion process from side. The flume is connected at its two ends by metallic pipe to facilitate circulation of water from the reservoir which can be controlled separately by valves. Test section of the flume base is fixed bed since the study considers dune erosion and sediment transport above dune base elevation. Two wave gauges, namely WG1 and WG2, were used to collect the water

surface elevation data; and gate 2 is installed and operated manually to achieve controlled overwash as shown in Figure 3.1.

Figure 3.2 Wave flume in Hydraulics Laboratory

Figure 3.3 Dam-break gate in wave flume

3.2.2 Partition Wall

A thin vertical partition wall of 0.80 m height and 4 m length is installed along the middle of the flume at the test reach to divide it into two parts (Figure 3.4). The steel wall is thin enough that it does not affect the water flow. This measure enables to conduct simultaneous runs for two different dune condition. It also facilitate to observe overwash process in wet and dry dune simultaneously for the same hydrodynamic condition.

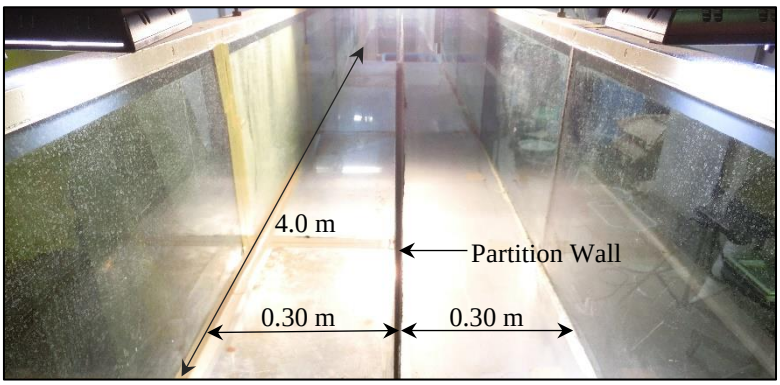

Figure 3.4 Vertical partition wall to separate WD and DD during experiment

3.2.3 Laser Displacement Sensor

A high speed, high accuracy Charged Couple Device (CCD) Laser Displacement Sensor manufactured by Keyence Corporation, Japan; is employed in this study as shown in Figure 3.5. The LK-G505 model has measurement accuracy of ±0.001 mm and the sampling cycle of 200 μs with a storage cycle of 20 ms. It can be used as a profiler to collect the bed elevation data precisely and accurately. Therefore, to collect the bed profile data the device is run attached on a motorized cart. To estimate bed elevation at a point, horizontal distance of that point from a reference has to be known. To find this value, CCD sensor attached with the cart is moved for a certain distance. Knowing storage cycle and the recorded number of data of the sensor, the velocity can be calculated; which should be equal to the velocity of the cart. In this way the distance between two data points recorded by the sensor is found. Similarly, the elevation versus horizontal distance, that is, bed profile is measured.

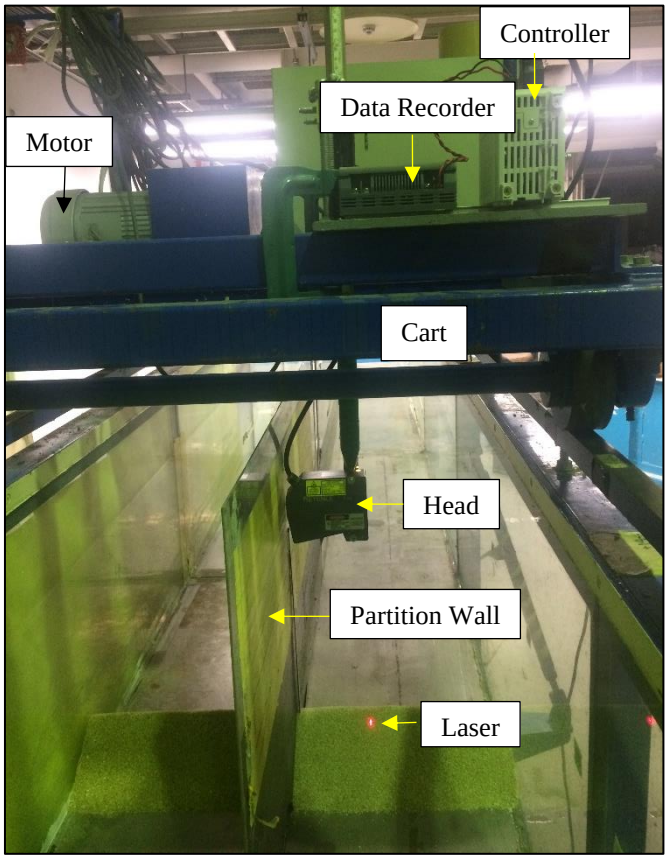

Figure 3.5 CCD Laser Displacement Sensor

3.2.4 Motorized Cart

A motorized cart (as shown in Figure 3.6) is deployed to move the CCD sensor at a constant speed along the cross-shore. The cart is moved for a certain distance and the time is recorded. This process is repeated for ten times and the average is taken as the constant speed of the cart.

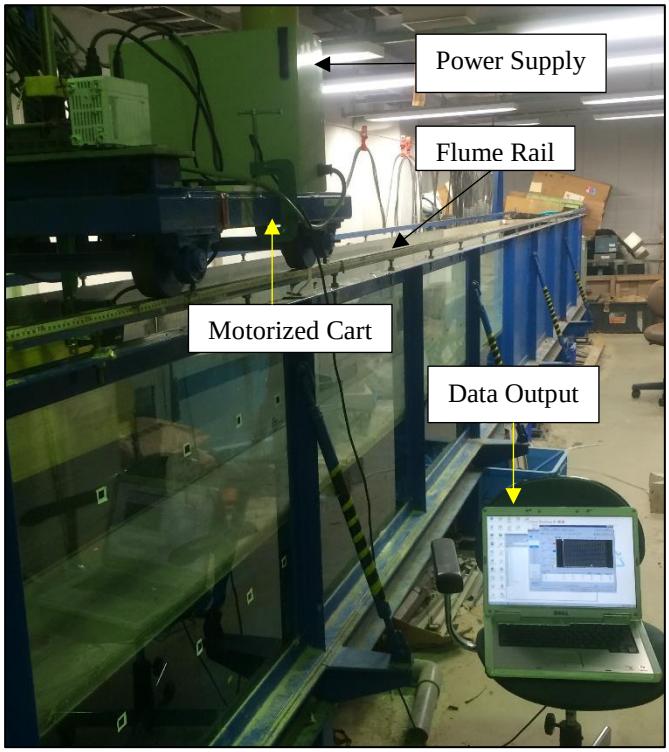

Figure 3.6 Motorized cart over the flume rail

3.2.5 Bed Slope

Two slopes are constructed (Figure 3.1) to investigate the nature of overwash and the influence of bed slope in sediment transport: (i) steep slope (1V:7H) and (ii) mild slope (1V:28H).

3.2.6 Dune Construction

In general, dunes have different shapes like triangular with round crest or trapezoidal. However, this study focuses on dune sediment transport especially in initially wet and initially dry condition. To investigate this mechanism, a triangular shaped dune with relatively steep slopes are selected. This geometry facilitate comparatively clear distinction during overwash between wet and dry dune. For dune construction, transparent plastic mold is fabricated to achieve same dune geometry in all the experiments. Therefore, the size of the dune results in 30 cm, 20 cm and 7 cm for length, width and height, respectively. Same amount of sand was taken for the construction of DD and WD. For DD, the mold is filled with sand of normal condition and was placed on the bed. For WD, firstly, the mold is filled with dry dune and then,

water is sprinkled gently on the surface in such a way that water reaches the farthest corner and lowest part of the dune and it is made sure that all the grains are wet. Then it was placed on the flume bed. Figure 3.7 shows the stepwise process followed to place the sand in the plastic mold and placement on the flume test reach to get the designed dune size and shape.

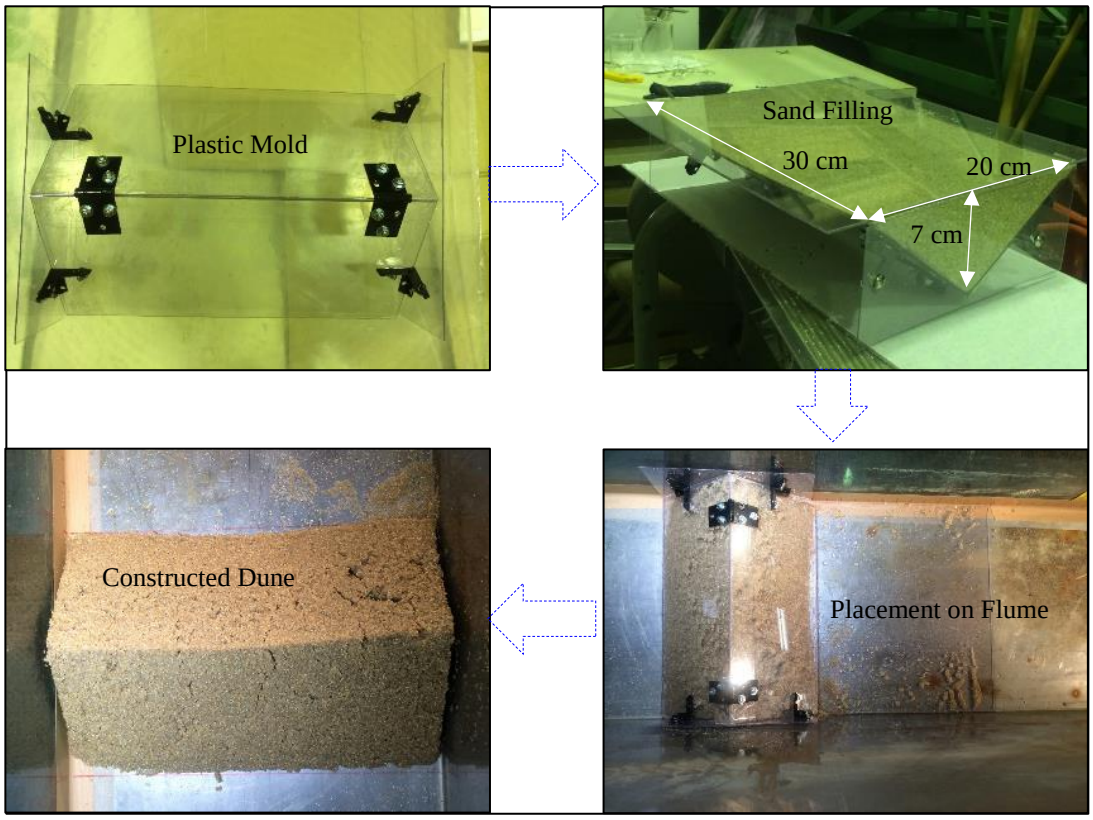

Figure 3.7 Steps of sand dune preparation on the wave flume

3.2.7 Generation of Bore

Tsunami and storm surge waves are simulated in the laboratory by creating dam-break waves or bores. The still water level (*H1*) was 0.32 m throughout all the experiments. Only the water level (*H2*) on the other side of the gate (Figure 3.1) is changed to generate the bore. Three bore conditions on the basis of water surface elevation difference (ΔHi in Figure 3.1) were investigated, namely, small bore ($\Delta H1$ = 6 cm), medium bore ($\Delta H2$ = 8 cm) and large bore ($\Delta H3$ = 10 cm).

3.2.8 Sand Types

To investigate the influence of sand sizes during sand dune overwash, three types of sand is utilized. (i) Coarse, (ii) Medium, and (iii) Fine with median grain size of 0.90 mm, 0.60 mm and 0.15 mm; respectively.

3.3 Procedure of Experiment

Several trial runs had been conducted to design the experiments, e.g. selecting bore and dune size in such a manner that overflow of water over dune is taking place. On the basis of these runs, a total of 16 experimental runs were performed. Procedure of conducting the experiment is briefly mentioned below:

(i) With a particular type of sand, the dune was constructed for the two initial conditions: wet and dry; and placed on the test section of the flume. These two dunes are separated by the vertical partition wall.

(ii) Each dune is divided into five equal strip of 5 cm width across the shoreline as shown in Figure 3.8 and dune profile data is collected along these lines with CCD laser profiler before overwash occurs.

(iii) High speed video camera are used on overhead of dune and by the flume wall to record the overwash process.

(iv) Still Water Level (SWL) is maintained at 32 cm in the wave flume. Then, the dam-break gate is closed. The water level on the upstream side of the gate is raised (ΔH) to the desired level ($H2$) to achieve bore condition (e.g. $\Delta H = 6, 8, 10\ cm$).

(v) Two wave gauges are used to obtain incident wave parameters. Wave profile is measured by capacitance type wave gauge of 100 Hz sampling frequency. In steep slope experiments, first and second wave gauge is installed at 3 m and 11 m, respectively, from the dam-break gate. In mild slope experiments, first and second wave gauge is installed at 1 m and 12 m, respectively, from the dam-break gate.

(vi) The dam-break gate (Figure 3.1) is opened to release water suddenly to generate bore.

(vii) A vertical gate (Gate 2 in Figure 3.1) is installed and operated manually near the shoreline to prevent dune overwash by waves other than the first bore completes overwash. To ensure this, the gate is shut down after the first bore has receded.

(viii) Step (ii) is repeated after the overwash is finished.

(ix) Then all sediment is collected on separate tray for initially wet and dry dune from the flume bed beginning from the back dune edge (Figure 3.9) of the initial dune till the farthest distance where sand grain moved.

(x) For the first run, transported sediment is collected by making 2 cm strip along the flume as shown in Figure 3.10 and Figure 3.11. It helps to have an insight understanding of spatial extent and the inherent difference of sediment transport between initially wet and initially dry sediment condition.

(xi) The collected sediment is oven dried for 24 hours at $\pm 105^0$ C and then the mass is measured on an electronic scale and recorded.

(xii) Initial and final dune profile was plotted from the displacement sensor data.

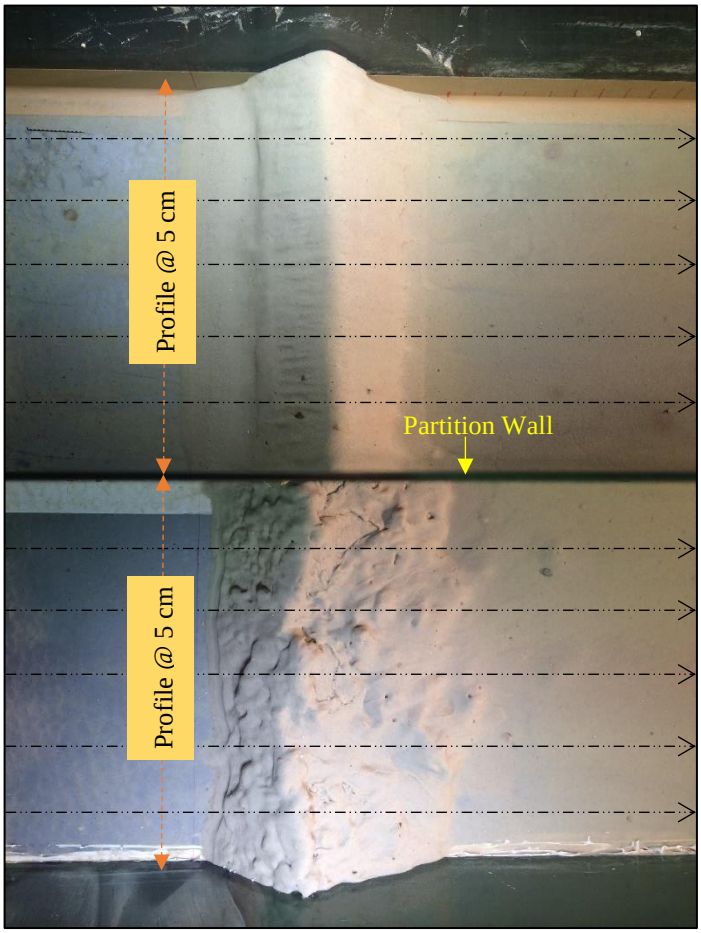

Figure 3.8 Lines along dune width for profile measurement

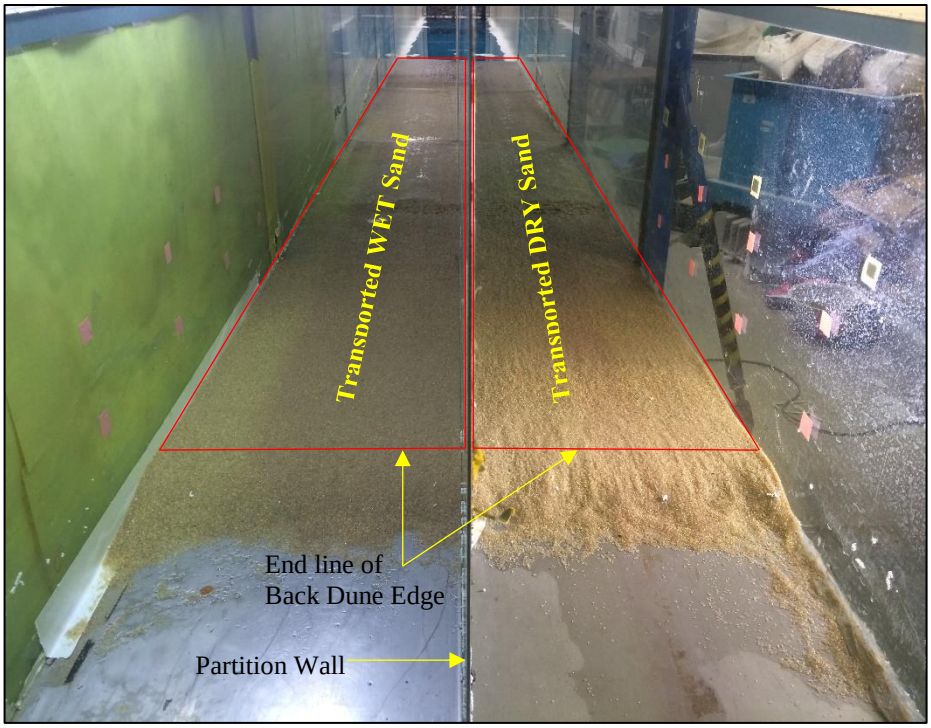

Figure 3.9 Transported sediment collection area (marked by red box) on the flume bed

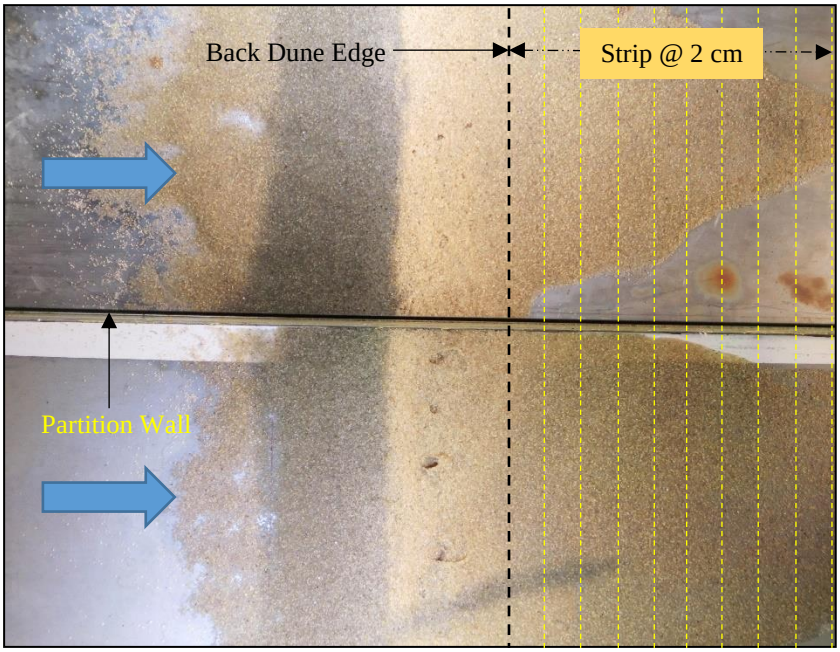

Figure 3.10 Method of sediment collection during primary experiment

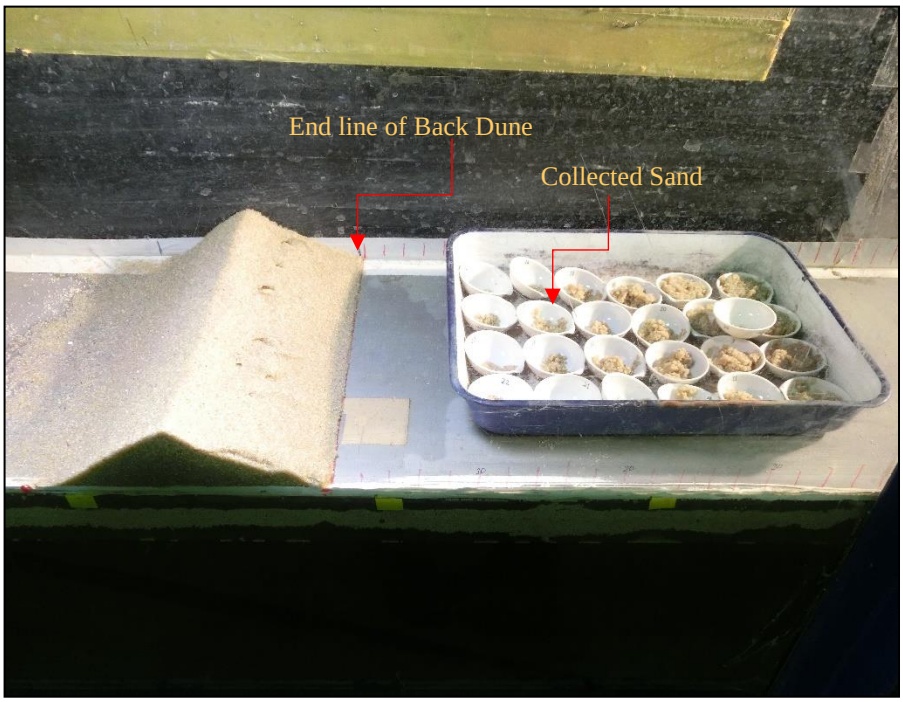

Figure 3.11 Collected sediment from each strip on single small cup

3.3.1 Reproducibility of the experiments

Run R2 is selected to check the reproducibility of the experiment. Because it showed small difference in sediment transport between initially wet and initially dry dune condition. It is found that more sand is transported from initially dry dune than initially

wet dune in regular experiment. The same response of sediment transport is found in the repeated experiment. Moreover, the recorded water surface elevation data of the incoming bore of the same bore size shows similarity. For example, almost same maximum wave height for experiments with three sands for the same bore B2 (ΔH = *8 cm*) on a particular slope, say steep slope. This is also the same for bore of sizes B3 (ΔH = *10 cm*) and B1 (ΔH = *6 cm*) as well. This is also the same for experiments on mild slope. That is almost same maximum wave height for experiments with three sands on steep slope, and almost same maximum wave height for experiments with three sands on mild slope case.

Therefore, it is expected and anticipated that the experiments are reproducible without significant deviation from one another.

3.4 Measurement

3.4.1 Sediment Grain Size

Figure 3.12 shows Laser Diffraction Particle Size Analyzer (Shimadzu SALD-3100) in the Hydraulics Laboratory employed for sediment grain size analysis. This instrument can accurately analyze grain sizes ranging from 0.05 μm to 3 mm.

Figure 3.12 Laser Diffraction Particle Size Analyzer (SALD-3100)

3.4.2 Angle of Repose

Angle of repose (φ) can be defined as the angle that the surface of sand pile under gravity makes with the horizontal (Mehta and Barker, 1994). Three sand types are taken to measure its angle of repose. 500 gm of sand is taken and slowly allowed to fall freely on a levelled surface. This form a cone shaped sand pile. The height and base width of the sand pile is measured to calculate the angle of repose. The process is repeated several times and the average is taken for analysis. The measured values are shown in Table 3.1 giving range of 28.7^0 to 33.7^0 which is in accordance with Wu (2008) and Hough (1957). However, Sleath (1984) defined angle of repose as, "If sediment is placed in an open box and carefully leveled and the box is then gradually tilted, there is observed to be a certain angle of tilt beyond which the sediment becomes unstable. This angle is what most engineers call the angle of repose". Wu (2008) defined, "The repose angle is the angle, with respect to the horizontal, of the slope formed by the sediment particles submerged in water under incipient sliding conditions". As suggested by Zhang et al. (1989) (from Wu, 2008), the repose angle can be estimated as,

$$\varphi = 32.5 + 1.27d \tag{3.1}$$

where φ is in degrees, and sediment size d is in mm. Equation 3.1 is calibrated for sediment sizes of 0.20 to 4.40 mm.

Angle of repose depends on angularity or roundness of grains. Roundness ($\Re$) is defined as the ratio of the average radius of curvature of the corners and edges of the particle to the radius of maximum sphere that can be inscribed (Wadell, 1932 and Mitchell and Soga, 2005). Santamarina and Cho (2004) presented a linear fit between angle of repose and roundness that can be expressed as follows:

$$\varphi = 42 - 17\Re \tag{3.2}$$

3.4.3 Porosity

To measure porosity (p), 100 ml of sand is taken in a graduated beaker and weighted. Then 150 ml of water is added to the beaker containing sand and stirred well. After this, volume of sand and water mixture is recorded. Porosity is calculated by dividing the volume of void by volume of sand. For each type of sand, this procedure is repeated

five time and average value is taken for analysis. However, investigation has been conducted to correlate porosity with median diameter by Komura (1963). Afterwards, this correlation is modified by Wu and Wang (2006) as follows,

$$p = 0.13 + \frac{0.21}{(d_{50} + 0.002)^{0.21}} \tag{3.3}$$

where d_{50} is in millimeters.

3.4.4 Fall Velocity

Fall velocity (w_o) of sediment particle (0.1 mm < d_{50} <1.0 mm) is calculated according to van Rijn (1993),

$$w_o = \frac{10\nu}{d_{50}}\left(\sqrt{1 + \frac{0.01\Delta g d_{50}^3}{\nu^2}} - 1\right) \tag{3.4}$$

3.4.5 Water Surface Profile

Following figures (Figure 3.13 to Figure 3.17) shows the dam-break wave profile measured at second wave gauge that represent tsunami like long waves generated by three bore sizes for two different slopes.

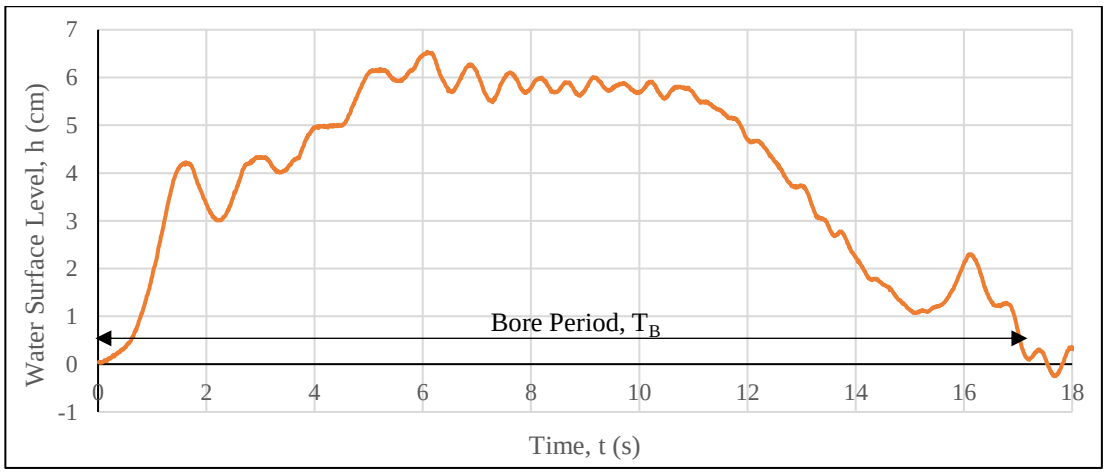

Figure 3.13 Water surface profile for bore B1 (ΔH2 = 6 cm) in steep slope cases

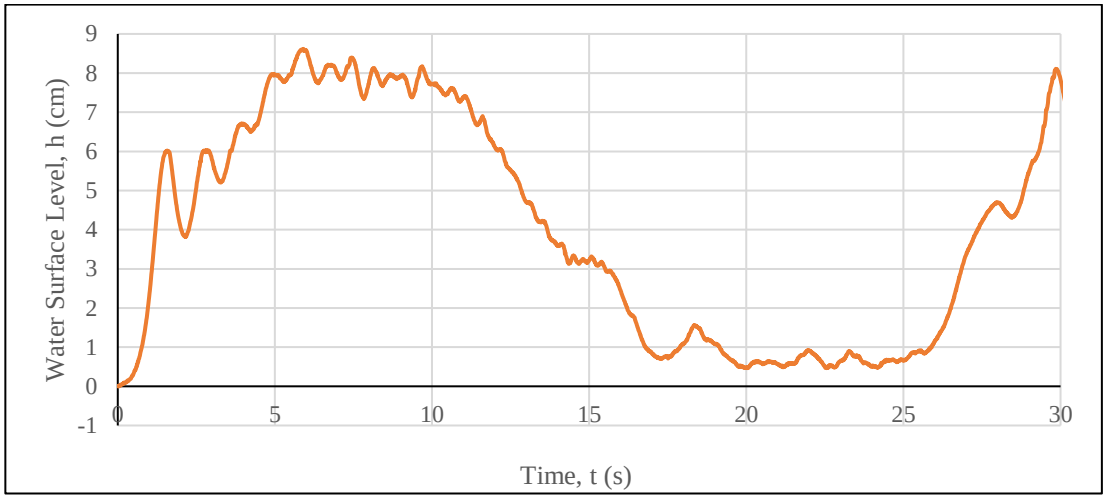

Figure 3.14 Water surface profile for bore B2 (ΔH2 = 8 cm) in steep slope cases

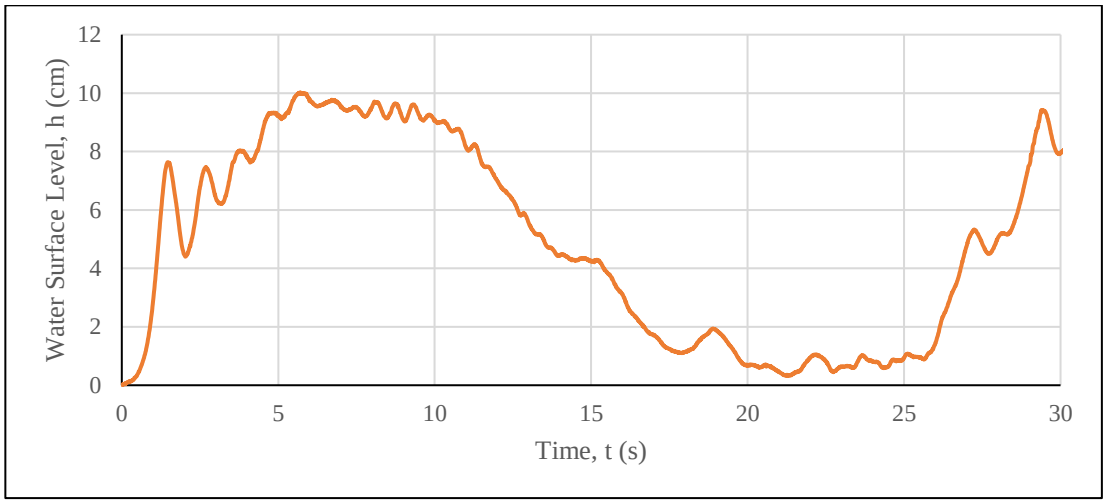

Figure 3.15 Water surface profile for bore B3 (ΔH3 = 10 cm) in steep slope cases

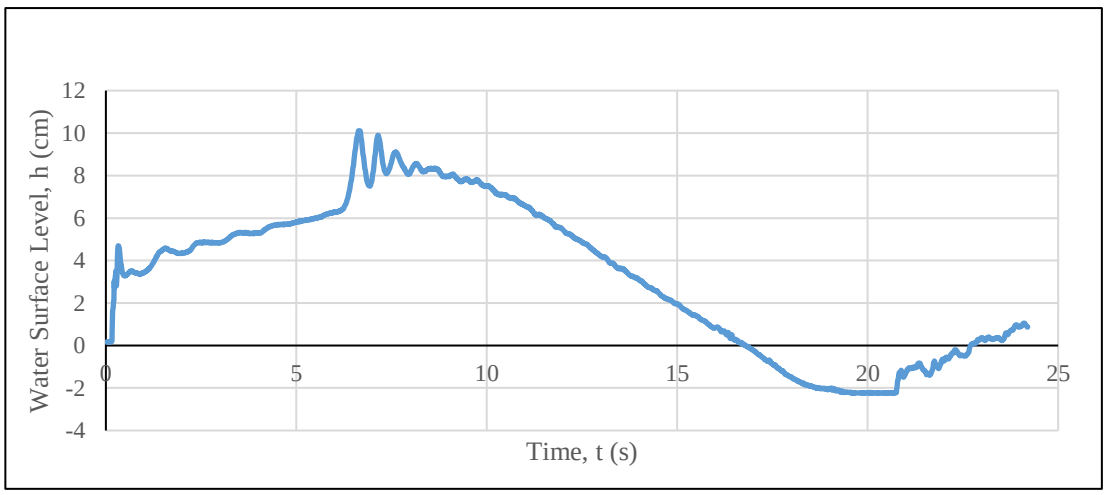

Figure 3.16 Water surface profile for bore B2 (ΔH2 = 8 cm) in mild slope cases

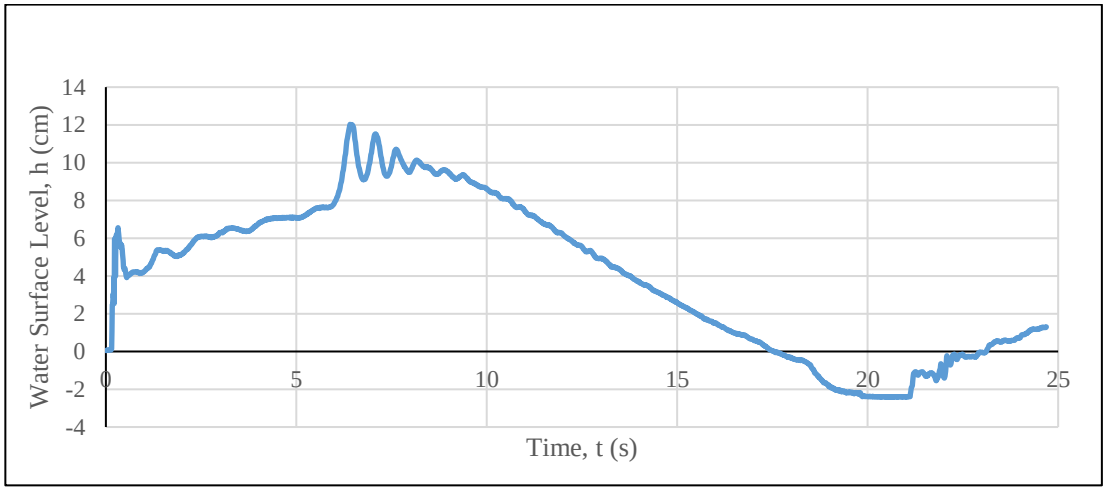

Figure 3.17 Water surface profile for bore B3 (ΔH3 = 10 cm) in mild slope cases

3.4.6 Bed Profile with Dune

Wave flume is divided into two parts for DD and WD. Each part splits into five equal strip of 5 cm width across the shore (as shown previously in Figure 3.8). Initial bed profile without dune is collected along five lines with CCD laser profiler. Then bed profile with dune; and lastly profile after overwash is recorded. To plot the cross shore dune profile, the measured five point values along the dune is averaged to obtain a single data point.

3.4.7 Waterfront Spreading Time through Dune

Observation during overwash of DD gives an estimation of the time required for it to become fully wet. This is accomplished analysis of the video recorded by high speed video camera set by the flume wall. The video is converted to all the photo frames recorded per second. Counting the number of frame till the entire dune cross-section becomes wet and dividing it with the 'frame per second' number gives the exact time. This time may be denoted as T_{ws}.

3.5 Summary of Experimental Features

Brief summary of the experimental features are mentioned in Table 3.1. Here water overflowing the dune is mentioned in fifth column as overtopping condition. Overtopping occurred only once in the first three run (R1~R3) while overtopping occurred three times for the next three run (R4~R6). In the rest experiments, inundation

type overtopping took place. For R10, no overtopping happened. Therefore, mild slope case has two bore size (B2 and B3) for overtopping to take place. It is seen that for R11~R13, inundation type overwash occurred but not for R4~R6. It reveals that, overwash duration and overtopping water volume is higher for mild slope than those of steep slope. Figure 3.19 shows schematic representation of the parameters involved in dune erosion mechanism.

Table 3.1 Experimentation features

Run Number	Slope Type	Sand Type	Bore ΔHi, cm	Overtopping Condition
R1	Steep	CS	6	Single Wave
R2	Steep	MS	6	Single Wave
R3	Steep	FS	6	Single Wave
R4	Steep	CS	8	3 Waves
R5	Steep	MS	8	3 Waves
R6	Steep	FS	8	3 Waves
R7	Steep	CS	10	Inundation
R8	Steep	MS	10	Inundation
R9	Steep	FS	10	Inundation
R10	Mild	CS	6	None
R11	Mild	CS	8	Inundation
R12	Mild	MS	8	Inundation
R13	Mild	FS	8	Inundation
R14	Mild	CS	10	Inundation
R15	Mild	MS	10	Inundation
R16	Mild	FS	10	Inundation

3.6 Properties of Sediment

Grain size analysis is performed by a laser diffraction particle size analyzer. The grain size distribution of these sands are shown in Figure 3.18. Some properties of the sands like angle of repose, hydraulic conductivity, porosity, standard deviation are given in Table 3.2.

For the estimation of hydraulic conductivity, *K*, the following equation is used,

$$K = \frac{k\rho g}{\mu} \tag{3.5}$$

where, k = intrinsic permeability (cm^2); ρ = density of water (gm/cm^3); g = acceleration due to gravity (cm/s^2); and μ = dynamic viscosity of water (gm/cms). Intrinsic permeability, *k*, was calculated according to Harleman et al. (1963),

$$k = C_1 d_{50}^2 \tag{3.6}$$

where, C_1 = a dimensionless constant (5.5×10^{-4} for sand grains); d_{50} = grain size for which 50% of the sand is finer (cm).

Lambe and Whitman (1979) mentioned the following expression proposed by Hazen,

$$K = 100 d_{10}^2 \tag{3.7}$$

where d_{10} = grain size for which 10% of the sand is finer (cm). *K* is in cm/s. It is obvious that permeability is influenced by finer particles in a soil mass. However, this expression assumes hydrodynamic stability of the soil in order to restrict movement of finer particles due to seepage force of the flowing water.

Geometric standard deviation is defined as,

$$\sigma_g = \frac{1}{2}\left(\frac{d_{50}}{d_{16}} + \frac{d_{84}}{d_{50}}\right) \tag{3.8}$$

Trask's sorting coefficient (Trask, 1932) is defined as,

$$S_o = \sqrt{\frac{d_{75}}{d_{25}}} \tag{3.9}$$

Typical designations are:

$1.0 \leq S_o \leq 1.5$: well-sorted sands

$1.5 \leq S_o \leq 2.0$: ordinarily-sorted sands

$2.0 \leq S_o$: poorly-sorted sand

3.6.1 Time Ratio

The hydraulic conductivity of the sand may be used to define a scale to explain the sediment transport mechanism. The maximum length required by the water particle through the fore dune face to reach back dune face is assumed as the width of the dune (=20 cm). Therefore, the time scale for infiltration, T_i is defined as,

$$T_i = \frac{W_D}{K} \tag{3.10}$$

where, W_D = width of dune (cm). When the unit of K is in cm/s, the unit of T_i is s. If the overwash duration is T_o (s), time ratio, R_T can be expressed as,

$$R_T = \frac{T_o}{T_i} \tag{3.11}$$

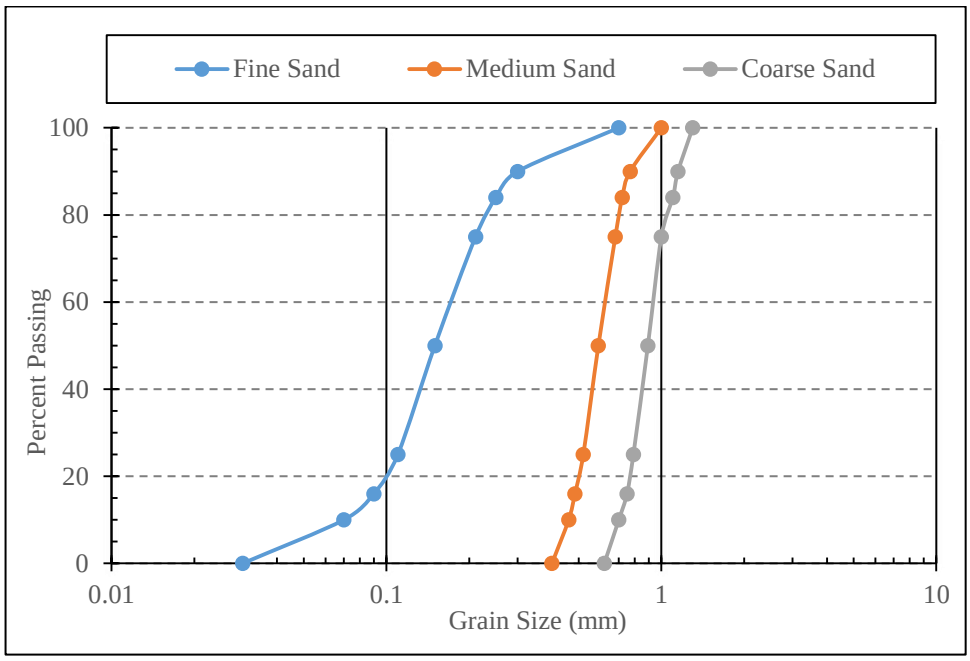

Figure 3.18 Grain size distribution for three sands used in the study

Table 3.2 Properties of sands used in the study

Sediment Properties	**Fine Sand (FS)**	**Medium Sand (MS)**	**Coarse Sand (CS)**
d_{10} (mm)	0.07	0.46	0.7
d_{16} (mm)	0.09	0.49	0.75
d_{25} (mm)	0.11	0.52	0.79
d_{50} (mm)	0.15	0.60	0.90
d_{75} (mm)	0.21	0.68	1.00
d_{84} (mm)	0.25	0.72	1.10
d_{90} (mm)	0.30	0.77	1.15
Standard Deviation, σ_g	1.67	1.22	1.21
Sorting Classification	Well Sorted	Well Sorted	Well Sorted
Angle of Repose, φ	33.7^0	28.7^0	29.7^0
Hydraulic Conductivity, K (cm/s)	0.012	0.194	0.437
Time Scale for infiltration, T_i (s)	1667	103	46
Porosity, p	0.36	0.41	0.30

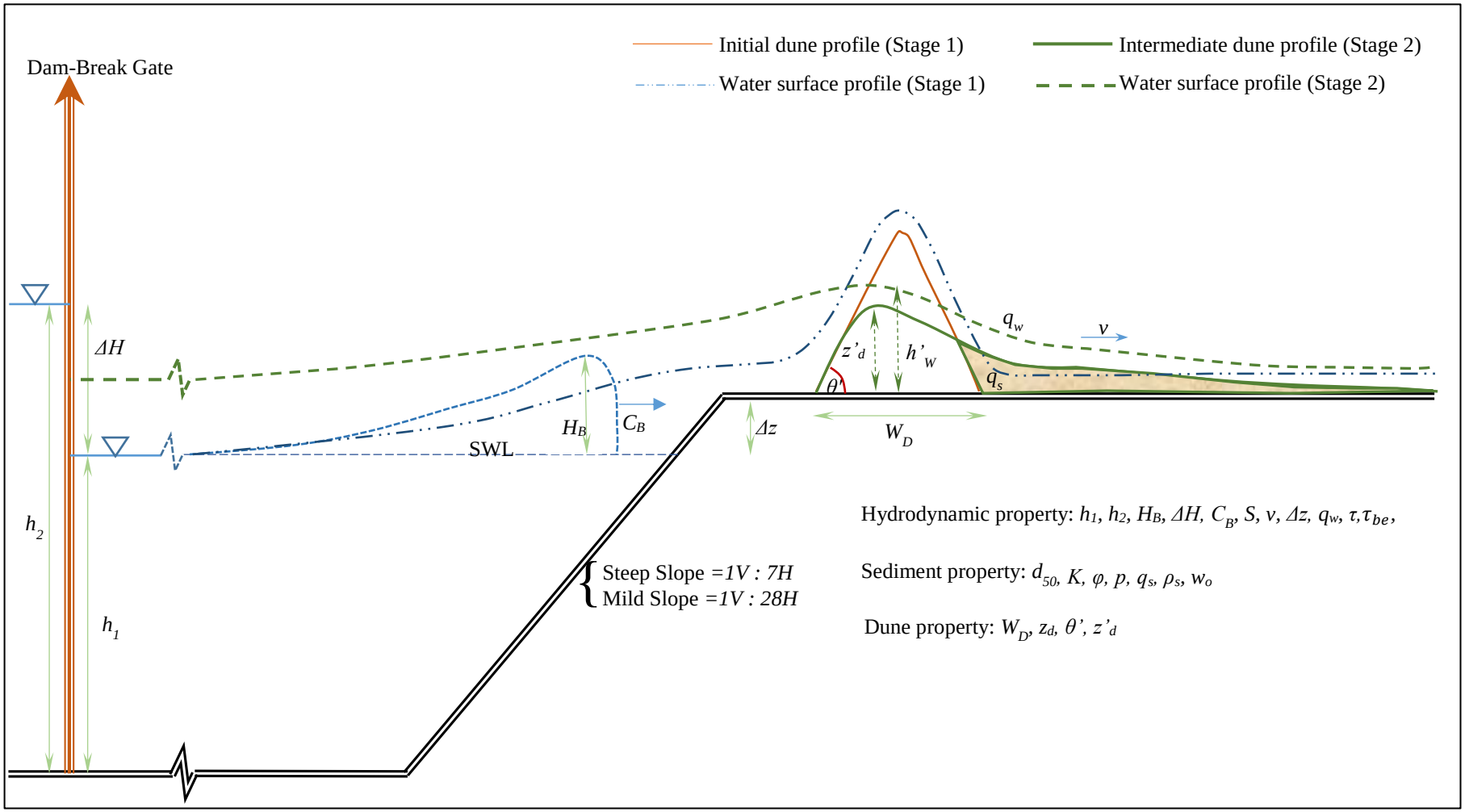

Figure 3.19 Schematic diagram showing parameters involved in dune erosion mechanism

CHAPTER FOUR

NUMERICAL MODELING

4.1 Introduction

Experimental study can be re-investigated by numerical analysis applying the mathematical models to predict the complex natural changes in the coastal areas due to extreme events like tsunami and storm surge- in a scientific way. Numerical simulation helps to understand processes involved in a phenomena, as well as the level of importance and/or influence of a particular parameter in the overall system very easily but accurately, as long as it does not differ much with the observation. This depends on the performance/accuracy of simulating the natural phenomena: wave hydrodynamics, sediment transport, bathymetry change, beach area evolution or destruction. This chapter describes these aspects model formulation and numerical schemes applied in the simulation.

The Saint-Venant (SV) shallow water equations is applied to describe the dam-break hydraulics. Dam-break waves are similar to the long waves e.g. tsunami or storm surge. SV equations can be used to simulate the waves resulting from tsunami or storm surge and propagation of these waves towards the shore at relatively shallow depth. These are also successfully used to analyze the broken wave propagation and run-up over the beach. Wave carries sediment as suspended load and bed load. When the wave reaches the beach, it may cause deposition or erosion resulting a net change of the foreshore and backshore area. Therefore, the broken or unbroken long waves causes a drastic evolution or damage of coastal area.

4.2 Model Development

This model is the extended version of Shimozono et al., 2007 model. Therefore, some of the sections are mainly from that model. Nonlinear shallow water equation is used in many literatures for the simulation of tsunami on the assumption of hydrostatic pressure. Another equation widely used in coastal engineering is Boussinesq-type equation which accounts for dispersion effects due to non-hydrostatic

pressure. Since dispersion term has an role of anti-steepening, simulation based on NSWEs predicts wave breaking far offshore. In addition, the present target is flow around dune with steep slope so that vertical acceleration cannot be negligible.

Sediment transport is modeled on the basis of advection equation with bottom boundary condition specified by a balance of upward and downward sediment flux. Horizontal diffusion term is not explicitly introduced since the equation is integrated with Shock Capturing Scheme, in which numerical diffusion is automatically given to preserve monotonous distribution of sediments in horizontal direction. For the upward flux, which is entrainment of sediment from bed layer, total-load sediment is computed with a single formula.

Mass conservation equation of water and sediments must be fully coupled since time-scale of the bed level change is not smaller than that of water surface. Thus, at every time step, bed level change is considered in the calculation of the flow. Although the effects of horizontally varying concentration and momentum transfer due to sediment exchange are also significant in the simulation of highly concentrated flow (Cao et al. 2004), they are not taken into account here.

4.3 Governing Equations

The governing equations can be written as follows:

$$\frac{\partial h}{\partial t}+\frac{\partial (uh)}{\partial x}+\frac{\partial z}{\partial t}\ =\ 0 \tag{4.1}$$

$$\frac{\partial (hu)}{\partial t}+\frac{\partial}{\partial x}\left(hu^2+\frac{1}{2}gh^2\right)+gh\left(\frac{\partial z}{\partial x}\right)=0 \tag{4.2}$$

$$\frac{\partial (hc)}{\partial t}+\frac{\partial (huc)}{\partial x}=E-D \tag{4.3}$$

$$\frac{\partial z}{\partial t}=\frac{D-E}{1-p} \tag{4.4}$$

where x = stream wise coordinate; h = total depth; u = depth averaged velocity; z = bed level; c = flux averaged volumetric sediment concentration; E = entrainment of

sediment flux from bed layer; D = deposition flux of sediment; g = gravitational acceleration; and p = porosity of bed material.

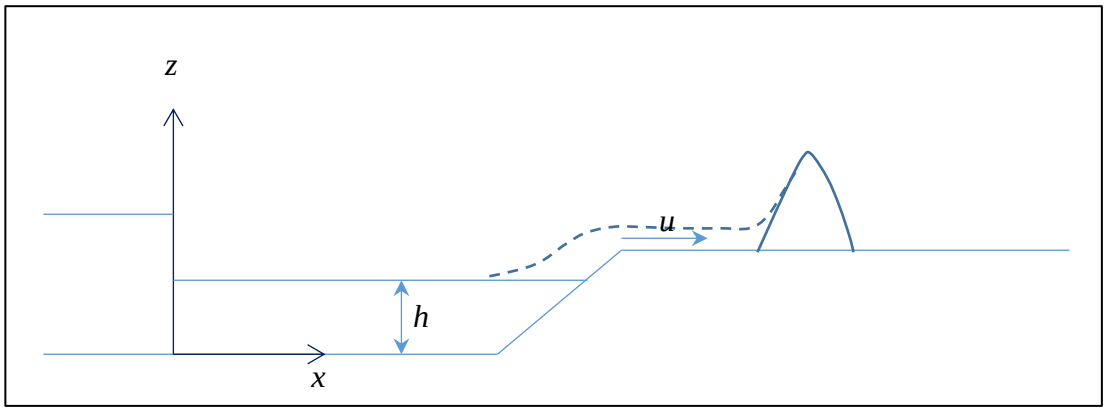

Figure 4.1 Definition sketch for governing equations

From equation (4.1) and equation (4.4), the mass conservation for the water sediment mixture can be expressed as:

$$\frac{\partial h}{\partial t}+\frac{\partial (uh)}{\partial x}=\frac{E-D}{1-p} \tag{4.5}$$

The right hand side of equation (4.5) is important because it represents the mass exchange between the sediment laden water and the erodible bed which is significant for suspended and bed load transport associated with the bed profile change (Cao et.al. 2004).

4.4 Model closure

The sediment entrainment, E from bed layer is calculated using total-load formula of Engelund and Hansen (1967),

$$E=0.05\frac{u^2}{h}\left\{\frac{\rho d}{(\rho_s-\rho)g}\right\}^{\frac{1}{2}}\left\{\frac{\tau_{be}}{(\rho_s-\rho)gd}\right\}^{\frac{3}{2}} \tag{4.6}$$

where ρ = density of water; ρ_s = density of sediment grain; d = grain size and τ_{be} = effective bottom shear stress. To account for gravity effect due to bed slope, stream wise component of gravitational force is added to bottom shear stress by Wu (2004)'s method,

$$\tau_{be} = \tau_b + \varepsilon\tau_c \frac{sin\theta}{sin\varphi} \tag{4.7}$$

where τ_b = bottom shear stress; τ_c = critical shear stress; θ = the bed angle with the horizontal; φ = repose angle; ε = coefficient related with wet and dry condition of sediment prior to overwash.

Bed shear stress (τ_b) is known as,

$$\tau_b = \rho u_*^2 \tag{4.8}$$

Shear velocity (u_*) is expressed according to Sleath (1984) as,

$$u_* = \frac{0.40u}{log\left(\frac{11h}{0.50d_{50}}\right)} \tag{4.9}$$

Critical shear stress is determined according to Wu and Wang (1999) as,

$$\frac{\tau_c}{(\gamma_s - \gamma_w)d_{50}} = \begin{matrix} 0.131D_*^{-0.55} & (fine\ sand) \\ 0.0685D_*^{-0.27} & (medium\ sand) \\ 0.0173D_*^{0.19} & (coarse\ sand) \end{matrix} \tag{4.10}$$

where non-dimensional particle size, D_* is obtained as,

$$D_* = d_{50}\left[\frac{\gamma_s - \gamma}{\gamma\nu^2}\right]^{\frac{1}{3}} \tag{4.11}$$

However, sediment entrainment model of Engelund and Hansen (1967) is modified by multiplying equation (4.6) with a sediment erosion coefficient, c_e representing subaerial dune sediment transport due to overwash and permeability of sediment grain.

Sediment transport model proposed by Cao (1999) is applied to evaluate the performance of reproducing the laboratory study in numerical simulation. This model is also used by Cao et al. (2004) to compute dam-break wave induced sediment transport. The model is based on Shields parameter. It can be written as,

$$E = \frac{160}{R^{0.8}} \frac{(1-p)}{\Psi_c} \frac{(\Psi - \Psi_c)hU_\infty}{h} \tag{4.12}$$

where $R = \sqrt{\Delta g d}\frac{d}{\nu}$, U_∞= free surface velocity (=*7u/6*, used by Cao et al. (1999)), Ψ = Shields parameter, Ψ_c = critical Shields parameter for initiation of sediment movement.

The deposition flux, *D* is evaluated with a general expression,

$$D = w_o c_a = \alpha w_o c \tag{4.13}$$

where w_o = fall velocity of sediment; c_a = local near bed sediment concentration in volume which is assumed to be proportional to the depth-averaged volumetric sediment concentration following Cao et al. (2004) and Wu and Wang (2007); $c_a = \alpha c$; α = ratio of the near bed and depth-averaged sediment concentration or non-equilibrium adaptation coefficient; c = depth-averaged volumetric sediment concentration. For α, different values are used by many researchers. In the present study, α = 2 was selected in Shimozono et al. (2007) following Cao et al. (2004).

However, conventional approximations are required to recast the erosion and deposition formulations to be applied in overland flow over sand dune. First, a deposition coefficient (c_d) is introduced to account for high deposition observed during experiment and determined empirically. It is evident from the observation and simulation that this coefficient depends upon sediment size, wet/dry condition of sediment and nature of overwash. Hence, equation (4.13) becomes,

$$D = c_d \alpha c w_o \tag{4.14}$$

Second, there are different methods to determine adaptation coefficient (α) as proposed by Lin (1984), Armanio and di Silvio (1986) and Zhuo and Lin (1998). Significant differences among these formulas are reported by Wu and Wang (2007). Here α is set as,

$$\alpha = min\left[\alpha_0, \frac{(1-p)}{c}\right] \tag{4.15}$$

where α_o is a coefficient, specified empirically. Cao et al. (2004) and Wu and Wang (2007) has taken a value of 2 in their study of dam-break flow over erodible sediment bed. Since, sediment deposition nature and character in the present study is quite

different than above mentioned studies, α_o is determined empirically and used in computation. It is evident from the observation and simulation that α_o depends upon sediment size, wet/dry condition of sediment and nature of overwash. Equation (4.15) ensures that near-bed sediment concentration (c_a) must not be greater than bed material concentration (*1-p*).

4.5 Numerical scheme

Governing equations are solved by a finite difference scheme with shock capturing property. TVD-MacCormack (Vincent and Bonneton, 2001) scheme is employed in the study. The scheme is flux limited version of MacCormack scheme which has been widely used for hyperbolic equations. Non-physical oscillation associated with the classical MacCormack scheme is suppressed by correcting the flux to satisfy TVD condition (Harten 1983).

The reason for choosing this scheme is its superiority to keep the integration of source term in second order not like in other schemes. To describe the numerical scheme, governing equations are rewritten as follows:

$$\frac{\partial \boldsymbol{Q}}{\partial t} + \frac{\partial \boldsymbol{F}}{\partial x} = \boldsymbol{S} \tag{4.16}$$

$$\boldsymbol{Q} = \begin{bmatrix} h \\ hu \\ hc \end{bmatrix} \tag{4.17}$$

$$\boldsymbol{F} = \begin{bmatrix} hu \\ hu^2 + \frac{1}{2}gh^2 \\ huc \end{bmatrix} \tag{4.18}$$

$$\boldsymbol{S} = \begin{bmatrix} \big((D-E)/(1-p)\big) \\ -gh\left(\frac{\partial z}{\partial x}\right) \\ E - D \end{bmatrix} \tag{4.19}$$

The present numerical integration process can be divided into three steps.

(i) Predictor step:

$$Q_i^p = Q_i^n - \frac{\Delta t}{\Delta x}(F_{i+1}^n - F_i^n) + \Delta t S_i^n \tag{4.20}$$

$$z_i^p = z_i^n + \Delta t \frac{D_i^n - E_i^n}{1-p} \tag{4.21}$$

(ii) Corrector step:

$$Q_i^c = Q_i^n - \frac{\Delta t}{\Delta x}\left(F_i^p - F_{i-1}^p\right) + \Delta t S_i^p \tag{4.22}$$

$$z_i^c = z_i^n + \Delta t \frac{D_i^p - E_i^p}{1-p} \tag{4.23}$$

(iii) TVD step:

$$Q_i^{n+1} = \frac{1}{2}\left(Q_i^p + Q_i^c\right) - \frac{\Delta t}{\Delta x}\left(F^T_{i+\frac{1}{2}} - F^T_{i-\frac{1}{2}}\right) \tag{4.24}$$

$$z_i^{n+1} = \frac{1}{2}\left(z_i^p + z_i^c\right) \tag{4.25}$$

Where F^T is correction flux.. The predictor and the corrector steps are fully explicit; while the TVD step is implicit. Because the integration of the dispersion term, which contains time derivatives of the variables, is included. If the bed level *z* and water depth *h* at new time step are approximated as solutions of the predictor and corrector step, (4.24) becomes tri-diagonal about velocity *u* so that Thomas algorithm can be applied.

The correction flux F^T is calculated by the conservative flux of the first order upwind scheme and second order Lax-Wendroff scheme as follows:

$$F^T_{i+\frac{1}{2}} = (1-\Phi)\left(F^{UP}_{i+\frac{1}{2}} - F^{LW}_{i+\frac{1}{2}}\right) \tag{4.26}$$

where Φ is the flux limiter function which ensures the scheme is total variation diminishing (TVD). As solution become discontinuous, Φ approaches to zero so that

numerical dissipation associated with the first order upwind scheme is introduced to eliminate spurious oscillation. Minmod and Superbee flux limiter (Toro 2001) are applied for flux correction which respectively gives maximum and minimum numerical dissipation in the extent of TVD region (Sweby 1985). F^T can be evaluated by using Roe's approximate Riemann solver (Vincent et al. 2001).

CHAPTER FIVE
RESULT AND DISCUSSION

5.1 Introduction

Experimental observation, sediment property and incident bore parameter are analyzed to have in depth understanding of dune erosion phenomena while overwash takes place due to tsunami or surge like waves. This chapter starts with the experimental results obtained in the laboratory along with their analysis; specially focusing initially wet and dry condition of the dune. The influence of sand grain size in sediment transport process is analyzed. Finally, results and discussion of numerical modeling are presented.

5.2 Mechanism of Sediment Transport for Dry and Wet Condition

While water flows over dune, sand particle will experience pressure force (F_p, with added hydrodynamic mass), lift force (F_L) and drag force (F_D). Forces involved in overwash mechanism are schematically shown in Figure 5.1. For small particles (d_{50}~0.20 mm), the drag force tends to dominate the pressure force (Nielsen, 1992).

For wet dune (WD) condition, considering only the first wave impact on the fore dune and no further movement of water over dune crest, it can be said that due to the first wave impact, infiltration (I_{in}) through pore space will tend to increase permeability (K) as well as exfiltration (I_{ex}) on back dune side. Consequently this exfiltration will try to mobilize sediment. But this process is not the same for dry condition. In dry dune, firstly the grains absorbs water, then the voids are filled with water and then these pores will be connected to result exfiltration. This will take relatively long time when compared with wet sand situation.

In wet sand dune, voids are filled with water and these pores are interconnected. Pore water pressure (P_w) and buoyancy force (F_b) will be developed. It is natural that buoyancy is higher in WD than dry dune (DD). Angle of repose is controlled by the frictional contact between the grains. Increase of water content more than a critical amount reduces the angle of repose (Webster 1919). When the saturated sand comes

in contact of moving/flowing water, mobility of sand grain from its initial location on dune surface increases. Exfiltration for wet sand should be higher as it has more water to come out contributing to mobility of wet sand. This is evident from Figures 5.2 and 5.3 showing more sand transport in initially wet sand condition.

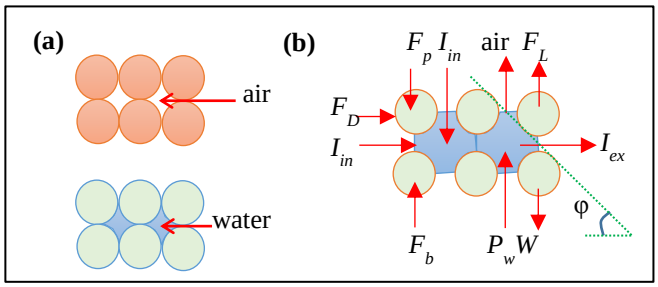

Figure 5.1 Schematic diagram showing (a) initially dry (top) and wet (bottom) dune; (b) the mechanism/ forces involved in overwash

On the other hand, in dry dune condition, the pores are filled with air only. When initially dry sand comes in contact of moving water, the angle of repose (φ) exhibit a high value because surface tension between the water and the grains tends to hold the grains in place and contributes to dune stability. Moreover buoyancy is less for initially dry sand. Infiltration (I_{in}) through the dune surface is higher but exfiltration is low for dry sand and it increases grain stability. This behavior can be observed from Figure 5.2 (data for this figure is presented in Appendix-A) and Figure 5.3 which explains the spatial distribution of overwashed sediment transport for CS. For this condition, less sediment is transported in initially dry dune. Figure 5.4 shows that during experiment air bubble comes out from the overflowing dry dune and left significant air escaping marks on the surface of the dune.

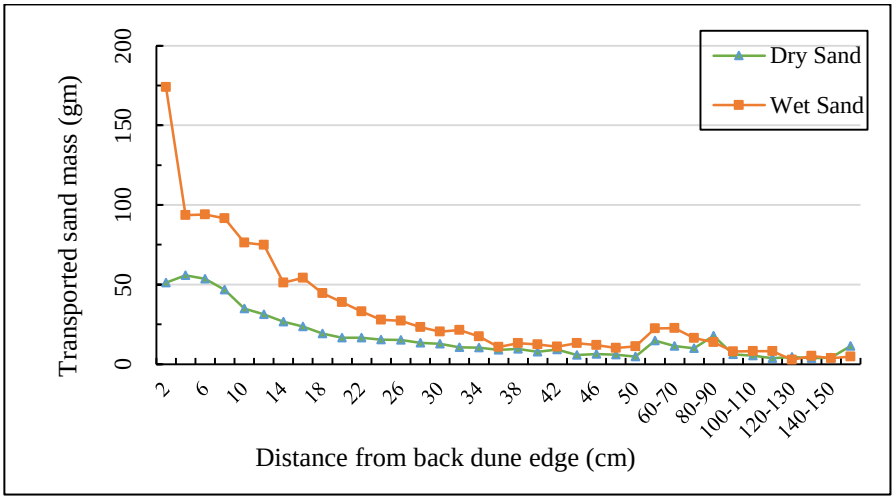

Figure 5.2 Distribution of sand mass transported from back dune edge (R4)

Figure 5.3 Higher sediment transport in wet sand dune than dry sand dune (R4)

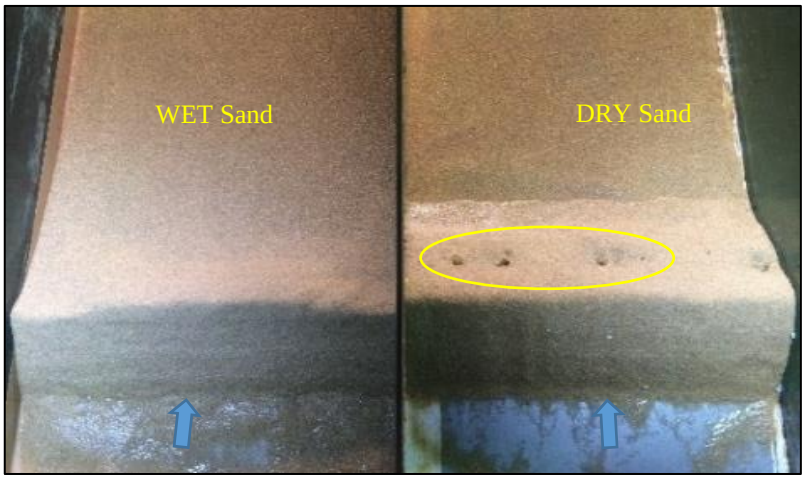

Figure 5.4 Air escaping marks left in DD (R5)

However, Figure 5.5 clearly depicts that more sediment was transported in initially dry dune for dune composed of fine sediment grains. This indicates that, there are few mechanisms responsible for dissimilar sediment transport due to dune overwash.

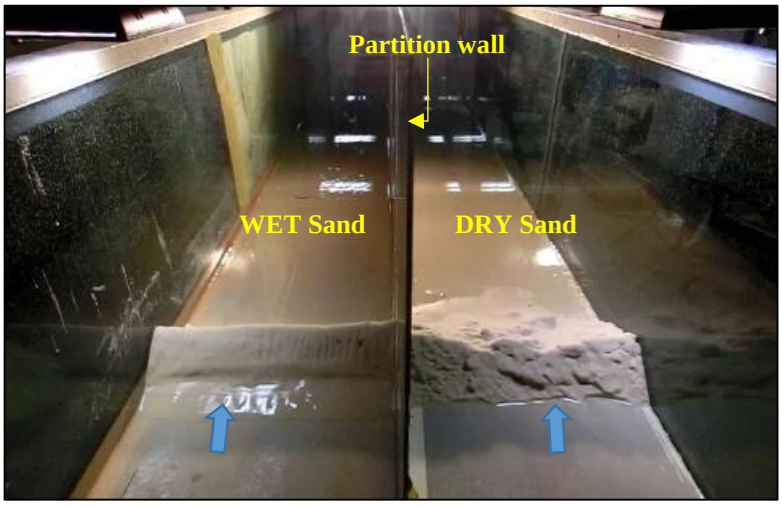

Figure 5.5 Higher sediment transported from dry dune for fine sediment (R6)

The above figures (Figure 5.3 to 5.5) represent experiments conducted on steep bed slope for B2 (ΔH=8 cm) bore size. This means, same initial hydrodynamic condition, initially same degree of saturation in wet dune as well as same dune size and shape for all the experiments.

Table 5.1 Summary of onshore transported sediment mass

Slope Type	Run Number	Sand Type	ΔH (cm)	Transported Dry Sand (gm)	Transported Wet Sand (gm)
Steep	R1	Coarse Sand	6	196	282
	R4		8	605	1173
	R7		10	1896	1859
Mild	R11		8	731	1286
	R14		10	2253	1958
Steep	R2	Medium Sand	6	150	113
	R5		8	437	908
	R8		10	1726	1780
Mild	R12		8	1738	1441
	R15		10	2089	2204
Steep	R3	Fine Sand	6	100	35
	R6		8	582	214
	R9		10	1731	283
Mild	R13		8	693	179
	R16		10	1599	970

5.3 Comparison and Discussion of Sediment Transport

The process of collection and measurement of transported sediment mass has been described in section 3.3. Table 5.1 gives the summary of dune sediment transport quantitatively for all the experiments. The influence of bed slope, wet/dry condition and grain size on sediment transport are explained in this section.

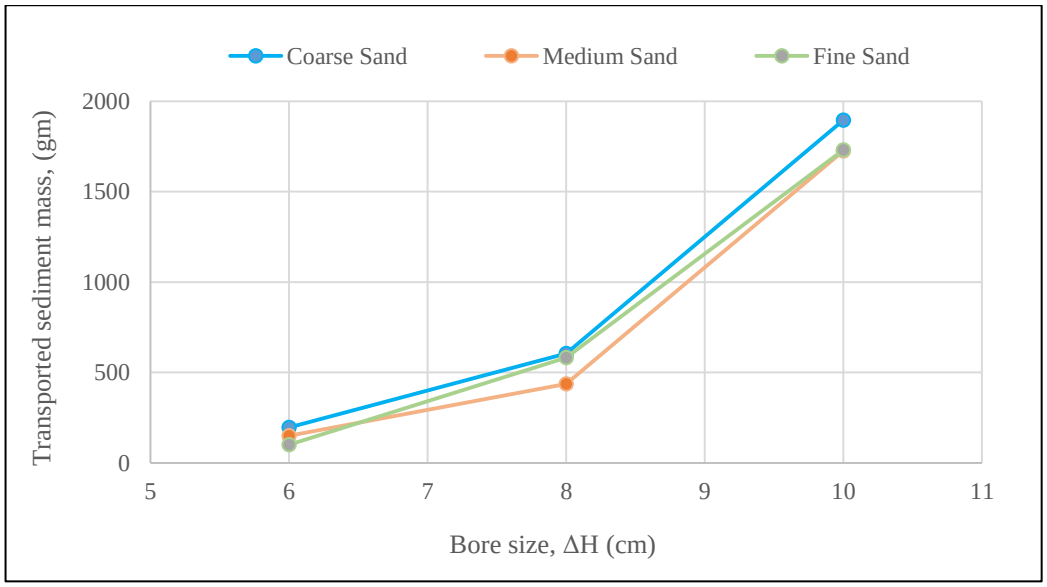

Figure 5.6 Comparison of onshore sediment transport for different bore and sands (initially dry) on **steep slope**

Figure 5.6 shows as the bore size increases from low to high, sediment transport also increases for all types of sand. When attention is paid from bore B2 (8 cm) to B3 (10 cm), it reveals that sediment transport increases faster at high bore. But fine sand B2 case results sediment transport more that medium sand and close to coarse sand. Analysis of the recorded video during this experiments shows that dune surface (group of sand grain) failure occurred resulting relatively more sediment transport. Less drag force acting on small grain, low permeability and low intergranular friction may be the reason to exhibit such failure process. Since the permeability of fine sand is very low, initial water mass on top of dune cannot penetrate the surface. Therefore, momentum of the water mass is expected to be greater at that location than high permeable sand. Relatively small inter-granular friction results less resistance against downward movement of dune surface sand mass.

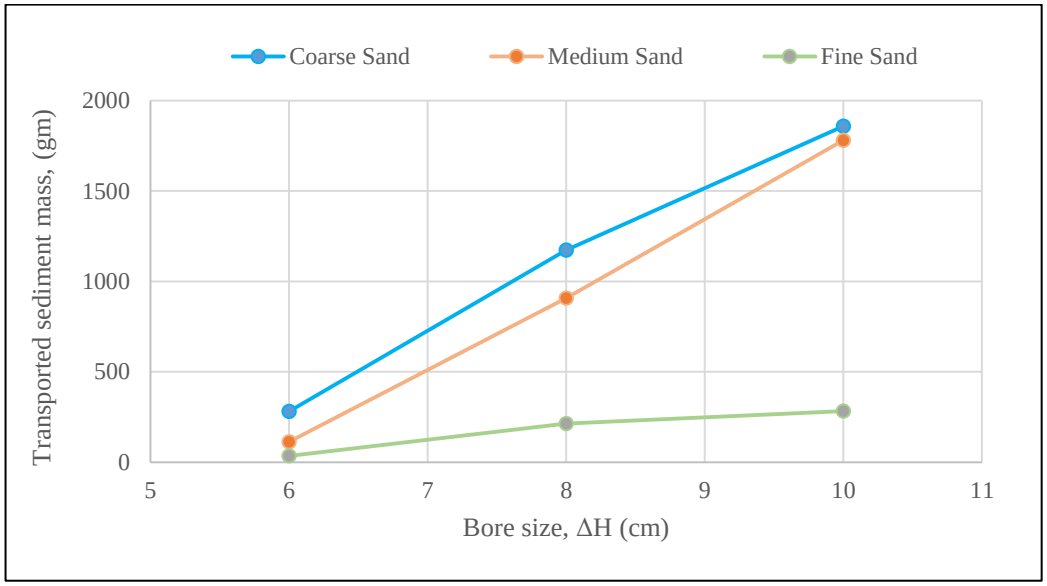

Figure 5.7 Comparison of onshore sediment transport for different bore and sands (initially wet) on **steep slope**

Figure 5.7 shows very less sediment transport for fine sand. This is due to the presence of suction as well as low permeability. It is observed after the experiment that the remained dune section at the test location is relatively harder when compared with dunes of medium and coarse sand. However, coarse sand shows higher sediment transport as the same is seen for dry dune case (Figure 5.6).

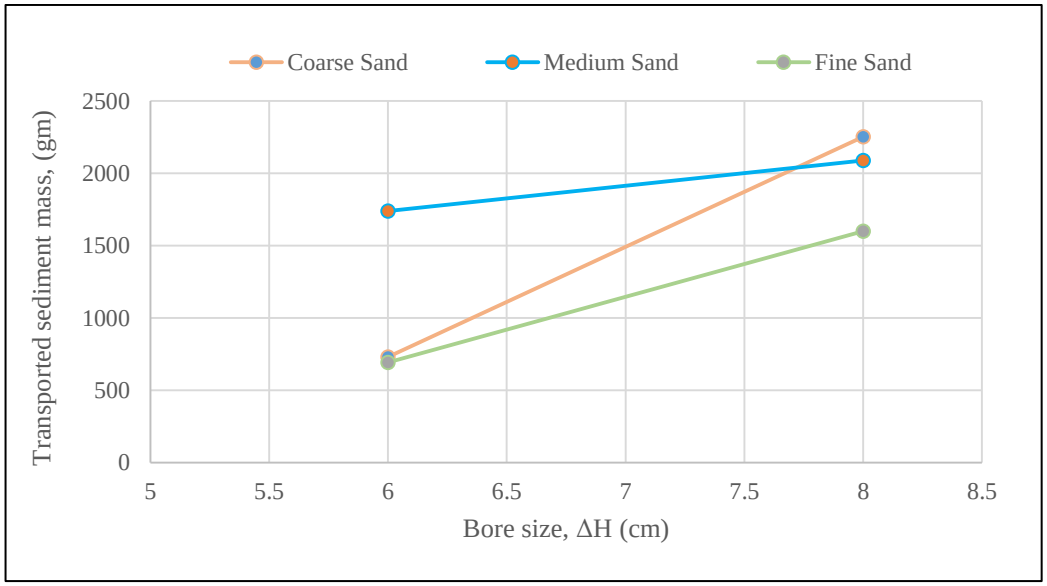

Figure 5.8 Comparison of onshore sediment transport for different bore and sands (initially dry) on **mild slope**

Figure 5.8 shows high sediment transport rate for medium sand from bore B2 to bore B3. Fine sand has minimum sediment transport as explained earlier. When compared with steep slope case (Figure 5.6) it reveals that higher sediment transport is seen for mild slope case. This is due to the higher water overtopping of dune in mild slope than in steep slope.

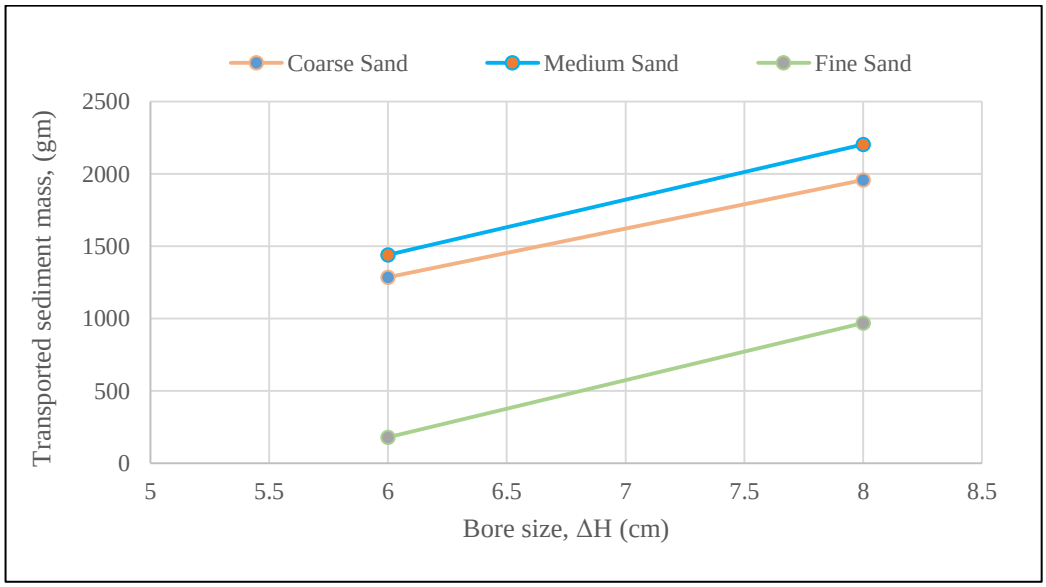

Figure 5.9 Comparison of onshore sediment transport for different bore and sands (initially wet) on **mild slope**

However, Figure 5.9 shows medium sand has higher sediment transport and also a similar rate of increase in sediment transport volume for all sands.

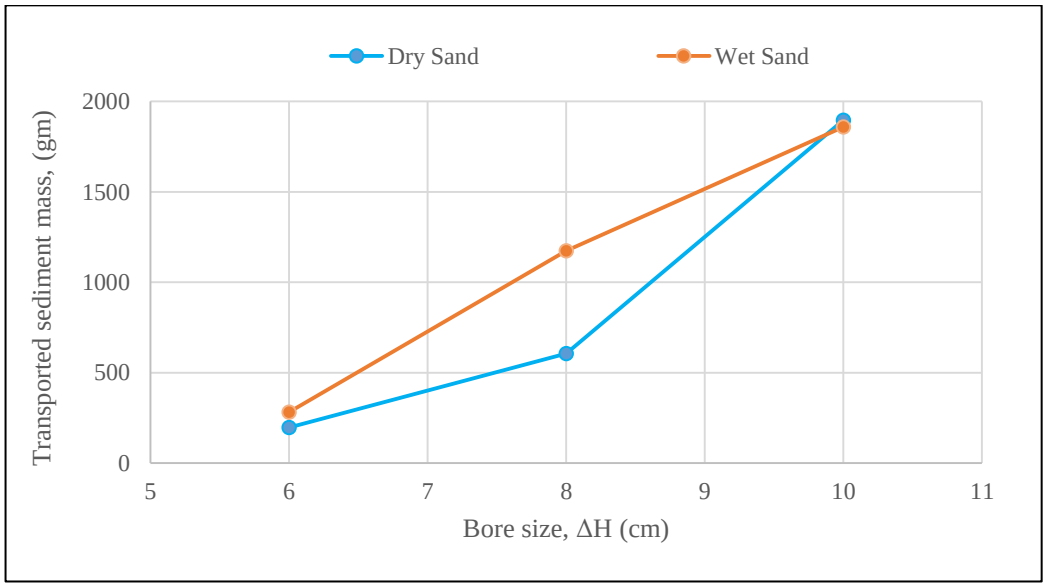

Figure 5.10 Initially dry and wet **coarse** sediment transport for different bore on **steep slope**

Figure 5.10 shows medium bore size has higher sediment transport difference for dry and wet dune. Because at low bore, dune overtopping water is less and the difference in dry and wet is not significant. In other words, this is the beginning or at initial stage of sediment transport process/mechanism for dry and wet case. However, for high bore size, dune overtopping water is very high resulting inundation overwash and therefore sediment transport takes place for long time which diminishes the difference between dune of wet and dry sand.

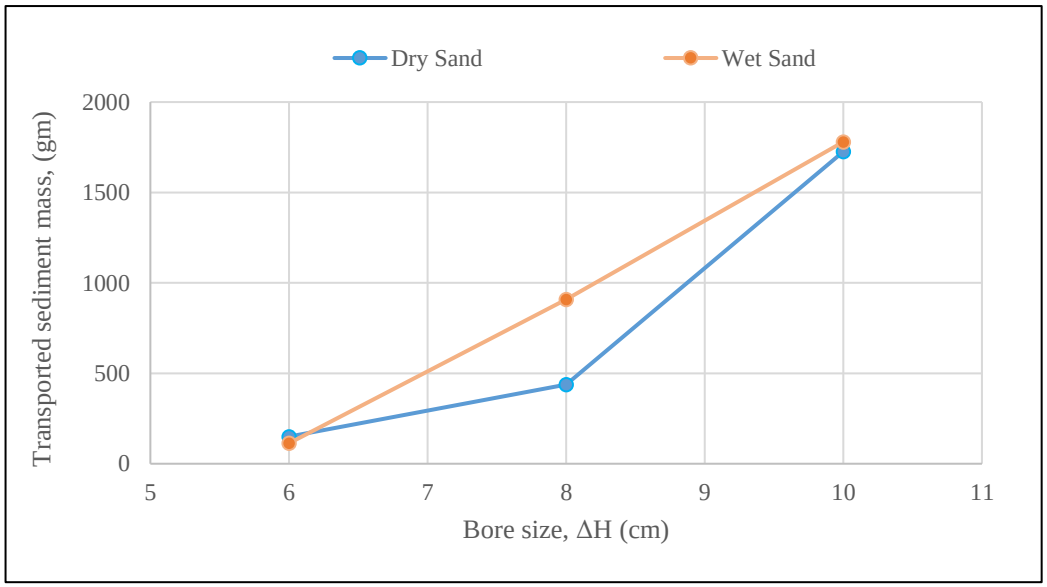

Figure 5.11 Initially dry and wet **medium** sediment transport for different bore on **steep slope**

Figure 5.11 shows a linear increasing rate for wet sand. Here the difference between the wet and dry dune is prominent in medium bore size as explained earlier.

However, Figure 5.12 shows that maximum difference in wet and dry sand dune is seen in high bore for fine sand. This is due to the suction and low permeability. When erosion occurs at the crest of dry dune, it allows more water to overflow and more sediment to transport from dune. But for wet dune, this crest erosion is less due to suction and low permeability. Consequently, overflow of water is less resulting low sediment transport. It is seen that for wet sand, sediment transport is almost same for bore B2 and B3.

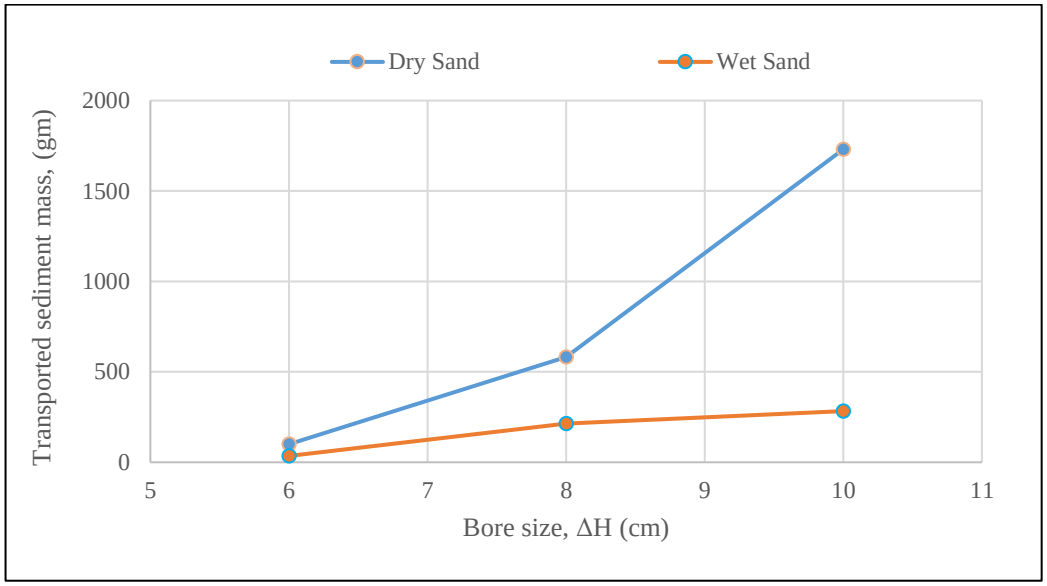

Figure 5.12 Initially dry and wet **fine** sediment transport for different bore on **steep slope**

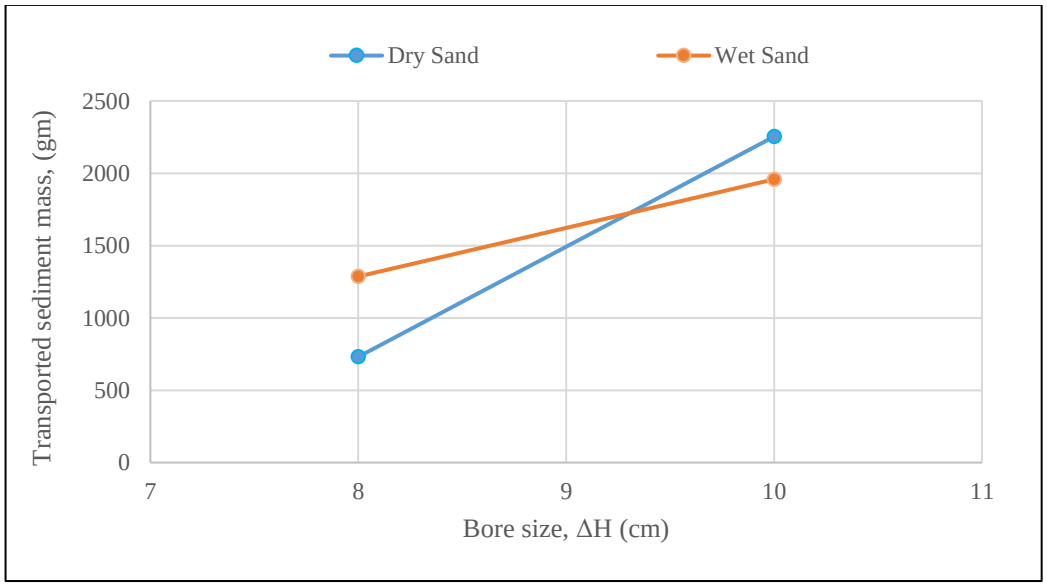

Figure 5.13 Initially dry and wet **coarse** sediment transport for different bore on **mild slope**

Figure 5.13 shows less sediment transport in dry sand for medium bore but the opposite for high bore. Therefore, it appears that permeability and buoyancy is important at the initial stage of dune overwash. At a certain bore size sediment transport become same for dry and wet dune. It is seen in Figure 5.31 that for bore B3, wet dune has relatively higher crest elevation than dry one. Figure 5.14 shows the opposite behavior than in Figure 5.13. Therefore, it appears that the pore distribution and grain size is influencing sediment transport mechanism for coarse and medium sand.

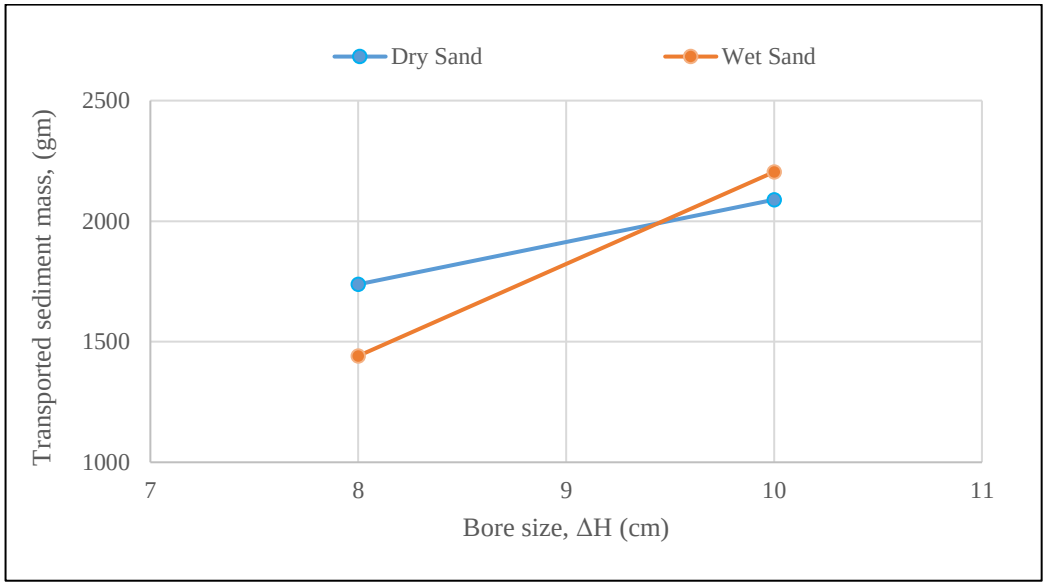

Figure 5.14 Initially dry and wet **medium** sediment transport for different bore on **mild slope**

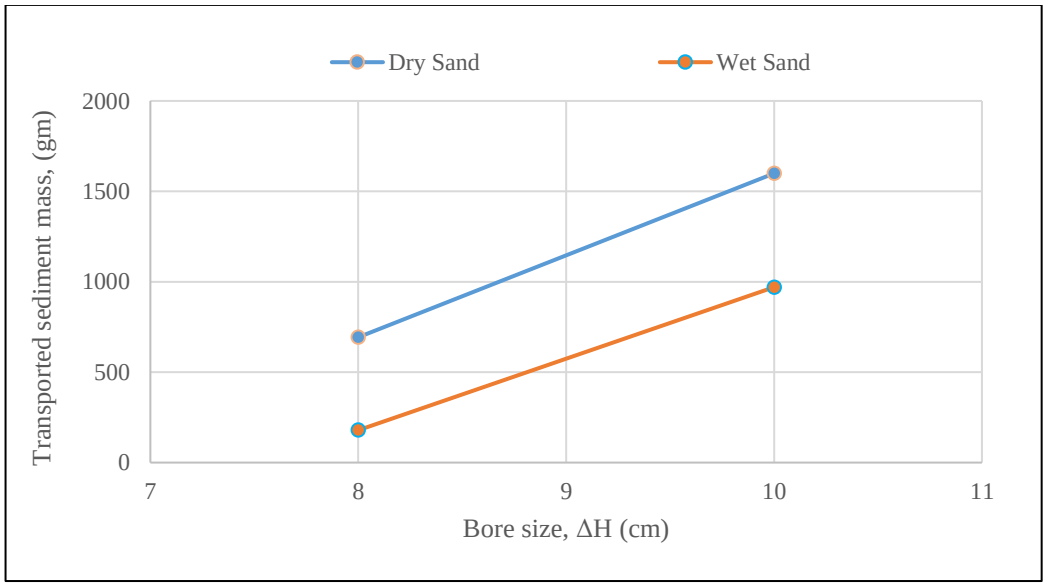

Figure 5.15 Initially dry and wet **fine** sediment transport for different bore on **mild slope**

Figure 5.15 shows that wet fine sand has the minimum sediment transport than dry sand.

5.3.1 Initially Wet and Dry Dune

In WD condition, FS has minimum sediment transport than for MS or CS. This is not consistent with the Shields parameter. Upon receiving water, dry sand (especially fine sand) gains cohesive force. High attraction/suction among grains and very low

permeability may be the reason for less sediment transport in wet fine sand. The cohesion (or apparent cohesion) between individual grains dominates the physical properties of granulates (Herminghaus, 2005). Therefore, dry and wet sand does not behave in a similar way during overwash. Angle of repose appeared to play an important role to mobilize MS and CS as they have high permeability but stabilizes FS as it has very low permeability. The effect of in/exfiltration is not significant in FS. However, DD condition for high ΔH, the Shields parameter can explain the phenomena as the sand remains in submerged condition for relatively long time and the effect of in/exfiltration and angle of repose diminishes. Important to mention that for the same reason, the difference of sediment transport between DD and WD of MS and CS becomes small in high ΔH (Figure 5.6).

5.3.2 Fine Sand

FS has significantly higher sediment transport for DD condition than WD condition for all the cases. Reasons may be due to the small pore spaces which reduce the permeability; and high porosity that maintain strong inter-granular attraction or suction in wet condition. Figure 5.16 shows more sand transport in DD. Figure 5.17 shows air escaping marks left on the surface of DD revealing the connectivity among the pores in initially dry dune. Therefore, is appears that mechanism of air escaping from dune may be a significant feature.

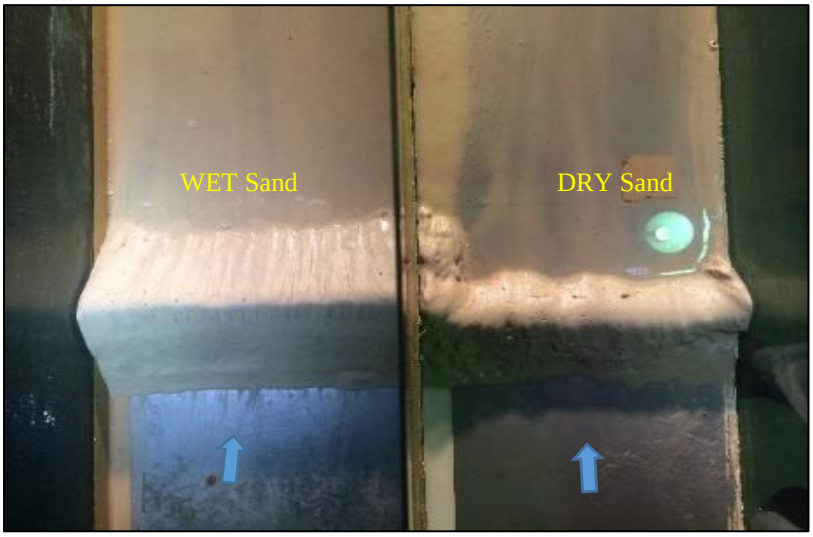

Figure 5.16 Higher sediment is transported in DD (R9)

Figure 5.17 Rough surface in DD leaving air escape marks (R13)

5.3.3 Coarse Sand

For CS, on the other hand, more sediment is transported in WD condition as shown previously in Figure 5.4, showing the cross-shore distribution of transported sand. CS has large pore i.e. lower porosity and high permeability (K) appeared to increase in/exfiltration and then mobilize the sand grains on the back dune face. This can be explained consistently with the change of the angle of repose (φ) dependent on the presence of air in the void space. Because in WD, the pore space is filled mainly with water, making a continuous flow line through the dune which helps to move water particle. This is not the same for DD as pore space is filled with air. In DD, the air escaping marks left on the back dune surface is shown in Figure 5.18. But no air escaping mark is left for high ΔH (Figure 5.19). CS has relatively higher sediment transport than MS for experimental runs in steep slope. Due to relatively low permeability and higher porosity, the transport in MS is less than that of CS. Therefore, CS appeared to be more sensitive to the in/exfiltration effect in transport mechanism.

Figure 5.18 Air in void is significant for low ΔH. Many air escaping marks left on back dune (R2)

Figure 5.19 Almost similar appearance in WD and DD for high ΔH. No air escaping mark left (R14)

5.3.4 Medium Sand

MS has relatively higher sediment transport for WD condition, especially for high ΔH values. However, for low ΔH values; the sediment transport is opposite. This may be due to the effect of porosity and sensitivity to time scale. For high ΔH values the effect of the angle of repose (φ) is negligible and the difference between mass of sand transport in DD and WD becomes smaller.

5.3.5 Effect of Bed Slope

It reveals that FS, MS and CS has higher sediment transport in mild slope than steep slope in all the cases. Mild slope experiments give longer overwash duration than steep slope cases resulting higher time ratio. Therefore, bed slope has significant sensitivity to the time ratio, R_T; longer the time ratio, higher the transport.

5.4 Deformed Dune Angle

A new parameter, Deformed Dune Angle (DDA) is introduced to investigate the influence of angle of repose for different sand. DDA (φ") is the angle formed with the horizontal by connecting two data points on the overwashed dune. To measure this angle, the profile plotting of the initial and final dune is used. Intersecting point 1 (Figure 5.20) is the crest of deformed (overwashed) dune and intersecting point 2 (Figure 5.20) is the intersection of initial dune surface and deformed dune surface on the landward side as explained in Figure 5.20.

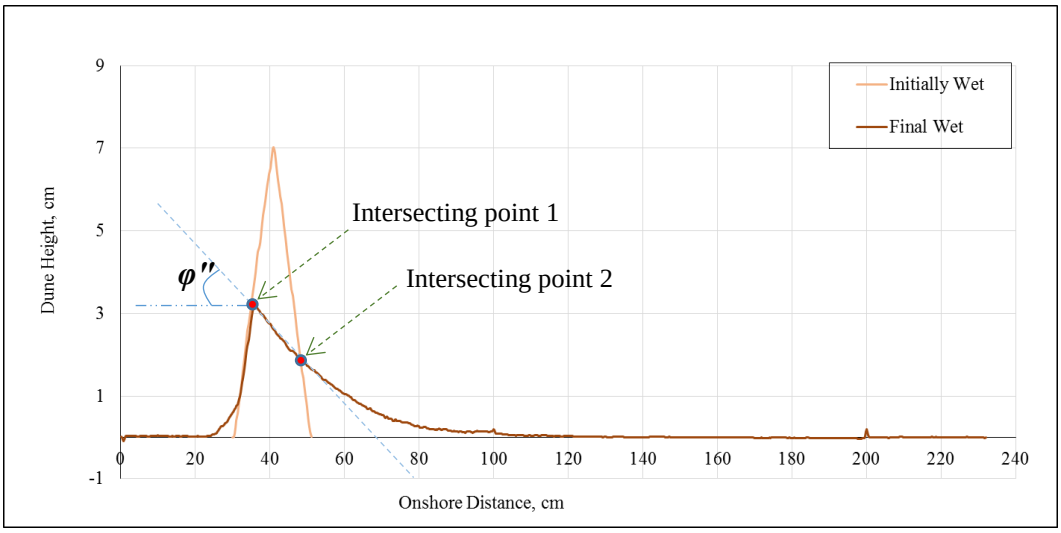

Figure 5.20 Definition sketch for DDA

Following the process as explained above, estimation of DDA for different experiments are done. These values are compared with the angle of repose of the respective sediment sizes. Figure 5.21 shows the role of angle of repose in mild slope experiments for bore sizes of B2 ($\Delta H2$=8 cm) and B3 ($\Delta H3$=10 cm). It is evident from this figure that coarse sand is more sensitive to dry and wet conditions for ΔH2 than medium sand as it exhibits greater difference between DDA. However, for ΔH3 the difference of DDA between wet and dry dune is not significant.

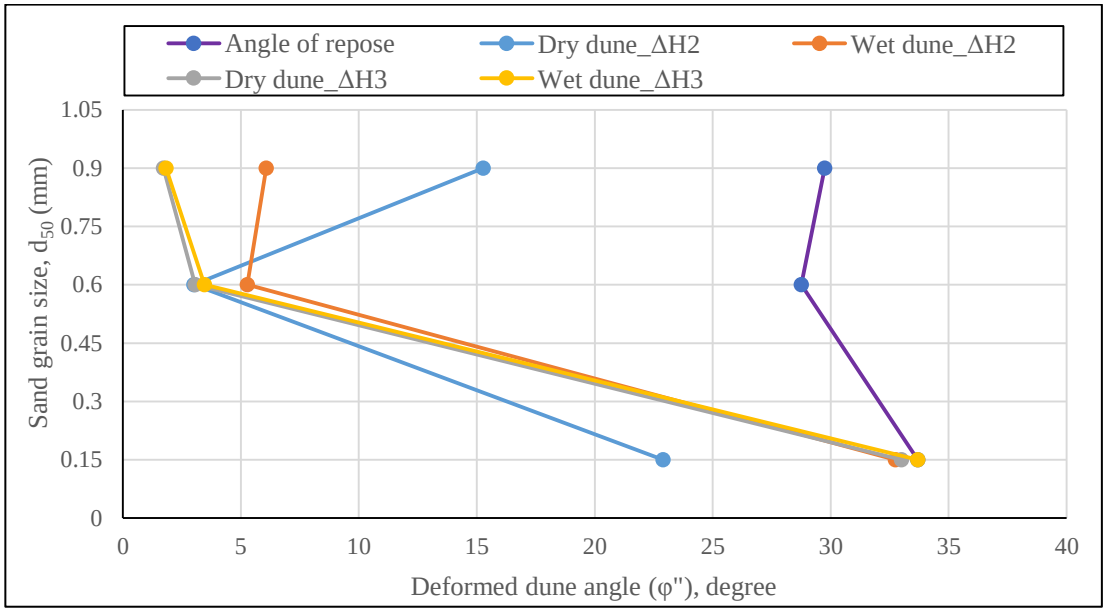

Figure 5.21 Comparison of DDA with angle of repose

The side slope angle of the initial dune is 35^0 for all experiments. Fine sand retains almost the initial profile especially in wet dune cases for ΔH2 and ΔH3. Wet fine sand shows increased value of repose angle due to cohesive force between grains (Mitarai and Nori, 2006). Hence for wet fine sand φ'' is close to φ. It is expected and observed from the final dune profile that fine sand will tend to retain deformed shape close to its repose angle as well as initial slope. The reason of this capacity to retain its initial slope and repose angle may be due to low permeability and suction force developed in wet condition. But coarse and medium sand has high permeability and almost no suction force among the grains which results a flat shape of the final dune profile giving a low value of DDA as can be seen from Figure 5.21.

5.5 Waterfront Spreading Time (T_{ws}) through Dry Dune

The estimation process of waterfront spreading time is described in section 3.4.7. This analysis is performed for bore B2 and B3 in steep slope and mild slope cases for dry dune only. Overwash occurring in B3 case takes relatively long time to recede which makes T_{ws} shorter.

Figure 5.22 shows six experiments conducted in mild slope. It is seen from the figure that FS needs longer T_{ws} in B2 than in B3 resembling its low permeability.

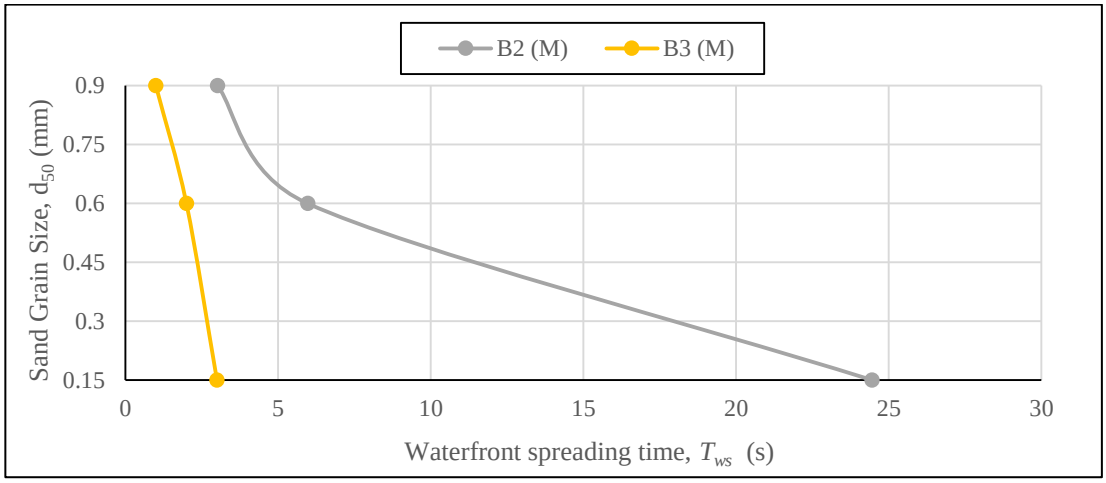

Figure 5.22 Waterfront spreading time in mild slope experiments

Figure 5.23 shows six experiments conducted in steep slope. It is seen from the figure that FS needs very long T_{ws} in B2 than in B3. However, CS and MS requires a close T_{ws} in B2 and B3. This is due to the very fast water overflowing the dune surface in steep slope. It is interesting to note that in B3, CS and MS takes same T_{ws} meaning that their sediment transport nature may be very close to each other.

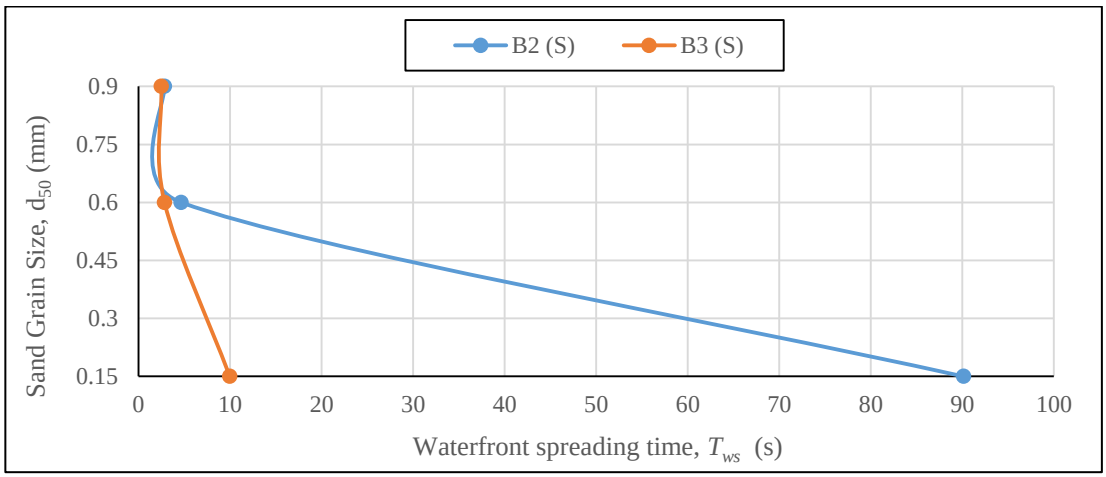

Figure 5.23 Waterfront spreading time in mild slope experiments

Figure 5.24 shows that dune overwashed in mild bed slope becomes completely wet earlier than steep bed slope. This is due to relatively high water depth over back dune slope in mild slope case resulting a quicker wetting. However, this difference is not so significant for B2 case other than FS as shown in Figure 5.25.

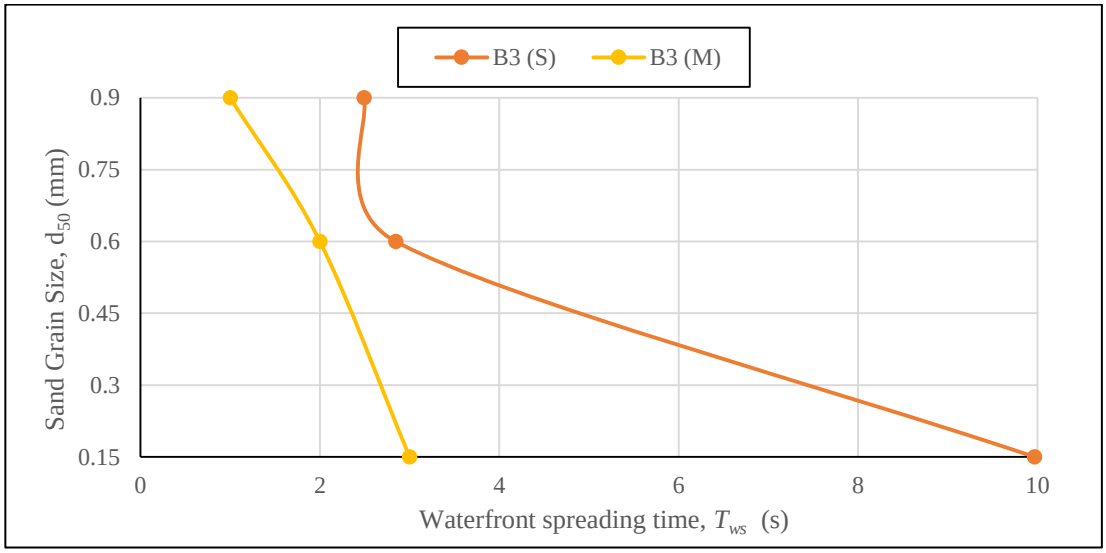

Figure 5.24 Comparison of T_{ws} in steep and mild slope experiments for B3

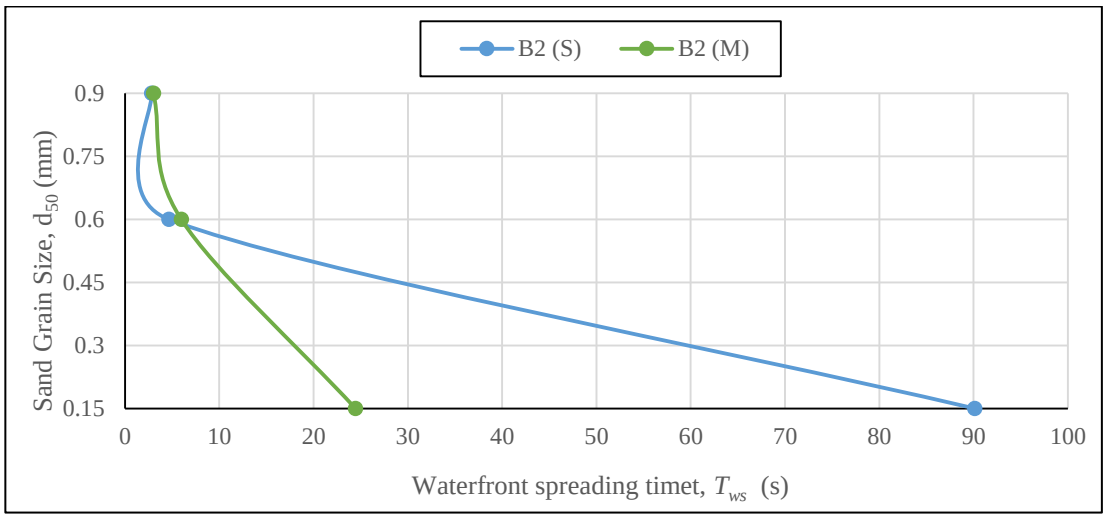

Figure 5.25 Comparison of T_{ws} in steep and mild slope experiments for B2

An overall view of T_{ws} for all the experiments is shown in Figure 5.26. It is evident from Figure 5.27 that time scale for infiltration (T_i) is very high than the time required for the entire dune section to become wet (T_{ws}) for all types of sands (specially FS). This may be due to:

i) The dynamic movement of flowing water: when the wave runup the fore dune face, the horizontal movement of water particle through the pore spaces rapidly increase.

ii) When water rundown the back dune slope, vertical movement of water particle through the pore spaces rapidly increase.

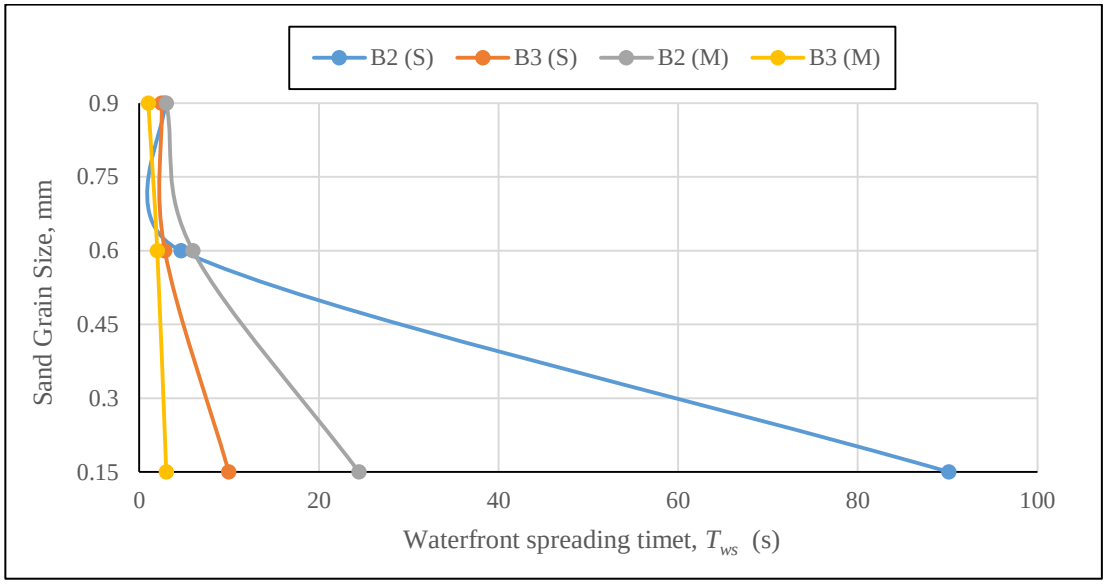

Figure 5.26 Comparison of T_{ws} and T_i for all experiments

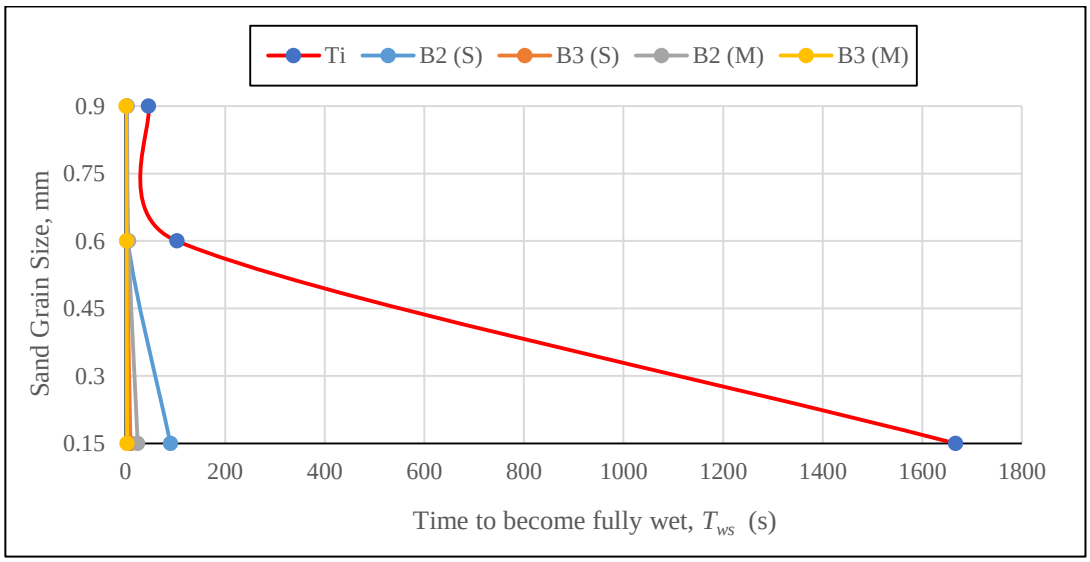

Figure 5.27 Comparison of T_{ws} and T_i for all experiments

5.6 Dune Profile

Bed profile with dune is recorded before and after experimental run for mild slope case. Profile gives an idea of sediment transport nature, especially the spatial extent of dune sediment movement can be clearly observed. It also helps to assess the performance of dune in relation to serve as a coastal protection structure. The magnitude of natural calamity like tsunami or surge causes the dune to transfer sediment volume in landward side. Therefore, an assessment of probable accumulation of sand can be possible from this post-overwash profile.

The following part shows profile of an experiment where both DD and WD are present with their initial and final state.

Figure 5.28 shows in WD crest is lowered more and it shifts a bit in seaward side. However the distance of sediment movement is around 2.30 m for DD and WD.

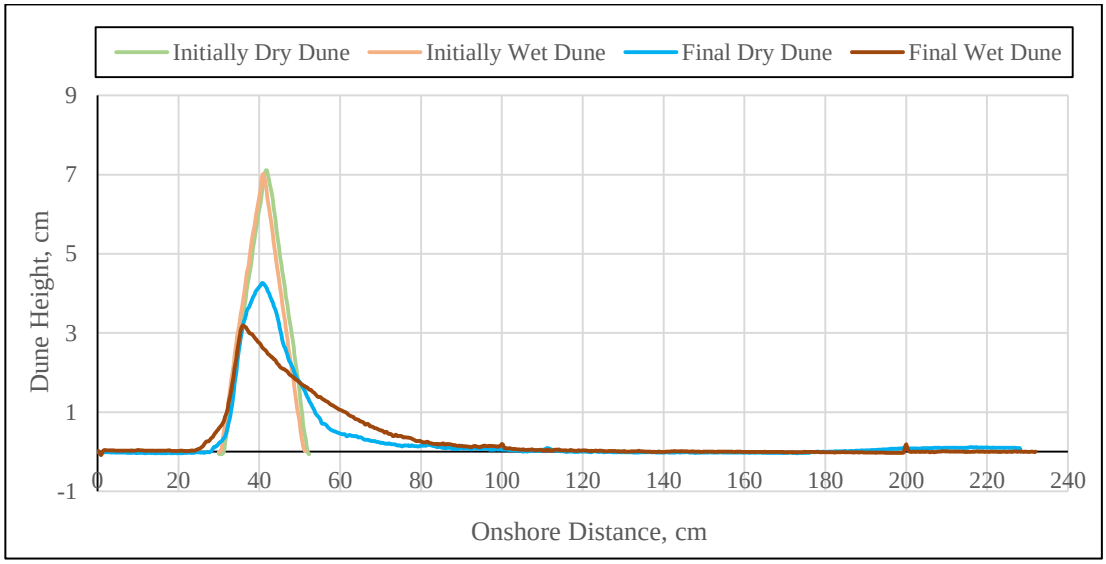

Figure 5.28 Profiles of coarse sand dune for ΔH2= 8 cm

Figure 5.29 shows in DD crest is lowered slightly more. Both crest shifts a bit in seaward side. The distance of sediment movement is more for DD than WD. The distance is less and lowering of crest more than CS (Figure 5.28). The reason could be initial resistance provided by the CS which resulted a relatively steep surface slope in back dune side causing higher flow velocity that takes sediment grain a longer distance than MS.

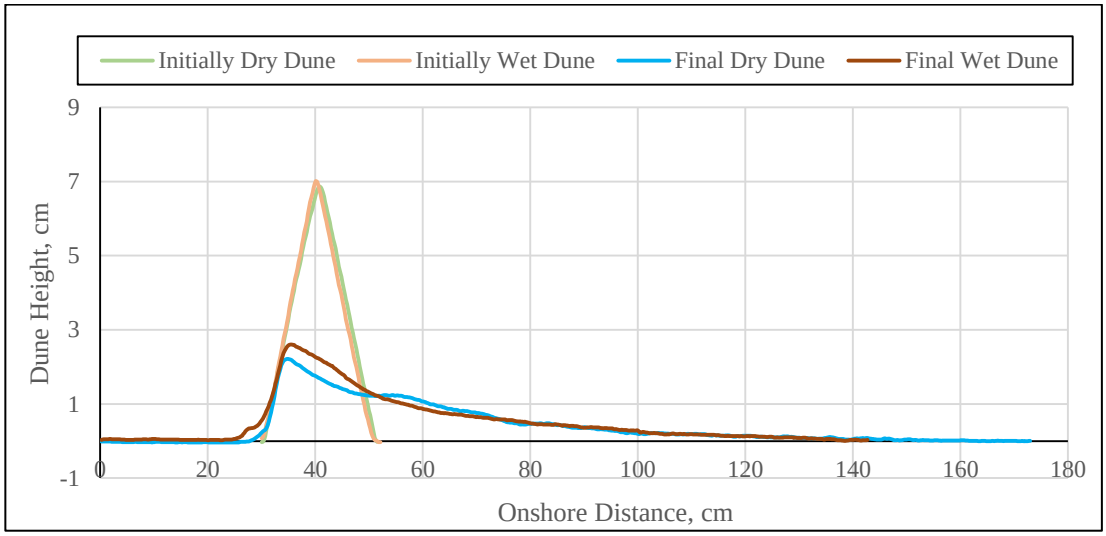

Figure 5.29 Profiles of medium sand dune for ΔH2= 8 cm

Figure 5.30 shows almost no change in dune shape for wet condition of FS. DD crest is lowered more and sediment moved longer distance than WD since wet FS grains have strong suction force that helps it to exhibit high resistance against erosion. It is clear that crest lowering in FS is minimum than CS (Figure 5.28) and MS (Figure 5.29).

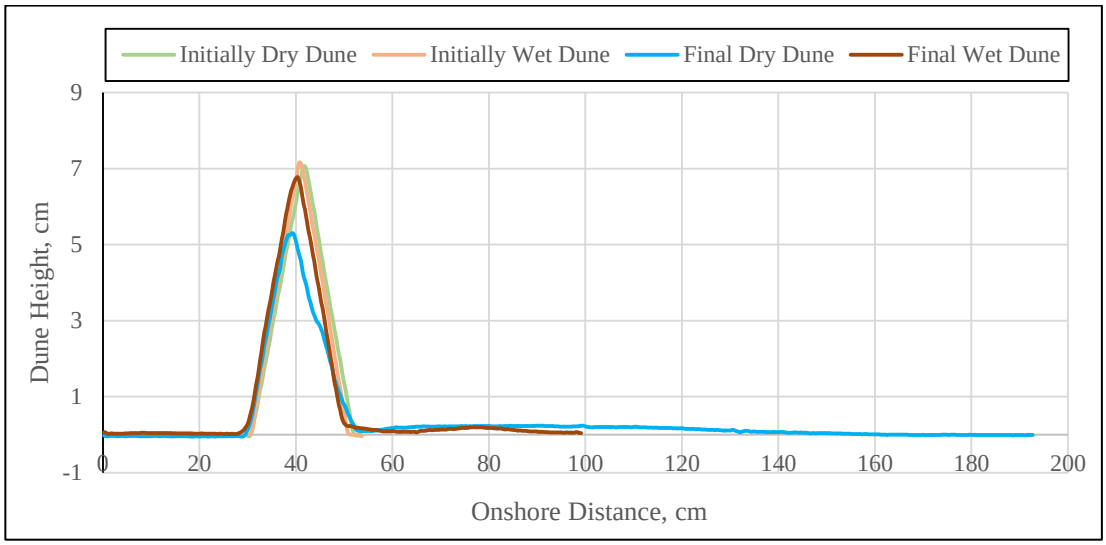

Figure 5.30 Profiles of fine sand dune for ΔH2= 8 cm

More flat deformed dune shape is seen in Figure 5.31. It shows almost same profile for CS in DD and WD. Since the bore size is large and carried huge amount of water, the difference is not prominent in terms of onshore sediment transport distance and crest height. This is also true for MS as can be seen in Figure 5.32. It appears that high recession velocity of water at the dune foot may cause the evolution of a second dune

peak (though small) near 60 cm distance. However, MS sediment moved to a longer distance (4.0 m) than CS (2.60) m, possibly due to its smaller grain size.

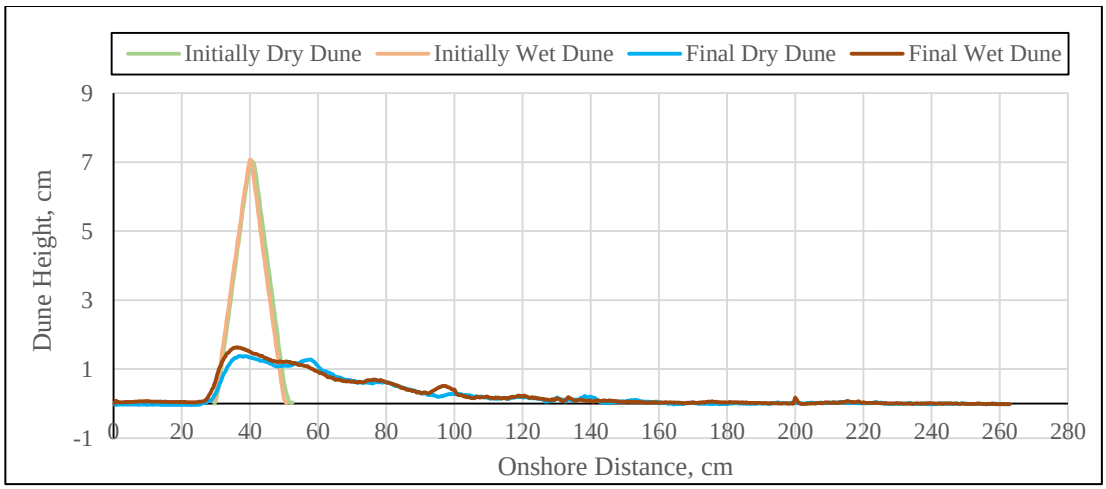

Figure 5.31 Profiles of coarse sand dune for ΔH3= 10 cm

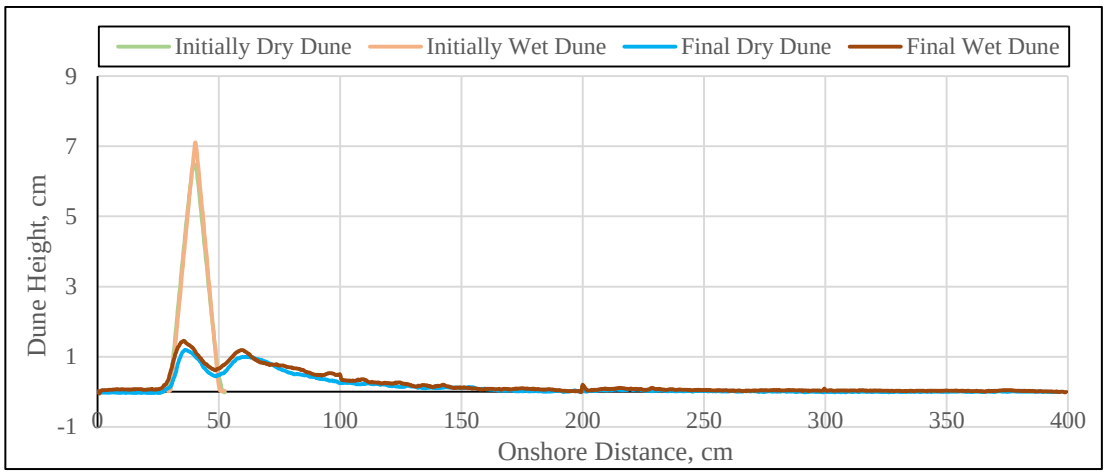

Figure 5.32 Profiles of medium sand dune for ΔH3= 10 cm

For B3 condition, FS shows dune crest lowered more for DD than WD as expected; and crest is shifted in seaward side as shown in Figure 5.33. However, the sediment moved almost same distance. This distance is less than CS and MS. Because relatively higher dune crest allowed less water over flow and consequently water could carry sediment up to 2.0 m.

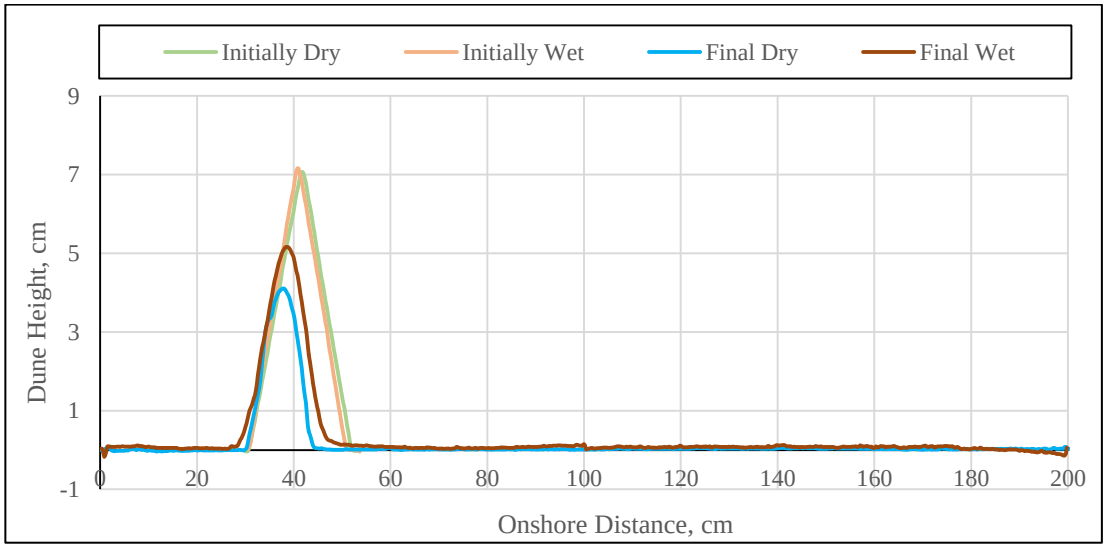

Figure 5.33 Profiles of fine sand dune for ΔH3= 10 cm

Figure 5.34 shows all of the initially dry sand dune profiles and Figure 5.35 shows all of the initially wet dune profiles. The general trend of back dune surface reveals a milder slope in dry and relatively elevated crest in wet condition. The reasons may be, buoyancy is higher in initially wet sand causing more sand grains to move farther downstream resulting receding velocity to be increased, even though this velocity may be ended earlier as the deformed crest height is higher. On the other hand, buoyancy in initially dry sand is less and water is absorbed by the dry sand and air voids are filled with water at the beginning of overwash causing a decelerated flow. This mechanism is important, even though this occurs within a short time. It is evident from these figures that wet fine sand has highest resistance potential against overwash while dry medium the least.

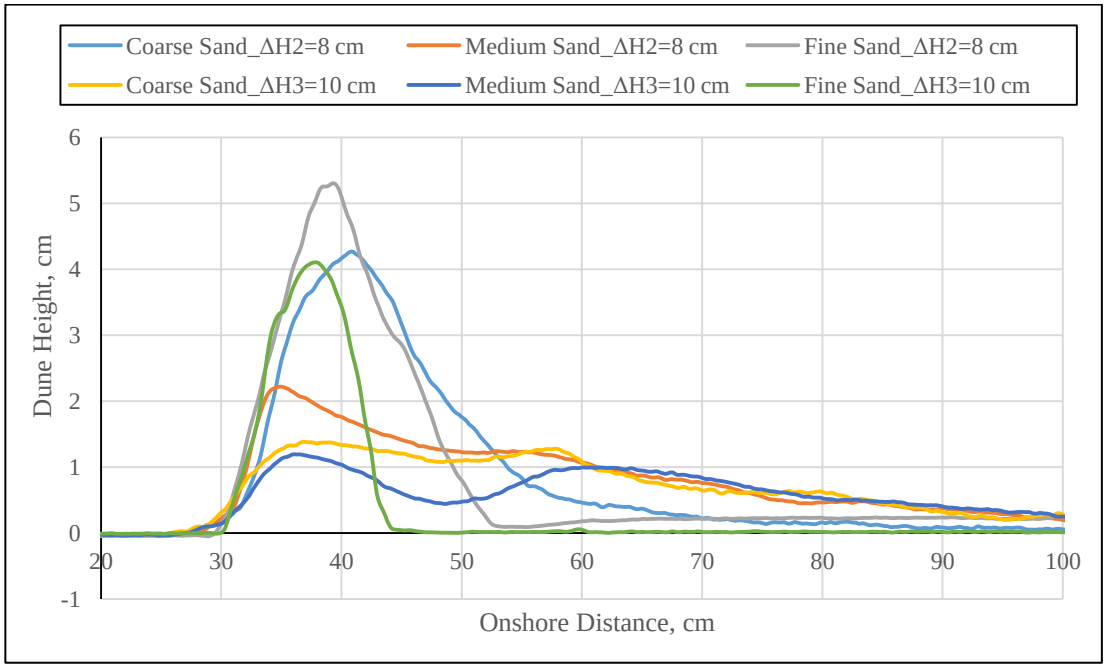

Figure 5.34 Final profiles of initially dry sand dune

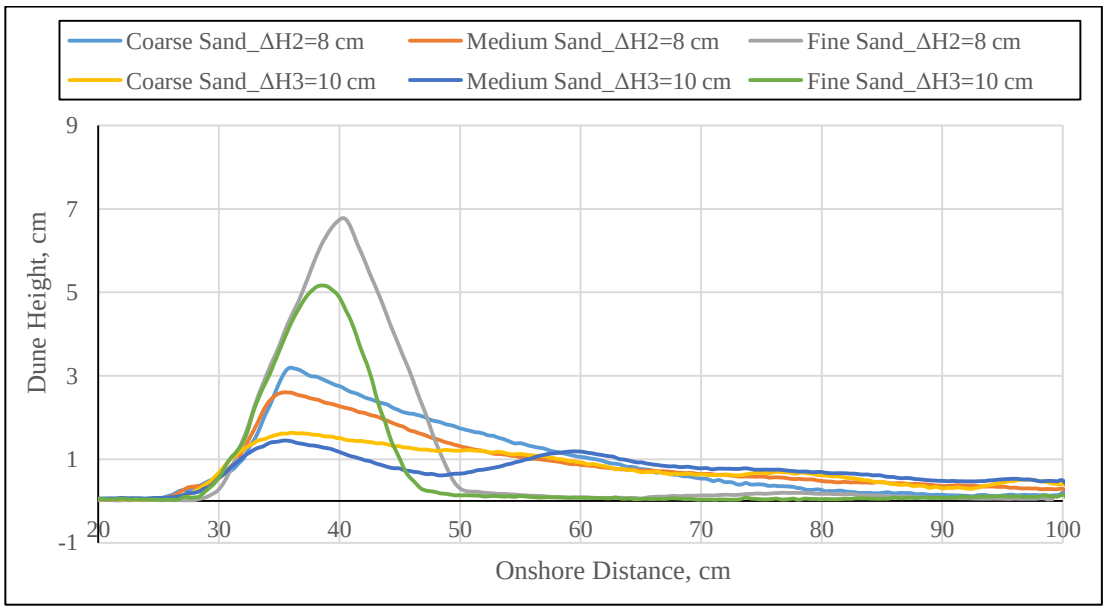

Figure 5.35 Final profiles of initially wet sand dune

5.7 Water surface profile during dune overwash

The following figures depicts the sand dune overwash observation during experimentation. The notation mentioned in Figures 5.36 to Figure 5.45 implies, e.g. MB1 ‘mild slope (M) bore 1 (B1)’; ‘steep slope (S)’. Time 0 s corresponds to wave front touching the fore dune base. With respect to this, timing of other stages are counted.

Figure 5.36 shows water slightly passes the dune crest and very small amount of sediment movement is observed. Stage 1 and 2 occurred at 0.18 s and 0.31 s, respectively and Figure 5.37 shows the pictorial view extracted from video recording.

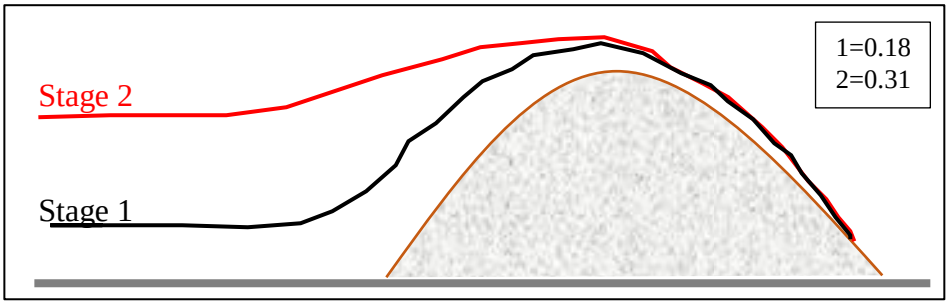

Figure 5.36 Water surface profiles during dune overwash **SB1**

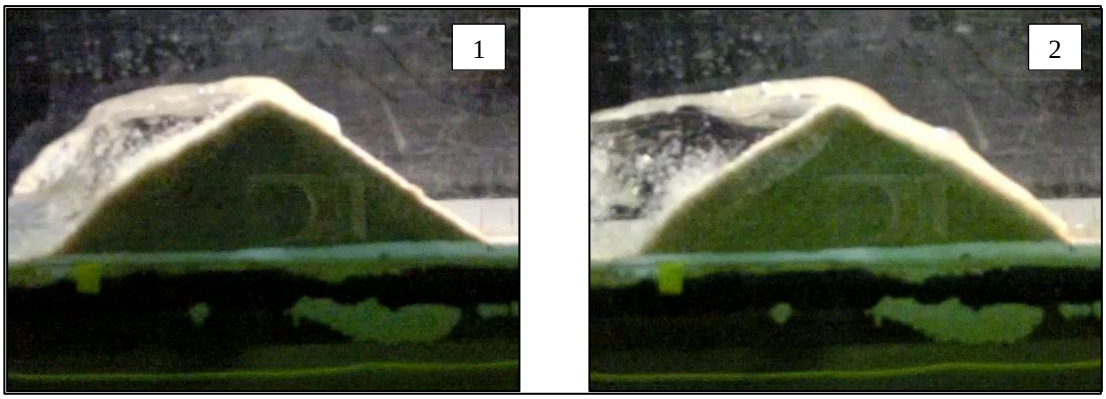

Figure 5.37 Pictorial view of water surface profiles during dune overwash **SB1**

Figure 5.38 shows five stages can be identified. Stage 1 occurred at 0.13 s and it overtopped the dune. Then a hydraulic jump formed which moved to downstream gradually. A second overtopping occurred on stage 5 at 1.45 s. Figure 5.39 shows the pictorial view extracted from video recording.

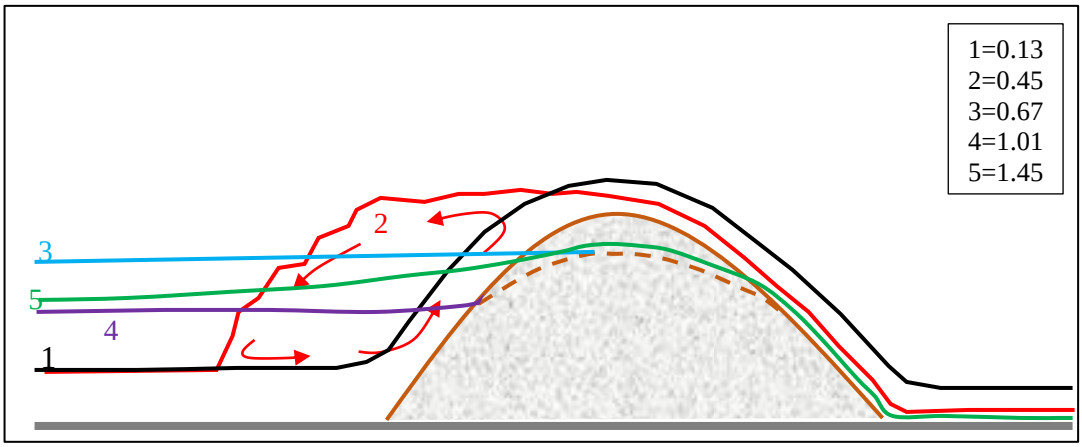

Figure 5.38 Water surface profiles during dune overwash **SB2**

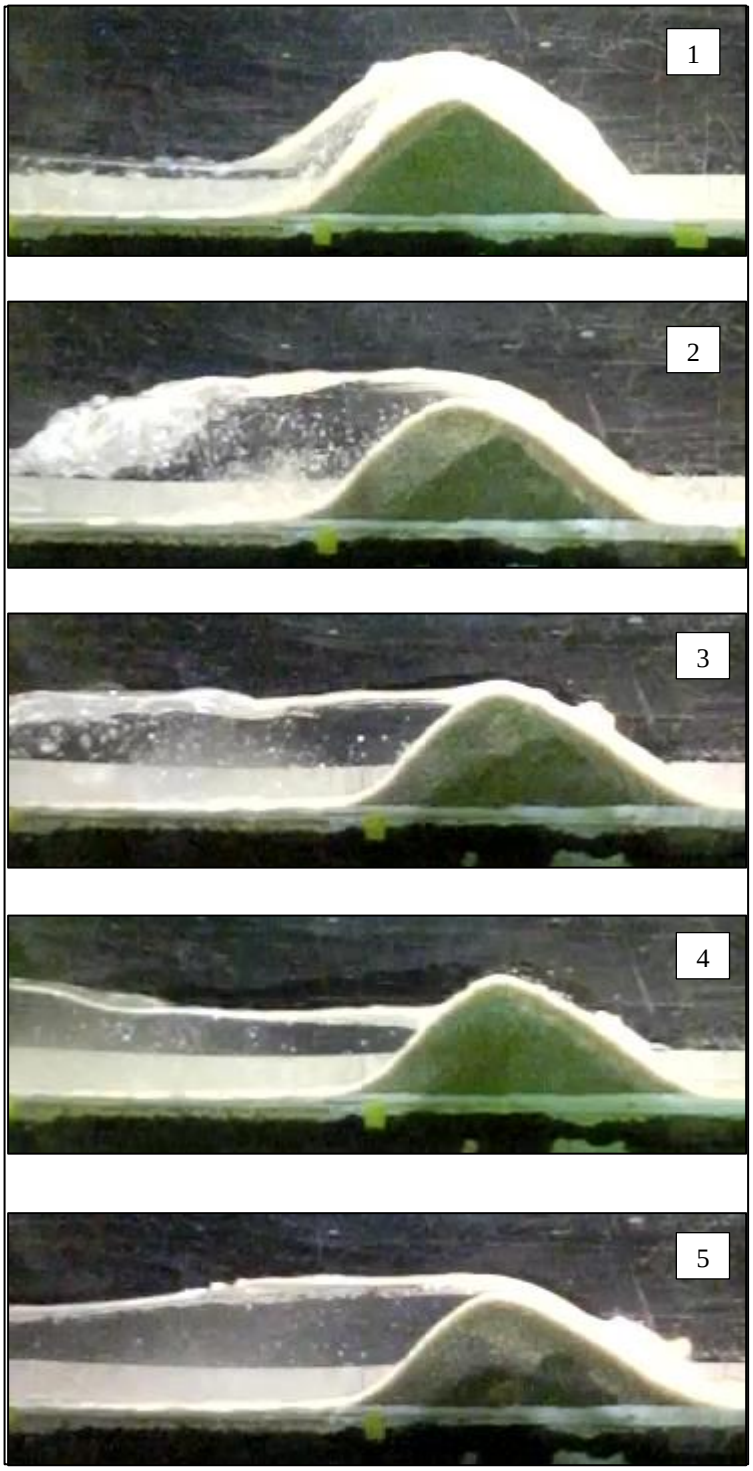

Figure 5.39 Pictorial view of water surface profiles during dune overwash **SB2**

Figure 5.40 shows six stages can be identified. Stage 1 occurred at 0.25 s and it overtopped the dune. Then a hydraulic jump formed which moved to downstream gradually. A second overtopping occurred on stage 5 at 1.74 s which continues to stage 6 at 2.19 s. Significant dune crest lowering resulting huge sediment transport. Figure 5.41 shows the pictorial view extracted from video recording.

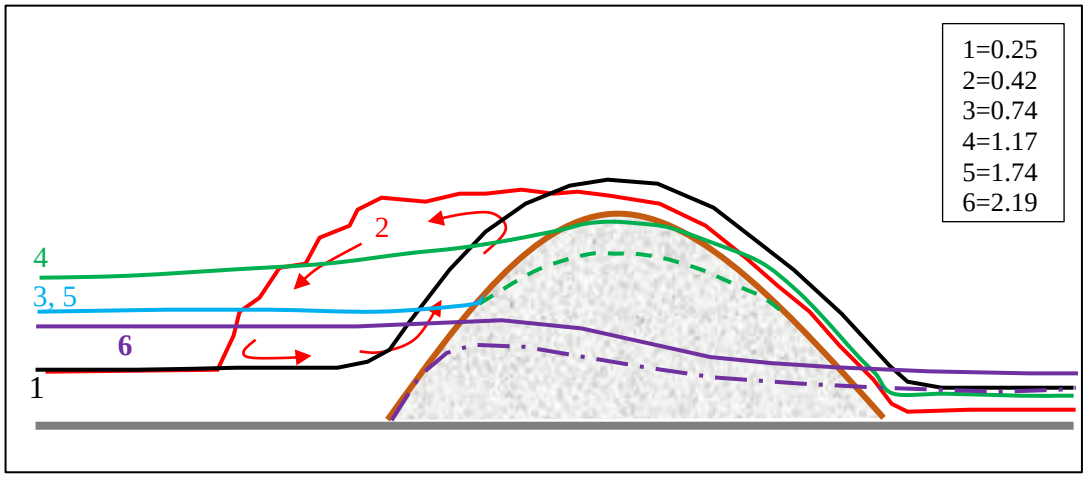

Figure 5.40 Water surface profiles during dune overwash **SB3**

Figure 5.42 shows four stages can be identified. Stage 1 occurred at 0.50 s and it do not overtopped the dune. Rather a hydraulic jump formed first which moved to downstream gradually and raised water level at dune base resulting overtopping, stage 2 at 1.58 s. The overtopping goes on to stage 4 at 7.49 s and continues till end. For all the time water level is higher than dune elevation. Significant sediment transport occurred. Figure 5.43 shows the pictorial view extracted from video recording.

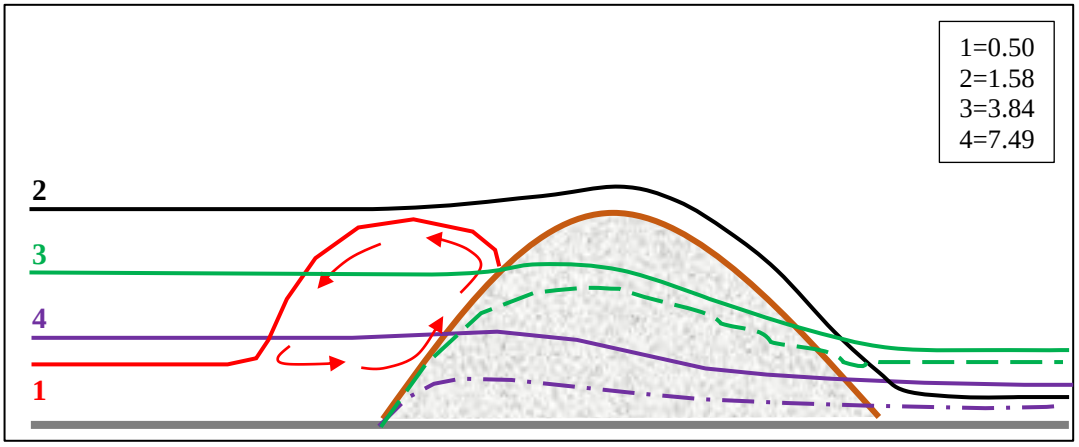

Figure 5.42 Water surface profiles during dune overwash **MB2**

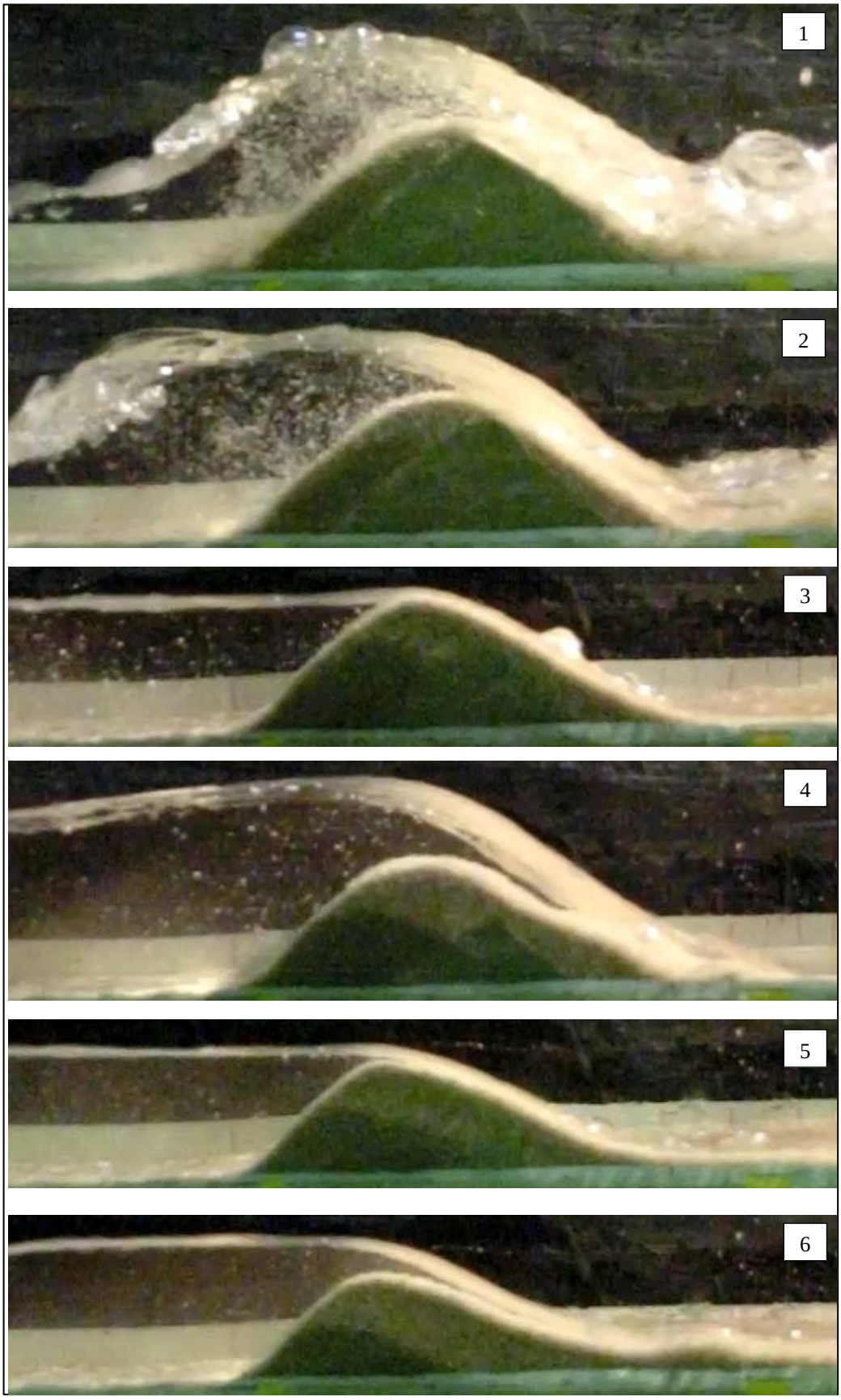

Figure 5.41 Pictorial view of water surface profiles during dune overwash **SB3**

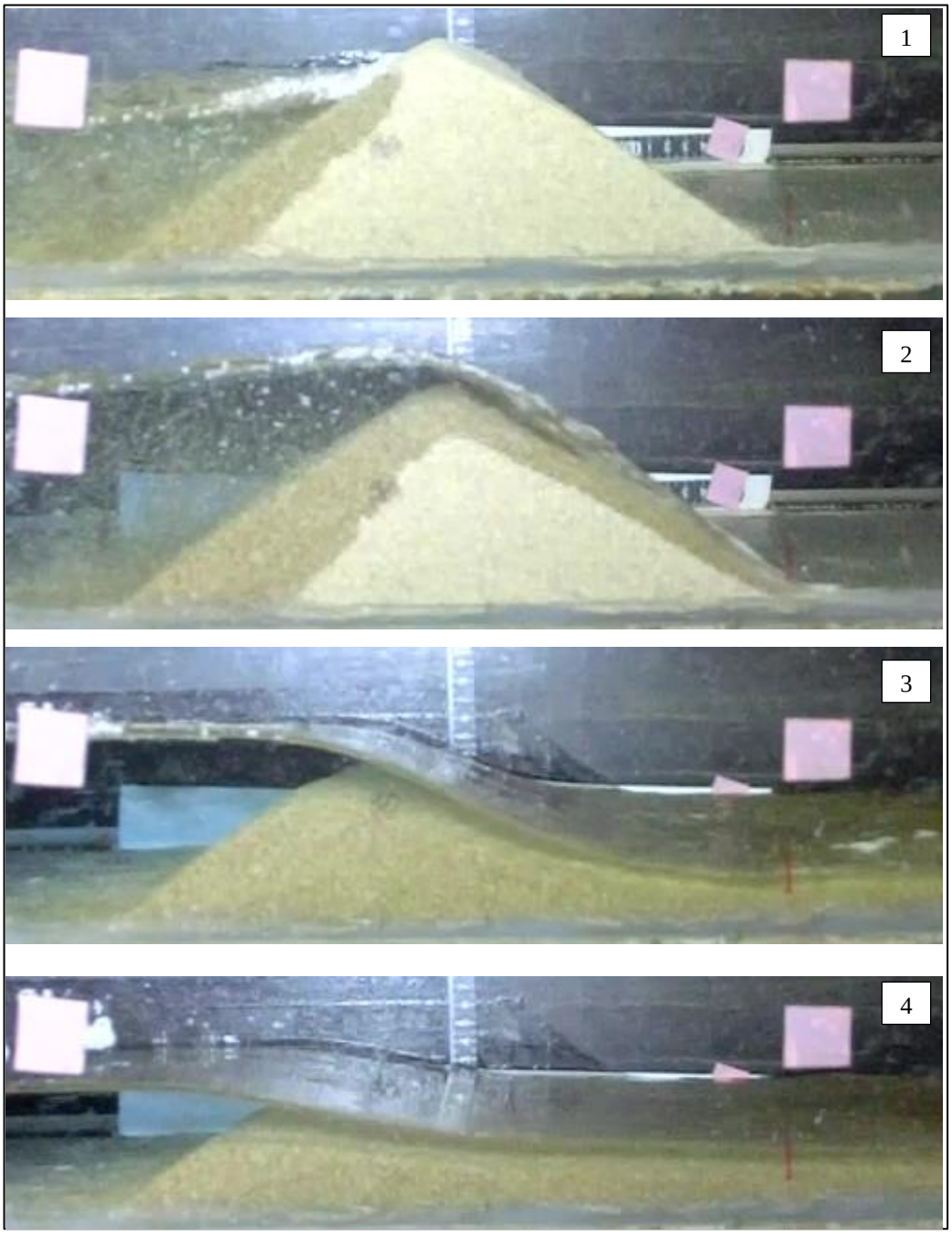

Figure 5.43 Pictorial view of water surface profiles during dune overwash **MB2**

Figure 5.44 shows four stages can be identified. Stage 1 occurred at 0.46 s and it do not overtopped the dune. Rather a hydraulic jump formed first which moved to downstream gradually and raised water level at dune base resulting overtopping, stage 2 at 0.95 s which is quicker than previous case. This is due to the larger bore size. The overtopping goes on to stage 4 at 7.09 s and continues till end. For all the time water level is higher than dune elevation. Significant sediment transport occurred at a faster

rate than Figure 5.43. Figure 5.45 shows the pictorial view extracted from video recording.

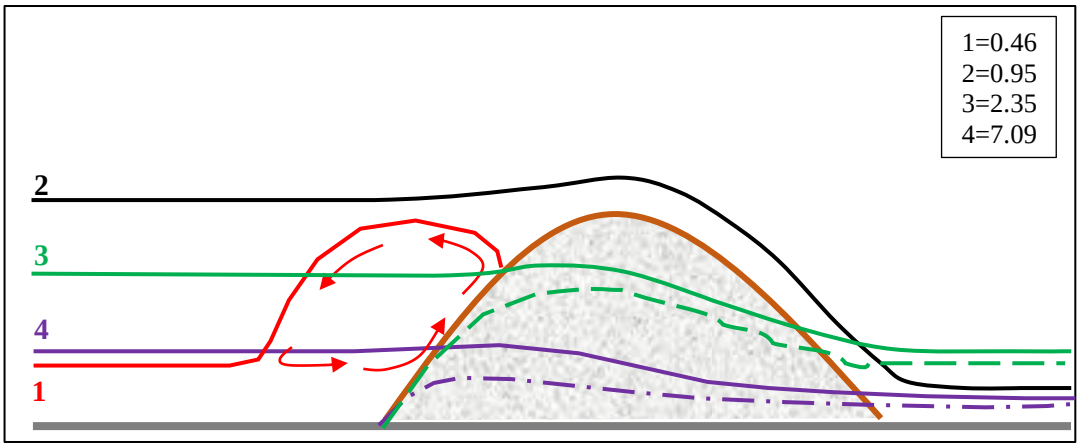

Figure 5.44 Water surface profiles during dune overwash **MB3**

5.8 Water Overtopping and Sediment Transport

The water overtopping rate is estimated using weir formula applied by Visser (1994). The formula is modified to recapitulate erodible dune phenomena considering the initial height of dune (z_d) and water depth (h_w); and remarkable final dune height (z'_d) and final water depth (h'_w) as shown in Figure 5.46. The word 'remarkable' implies that after attaining this condition, the dune sediment transport recedes to very small amount.

The modified formula can be stated as,

$$q_w = m\left(\frac{2}{3}\right)^{\frac{3}{2}}\sqrt{g}\left[\frac{(h_w - z_d) + (h'_w - z'_d)}{2}\right]^{\frac{3}{2}} \tag{5.1}$$

where q_w = water overtopping rate (cm^2/s), m = discharge coefficient ≅ 1.

Figure 5.45 Pictorial view of water surface profiles during dune overwash **MB3**

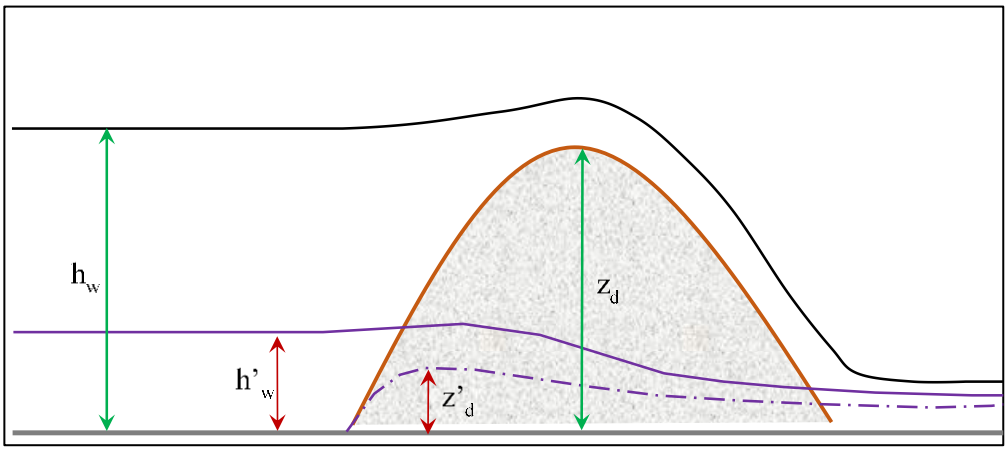

Figure 5.46 Schematic diagram representing water overtopping features

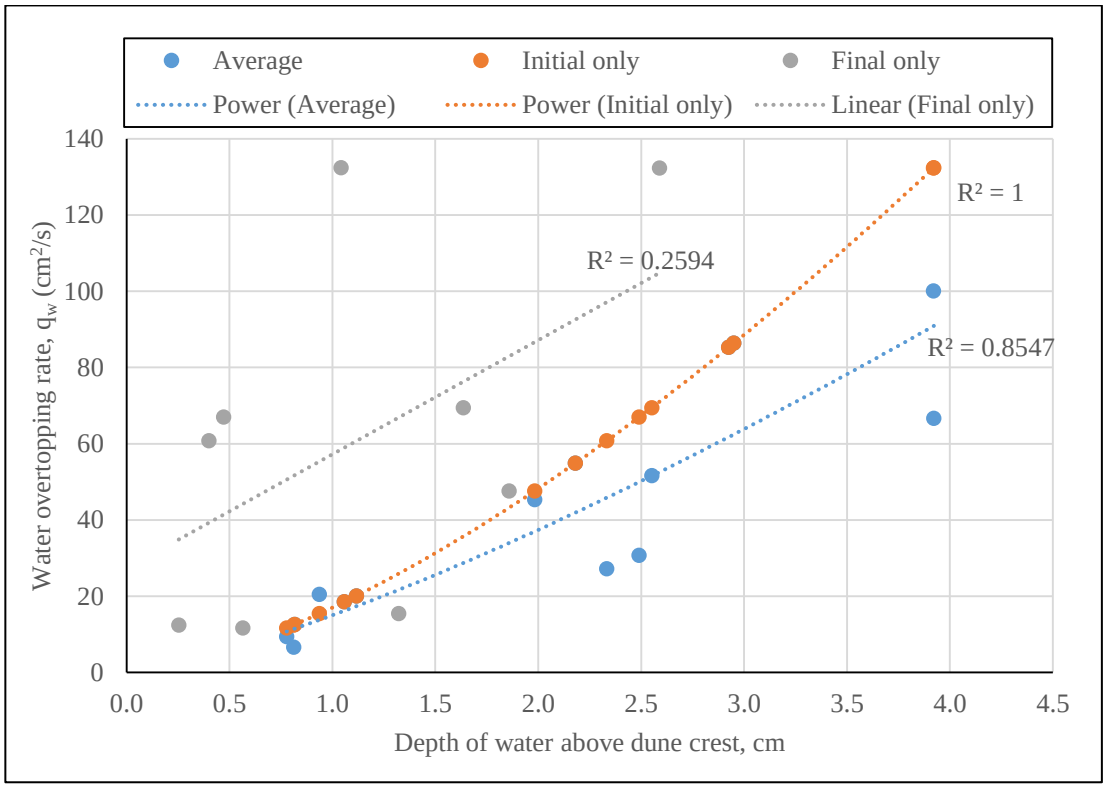

Figure 5.47 Water flow rate versus water depth above dune crest

The proposed expression of Equation 5.1 is examined by considering three conditions to measure depth of water above dune crest: (i) only initial, (ii) only final and (iii) average of initial and final to estimate q_w as shown in Figure 5.47. Since the original formula considers a weir composed of non-erodible material, only initial condition gives the best estimation of q_w followed by average of initial and final water depth above dune crest. Since, in the resent case the depth of water above the dune varies with time, therefore multiplying this flow rate by total overwash time will give

overestimation of total water volume overtopped. Therefore, average of initial and final water depth above dune crest is applied in this study to predict water overtopping rate. The estimated values of water overtopping rate are presented along with depth of water surface and corresponding dune height in Table 5.2.

Table 5.2 Overtopping water rate estimation for R1 to R16

Run Number	**Initial (h_w-z_d) (cm)**	**Final (h'_w-z'_d) (cm)**	**q_w (cm^2/s)**
R1	1.12	-	20.12
R2	0.82	-	12.58
R3	1.06	-	18.53
R4	2.93	-	85.3
R5	2.95	-	86.38
R6	2.18	-	54.9
R7	3.92	2.59	100.1
R8	3.92	1.04	66.68
R9	2.49	0.47	30.72
R11	0.81	0.25	6.627
R12	0.94	1.32	20.48
R13	0.78	0.57	9.386
R14	1.98	1.86	45.37
R15	2.55	1.64	51.64
R16	2.33	0.4	27.24

The computed q_w values of all the experiments and the corresponding sediment transport rate q_{sd} (dry dune condition), q_{sw} (wet dune condition) and q_s (general) are shown in Table 5.3.

Table 5.3 Overtopping water rate and sediment transport rate of R1 to R16

Run	q_w **(cm²/s)**	$q_{sd}=Vs/(BT_o)$ **(cm²/s)**	$q_{sw}=Vs/(BT_o)$ **(cm²/s)**
R1	20.1	11.2	16.1
R2	12.6	8.5	6.4
R3	18.5	5.7	2.0
R4	85.3	7.5	2.8
R5	86.4	5.7	2.3
R6	54.9	12.5	6.5
R7	100.1	4.6	4.5
R8	66.7	4.3	4.3
R9	30.7	4.2	1.4
R11	6.6	0.9	1.5
R12	20.5	2.1	1.7
R13	9.4	1.1	0.6
R14	45.4	2.0	1.8
R15	51.6	1.8	2.0
R16	27.2	1.1	0.4

The values mentioned in Table 5.3 can be plotted to obtain relationship between water and sediment transport rate that pass through the origin, i.e. when $q_w = 0$, $q_s = 0$.

Figure 5.48 illustrate water flow rate versus sediment transport rate for different sand. It is revealed that FS has a high rate and MS the lowest. Figure 5.49 depicts water flow volume versus sediment transport volume for different sand. This shows higher volume transported for FS but interesting to note that almost same sediment volume is transported in CS and MS for a given volume of water. However, a good correlation coefficient is evident in CS.

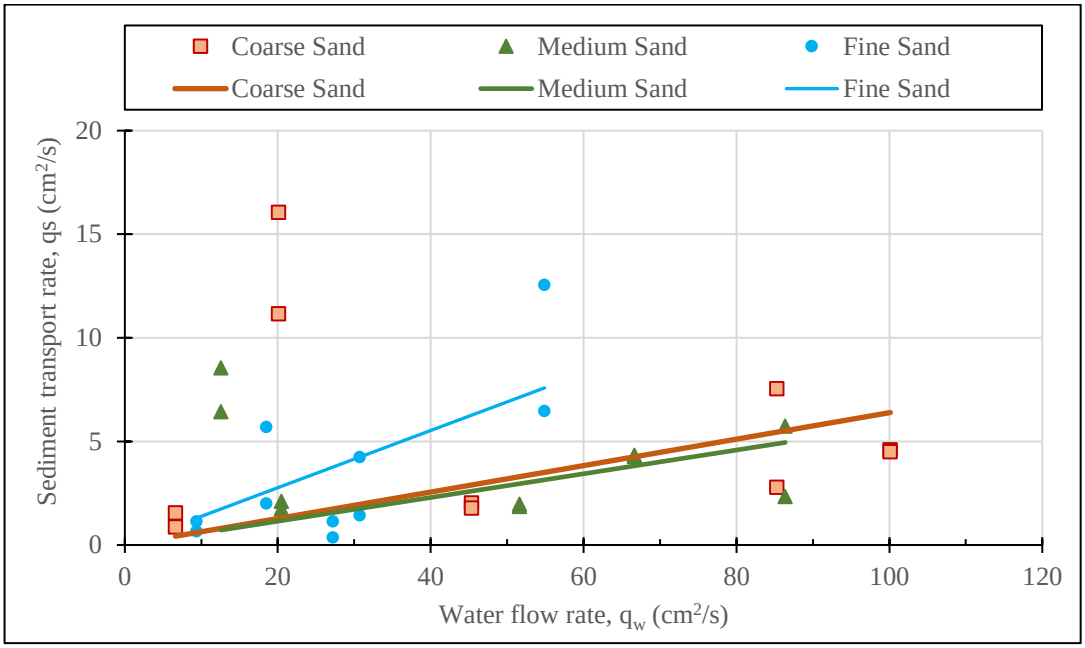

Figure 5.48 Water flow rate versus sediment transport rate for different sand

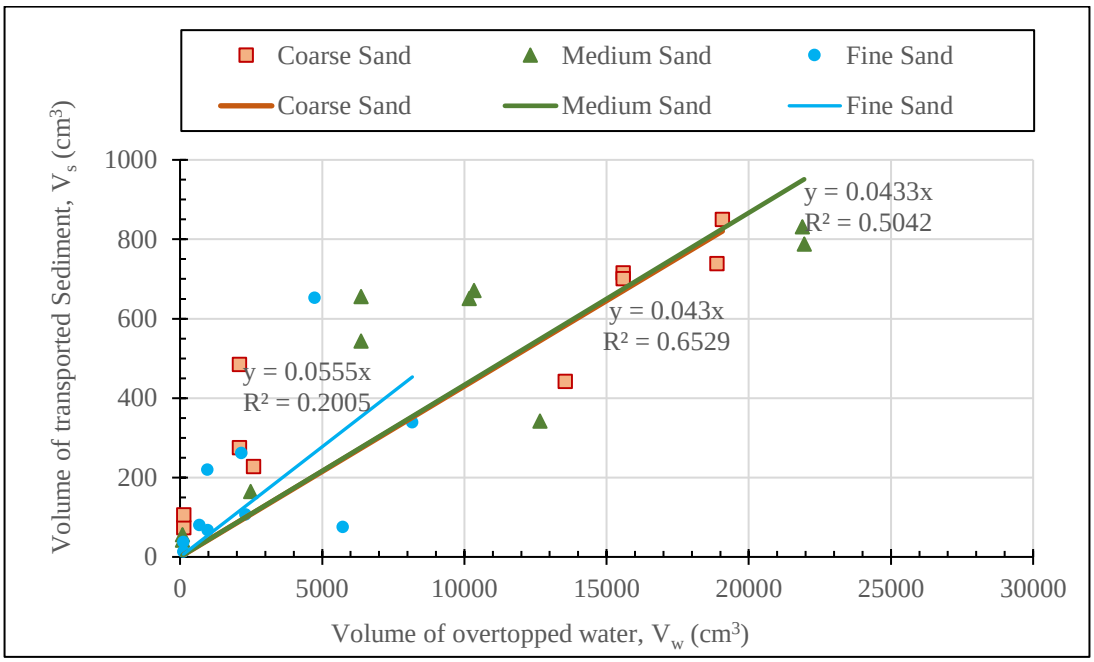

Figure 5.49 Water flow volume versus sediment transport volume for different sand

Figure 5.50 shows a power relationship between the transported water volume and sediment volume with a correlation coefficient (R^2) of 0.75. This shows an increasing trend of sediment transport volume at a decreasing rate. In general, this relationship may be used to assess the sediment transport volume from the known volume of water overtopping the dune during tsunami or storm surge.

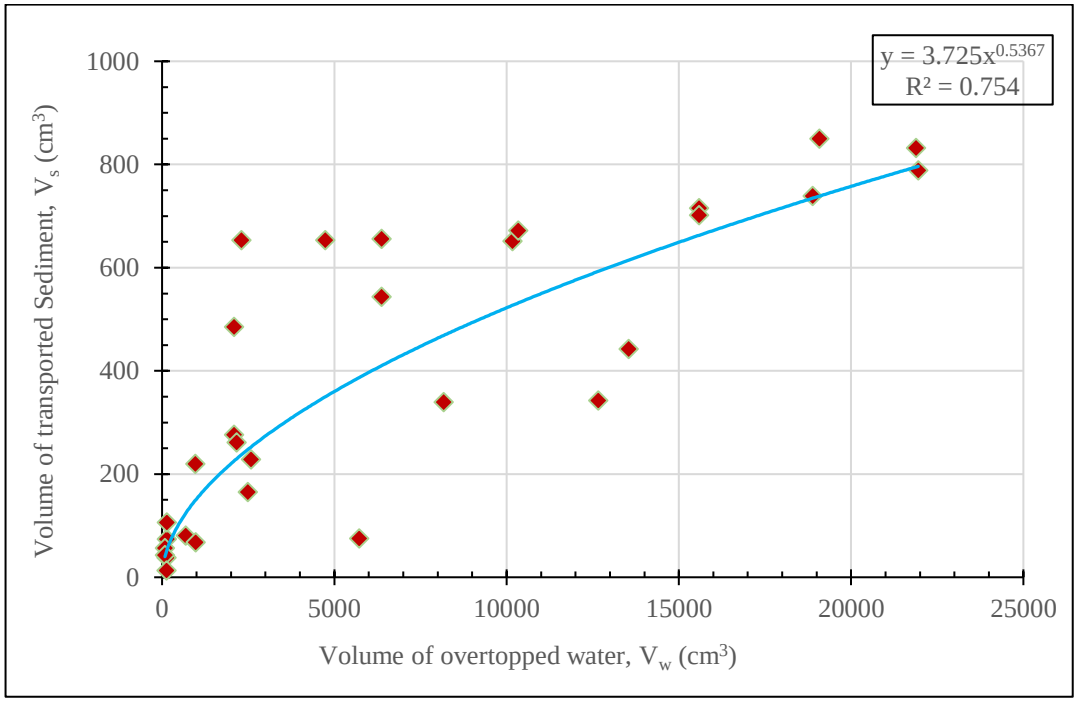

Figure 5.50 Water flow volume versus sediment transport volume for all experiments

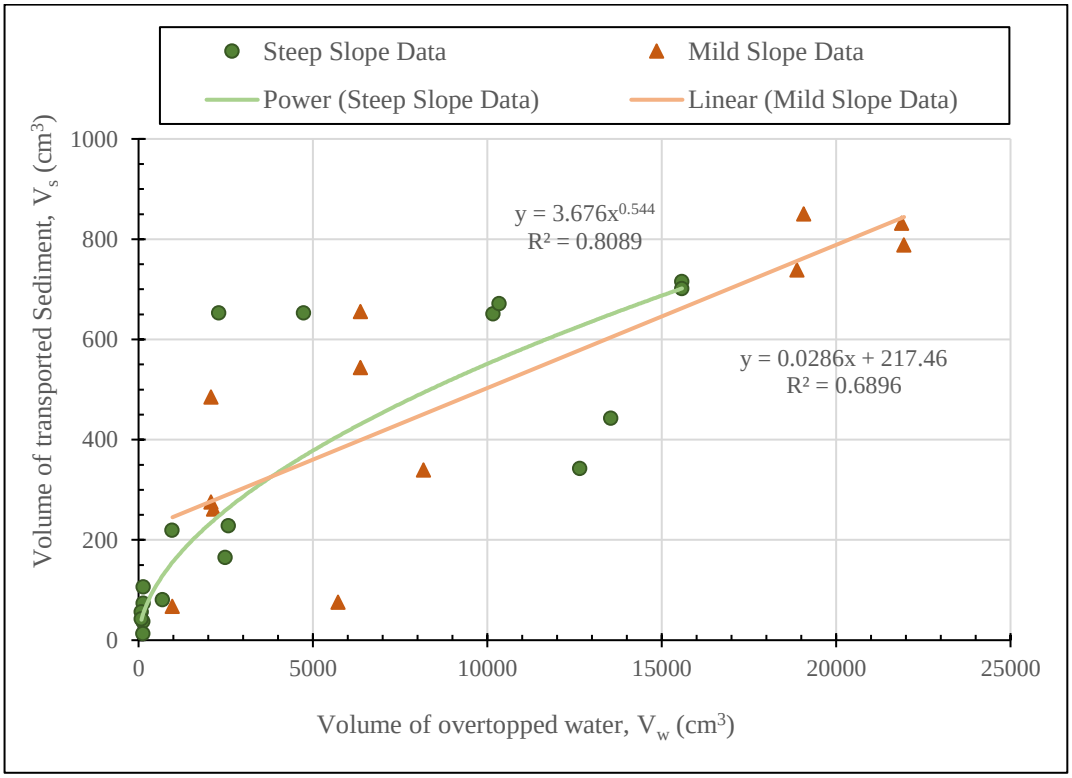

Figure 5.51 Water flow volume versus sediment transport volume for steep and mild slope

Figure 5.51 shows a better plotting than Figure 5.50 as it separates steep slope data and mild slope data. Steep slope data are best fitted by power relation with R^2 value of 0.81 while mild slope data best fits by a linear relation with R^2 value of 0.69.

The data presented in Table 5.3 can be analyzed in different aspects like type of slope, sediment grain size, initially dry dune (DD) or wet dune (WD) condition. Following figure illustrates influence and nature of these aspects considering overtopped water volume, overtopped water flow rate, sediment transport rate and sediment transport volume.

Figure 5.52 shows DD and WD condition on steep slope case. General trend reveals that higher sediment transport rate in DD than WD. This difference may be resulted due to the shorter overwash duration with high water flow rate.

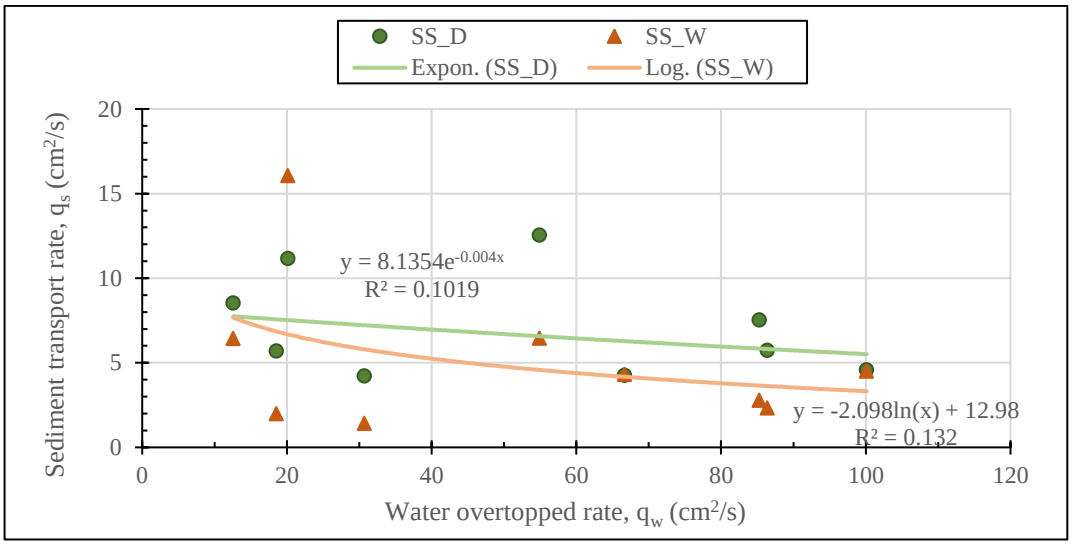

Figure 5.52 Water flow rate versus sediment transport rate of DD and WD for steep slope

Figure 5.53 shows DD and WD condition on mild slope case. General trend reveals that slightly higher sediment transport rate in DD than WD, though overlap is seen for low flow rate. However, the correlation coefficient gives better values than steep slope (Figure 5.52). It is evident from the two lines that an increase in overtopping flow rate decreases sediment transport rate.

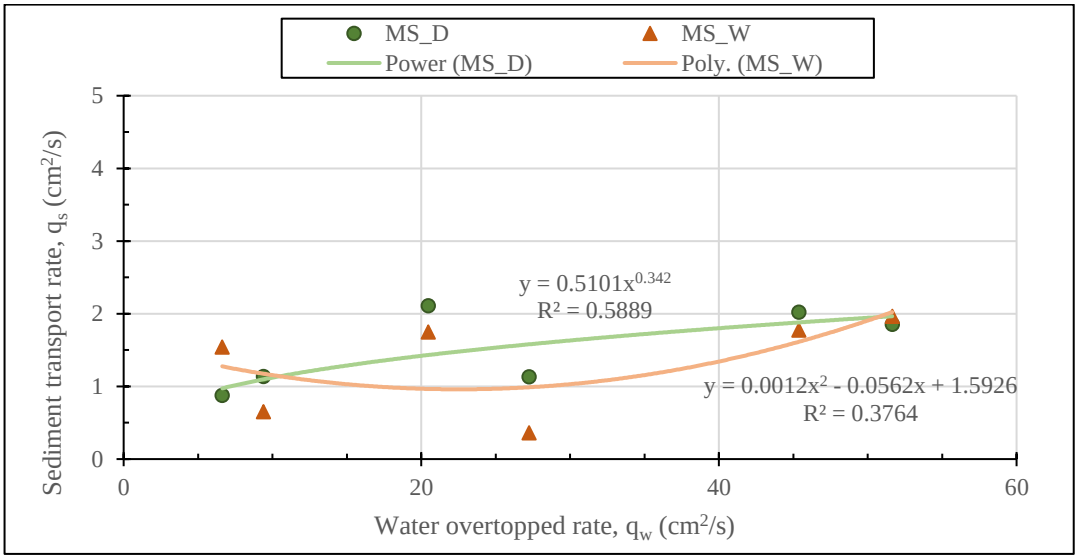

Figure 5.53 Water flow rate versus sediment transport rate of DD and WD for mild slope

Figure 5.54 shows DD and WD condition on mild slope case. General trend reveals that higher sediment volume is transported in DD than WD as is seen also in Figure 5.53. However, R^2 value is better here. DD condition express a power relation while WD condition shows linear relation. It is evident from the two lines that an increase in overtopping flow rate increases sediment transport rate (opposite trend in steep slope).

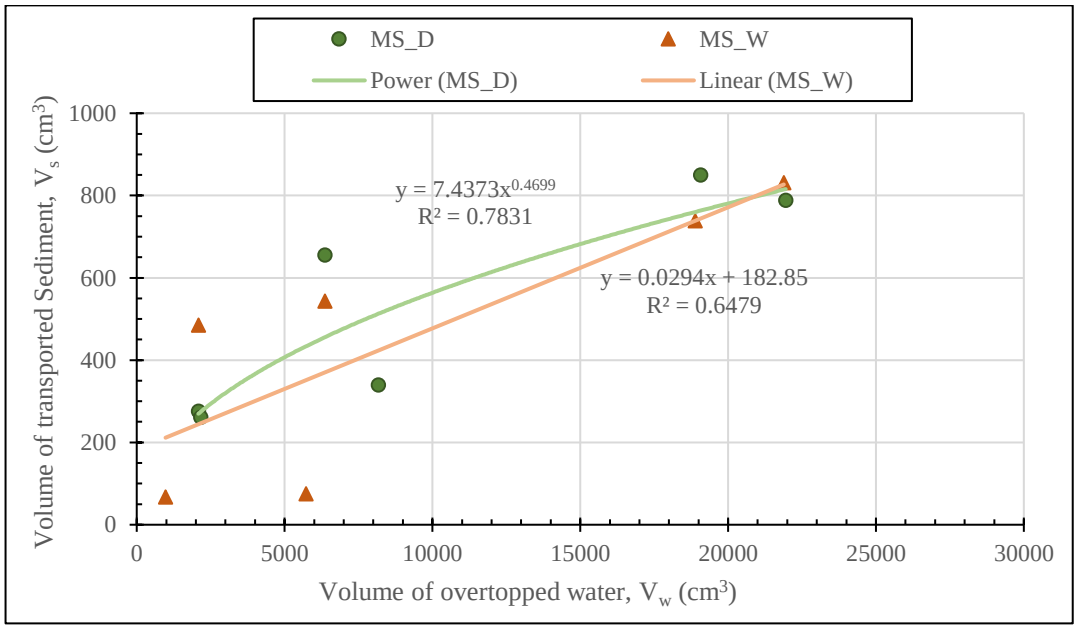

Figure 5.54 Water overtopped volume versus sediment transport volume of DD and WD for mild slope

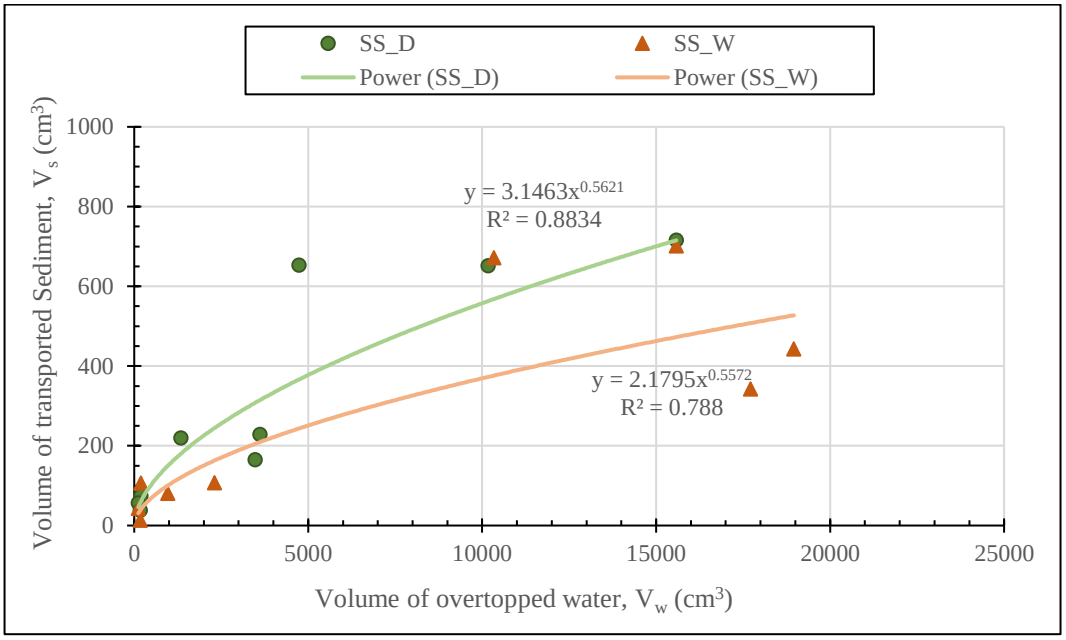

Figure 5.55 Water overtopped volume versus sediment transport volume of DD and WD for steep slope

Figure 5.55 shows DD and WD condition on steep slope case. General trend reveals that higher sediment volume is transported in DD than WD as is seen also in Figure 5.52. However, R^2 value is far better here than Figure 5.52. Both DD and WD condition express a power relation.

This figure clearly depicts the large difference in transporting sediment volume between DD and WD condition for a given higher overtopped water volume. Dry sediment can be carried easily by the overflowing water due to its less self-weight. Another notable point is, during steep slope experiments more sediment is transported in DD than WD for FS. This could create bias to higher sediment volume movement in DD condition.

5.9 Numerical Simulation

The model of Shimozono et al. (2007) is reset in this study with necessary adjustment to incorporate experimental conditions. Two slope is used with three different sand grain sizes for two bore sizes (B1, B2) with initially dry (DD) and initially wet (WD) dune condition. Numerically simulated dune profile after overwash and the relevant discussions are shown in the following subsections. Dotted line in figures refer to the initial position and firm line refer to the overflow simulated profile of the dune.

5.9.1 Sediment Entrainment Model

The existing model of Shimozono et al. (2007) applied total sediment load formula of Engelung and Hansen (1967). Simulation is also performed using sediment transport formula proposed by Cao (1999) which is also applied in Cao et al. (2004).

Figure 5.56 to Figure 5.58 show comparison of simulated dune profile applying sediment entrainment model of Cao (1999) and Engelund and Hansen (EH) (1967). Other components of the model remain exactly the same during computation. Three sediment type: coarse, medium and fine; and two slopes: are shown here. Important to mention that the incipient condition as described in the above sediment transport models remain as it is. But the models are not sufficient to reproduce sediment transport as is found in laboratory experiments. Therefore, modification of the existing sediment transport model is necessary to simulate the dune sediment transport mechanism.

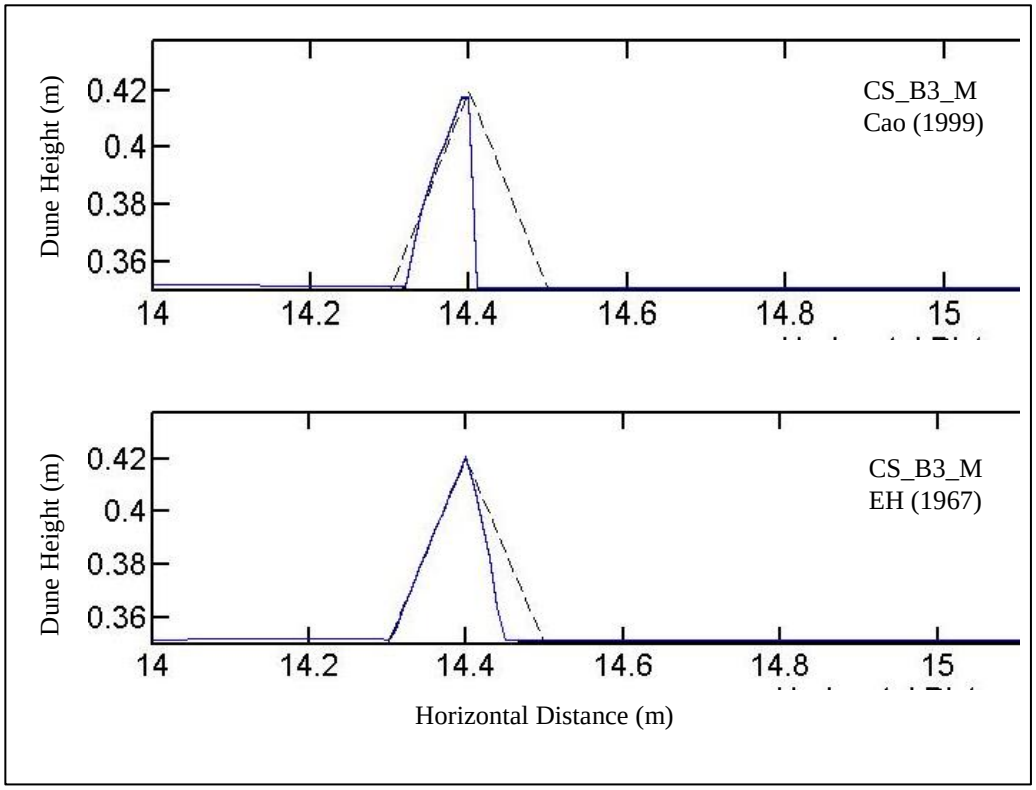

Figure 5.56 Comparison of sediment entrainment model (CS, mild slope)

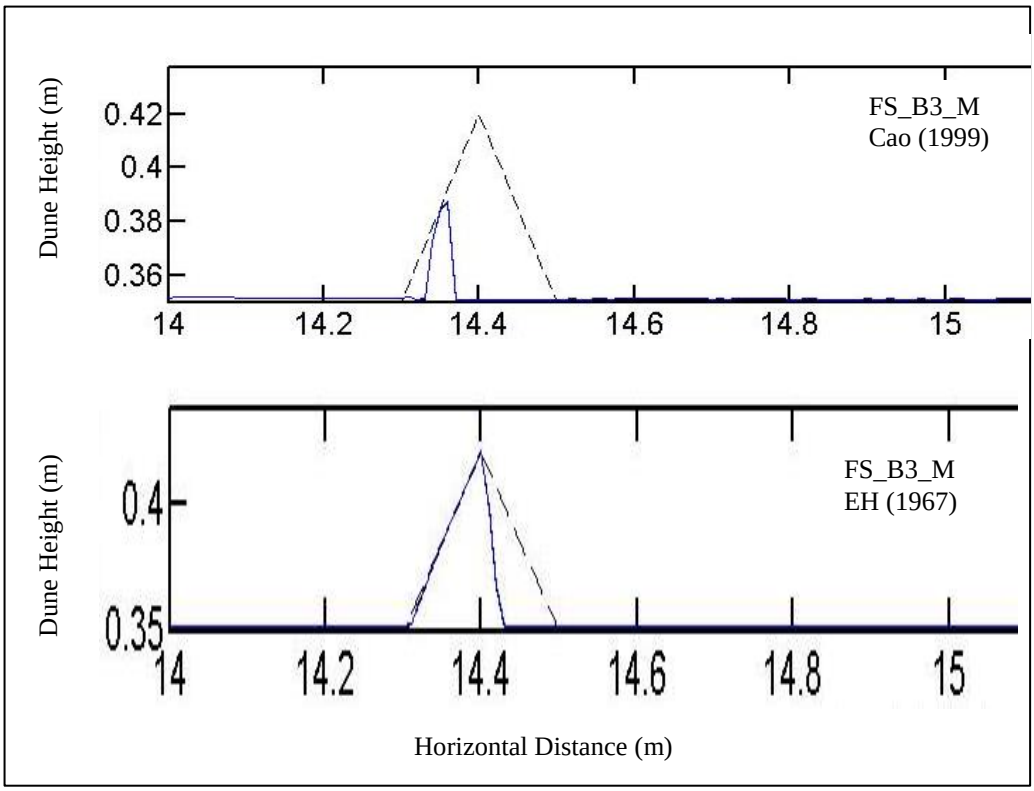

Figure 5.57 Comparison of sediment entrainment model (FS, mild slope)

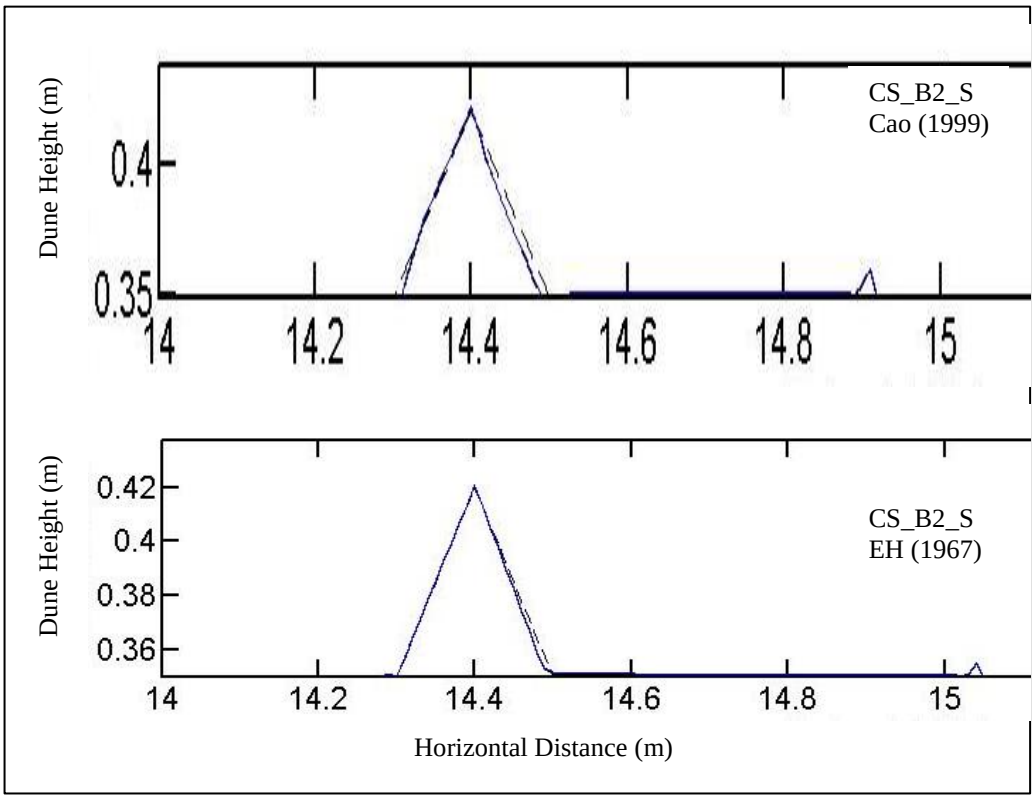

Figure 5.58 Comparison of sediment entrainment model (CS, steep slope)

5.9.2 Dune Erosion Simulation

Figure 5.59 shows dune profile plotted before and after overwash occurred for three different sand sizes on mild slope for B3 bore. It is clearly seen that maximum erosion takes place in fine sand, while minimum in coarse sand, though it is close to medium sand; but still, there is difference in the final shape (near crest). Therefore, the model considers the influence of grain size as is observed in the laboratory experiments.

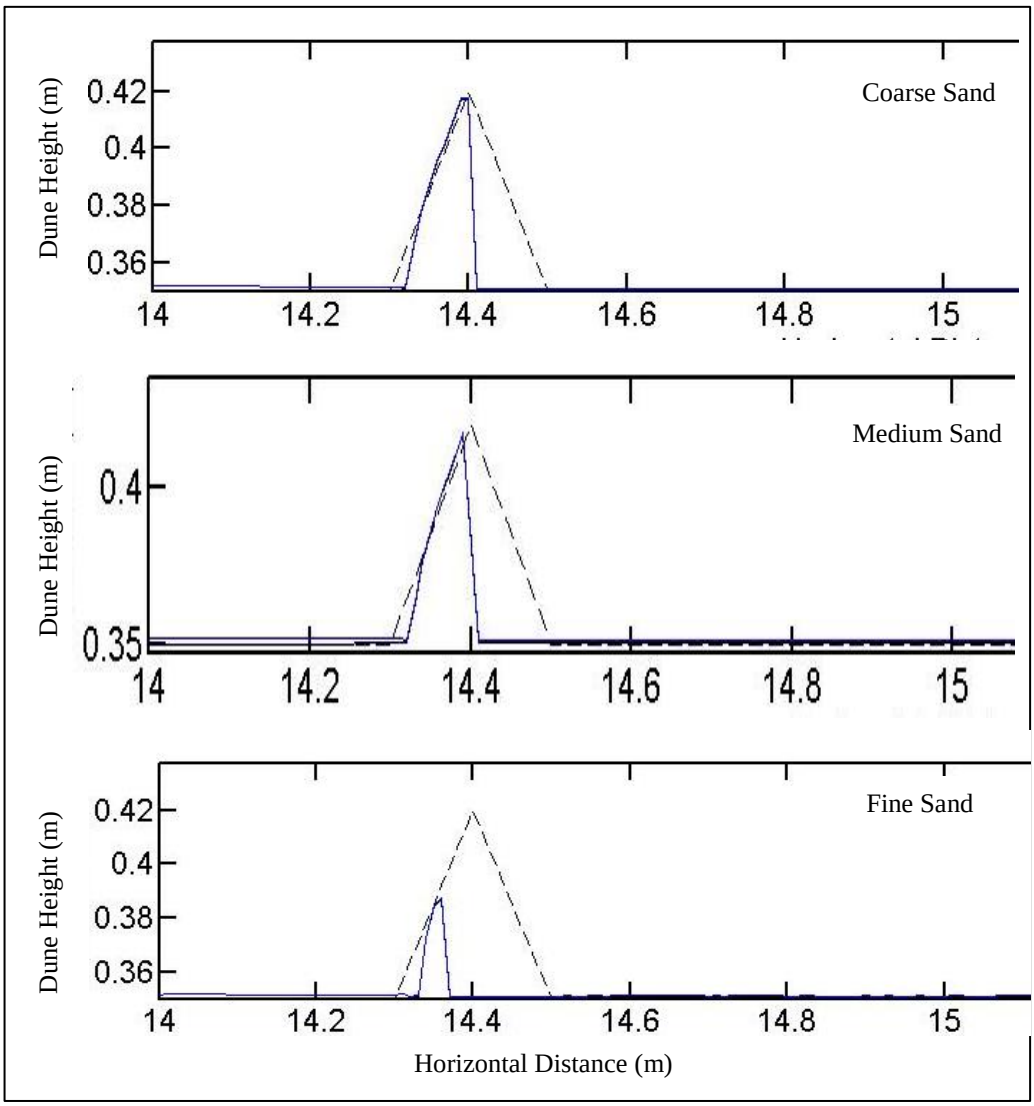

Figure 5.59 Comparison of simulated dune profile (mild slope, bore-B3)

The above simulations are performed based on the available sediment transport model that takes into account of the sediment sizes and establish incipient condition for that sediment. However, this simulated results disagree with laboratory observations (Figures 5.24, 5.25).

5.9.3 Sediment Transport Coefficients

Performing sensitivity analysis the following coefficients are determined for respective experimental conditions. Measured and simulated dune profile after overwash completion are matched to select the best set of coefficients. These coefficients are discussed in section 4.4.

5.9.4 Sensitivity Analysis

To describe determination process of the best set of coefficients, a typical case is presented here: dry coarse sand for B2 (8 cm). Coefficient set 1 of Table 5.4 is applied in simulation and the result is shown in Figure 5.60 which shows no overwash. Here, dotted line and firm line represents initial profile and final simulated profile, respectively.

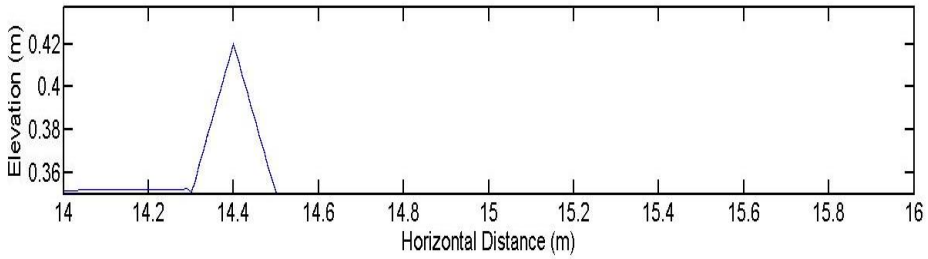

Figure 5.60 Simulated profile for coefficient set 1

Table 5.4 Sensitivity analysis

Set	Adaptation coefficient, α_o	Coefficient of sediment condition, ε	Coefficient of erosion, c_e	Coefficient of deposition, c_d
1	2	1	2.4	1
2	2	8.38	1	1
3	2	8.38	2.4	2.1
4	20	8.38	2.4	1
5	20	8.38	2.4	2.1

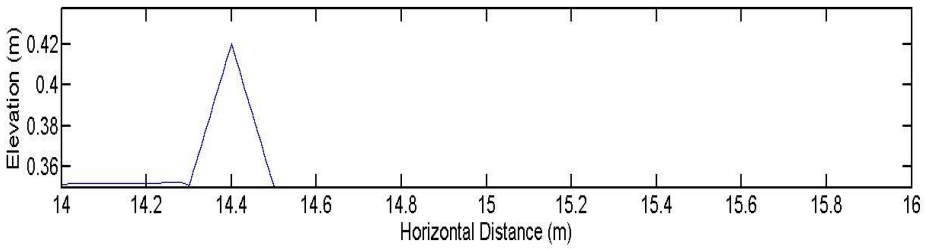

Figure 5.61 Simulated profile for coefficient set 2

For set 2 values, Figure 5.61 shows the same result. This means that sediment erosion on the dune crest will take place when both sediment erosion and sediment condition coefficients are adjusted.

For set 3, Figure 5.62 shows erosion as well as deposition of dune occurred. Therefore, the combination of the coefficient is getting better. However, still the erosion and deposition pattern requires adjustment.

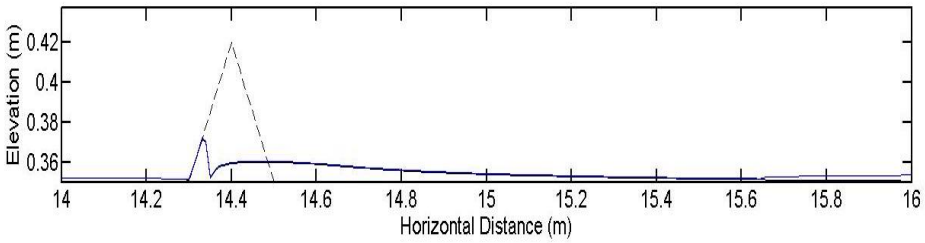

Figure 5.62 Simulated profile for coefficient set 3

Set 4 shows better simulation as can be seen in Figure 5.63. But erosion of the dune crest is higher than the actual as observed from measurement. Therefore, coefficient of deposition as well as coefficient of adaptation has to be adjusted together to get the best combination.

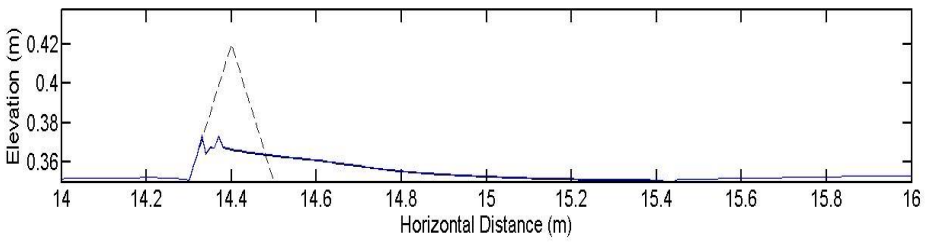

Figure 5.63 Simulated profile for coefficient set 4

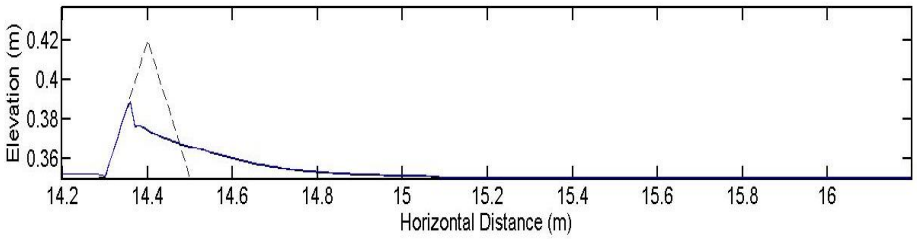

Figure 5.64 Simulated profile for coefficient set 5

Figure 5.64 shows the simulated profile for set 5. In the similar way the best set of coefficients are determined for other sand types, wet/dry condition, bore size. Table 5.5 shows the magnitude of these sets of coefficients. Next section shows comparison between simulated profile (by applying sediment transport coefficients) and measured profile.

Table 5.5 Sediment Transport Coefficients

Sand Type	**Bore**	**Dune Condition**	**Adaptation coefficient, α_o**	$\tau_c^* \varepsilon$	ε	**Coefficient of erosion, c_e**	**Coefficient of deposition, c_d**	τ_c
Coarse	B2	Dry	20	3.7	8.38	2.4	2.1	0.44
		Wet	20	8	18.11	2.4	2	
	B3	Dry/ Wet	10	3.7	8.38	2.4	2	
Medium	B2	Dry	20	5	16.11	2.4	2.1	0.31
		Wet	20	7	22.55	2.4	2.1	
	B3	Dry/ Wet	10	3.7	11.92	2.4	2	
Fine	B2	Dry	20	0.4	2.68	1	3	0.15
		Wet	20	0.2	1.34	1	3	
	B3	Dry	20	0.7	4.70	1	1.5	
		Wet	20	0.6	4.02	1	2	

5.9.5 Dune Profile Simulation: Fine Sand

Figure 5.65 shows the simulated and the observed profile of dune for fine sediment in wet condition for bore B2. The simulated profile and the measured profile are quite close. Shows a satisfactory agreement.

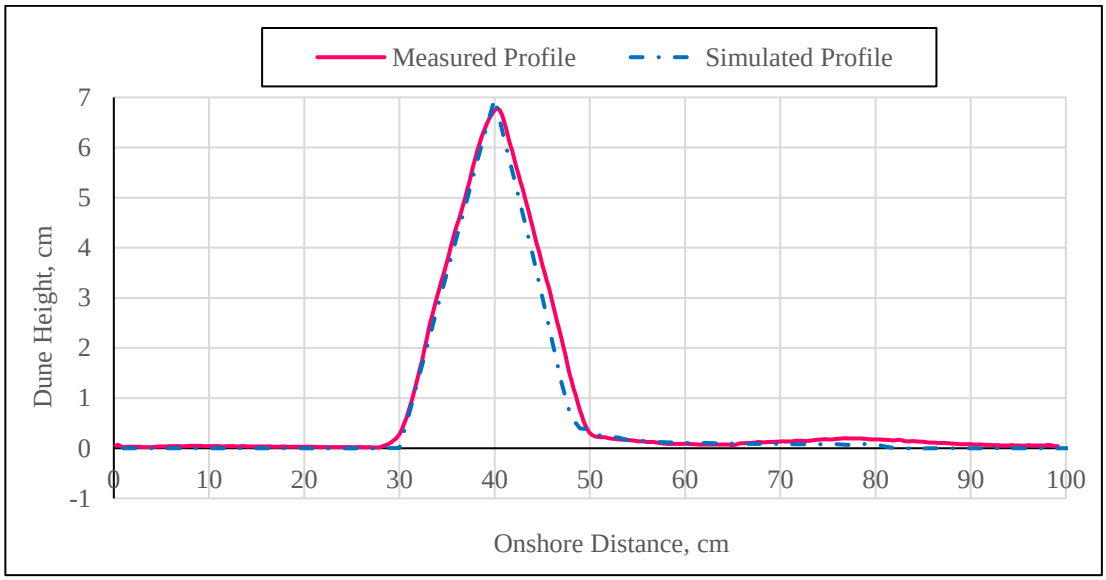

Figure 5.65 Comparison of measured simulated dune profile (FS, WET, bore-B2)

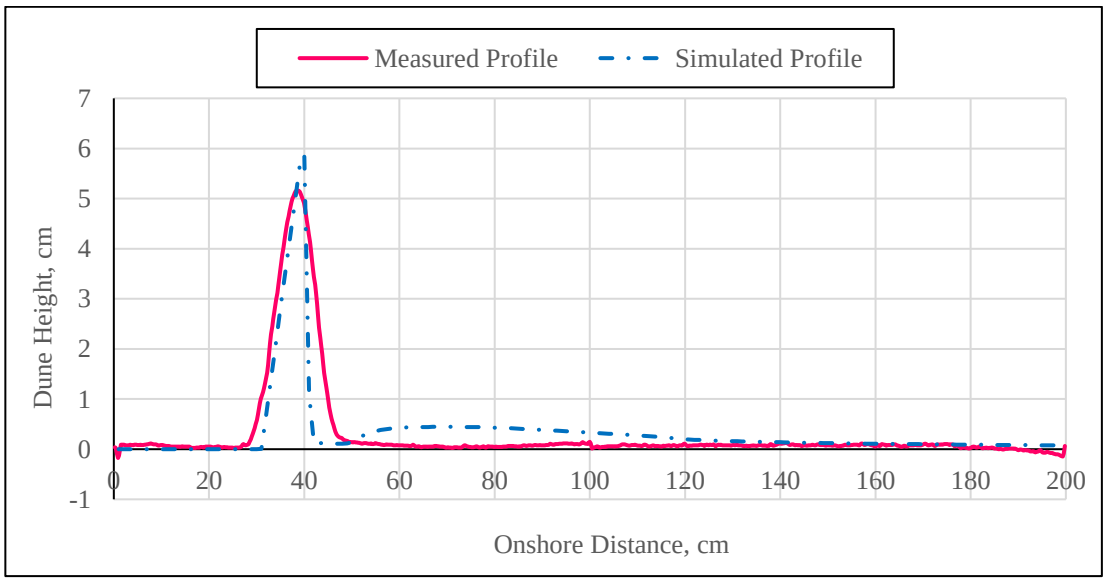

Figure 5.66 Comparison of measured simulated dune profile (FS, WET, bore-B3)

In Figure 5.66 the crest elevation of the simulated profile is higher than the measured one which is also seen in Figure 5.67. This reflects a relatively low overflow velocity computation at the crest.

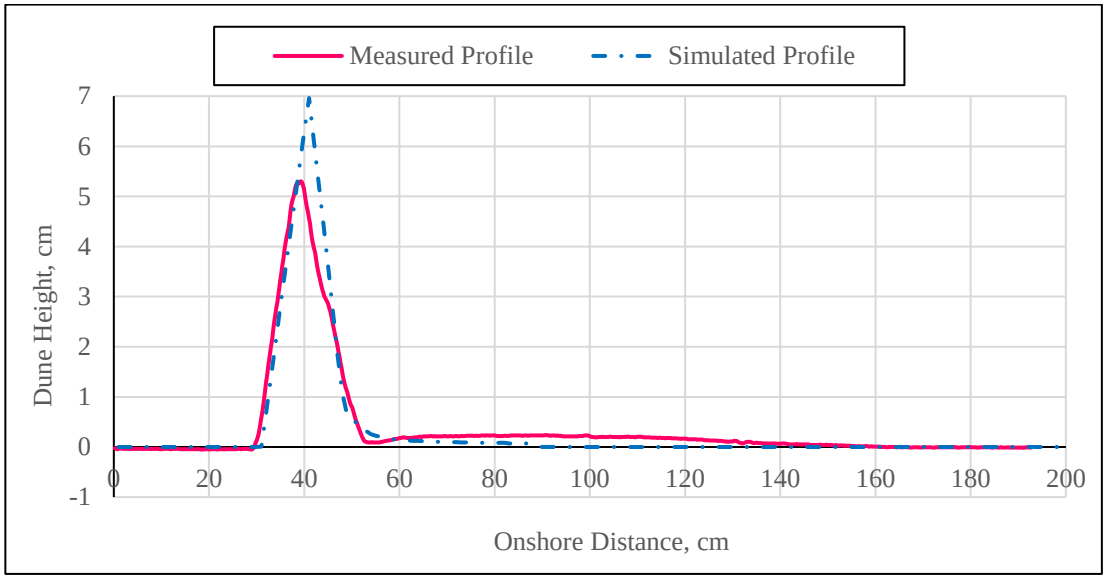

Figure 5.67 Comparison of measured simulated dune profile (FS, DRY, bore-B2)

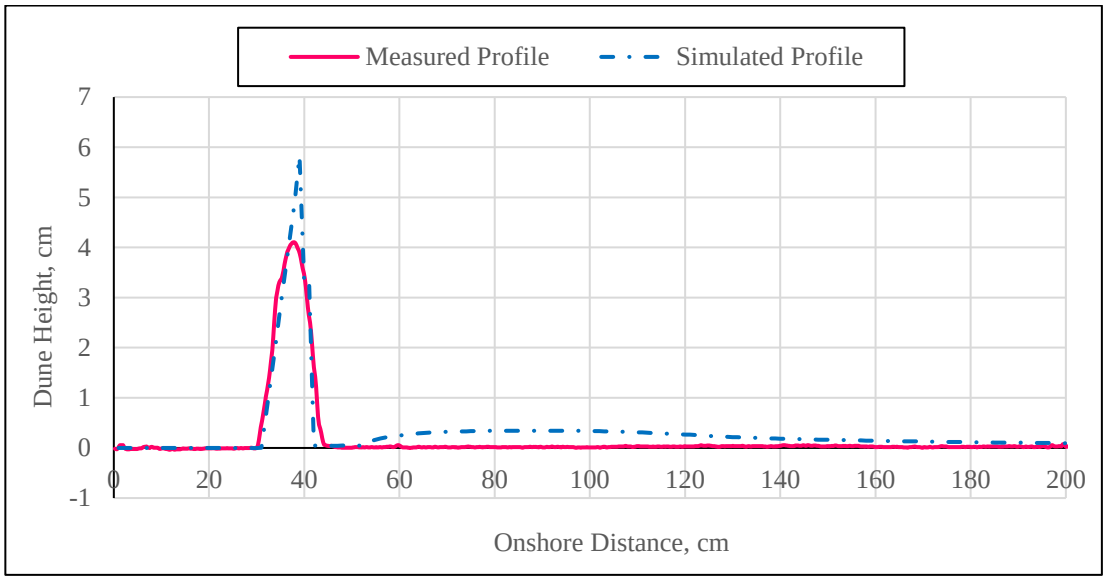

Figure 5.68 Comparison of measured simulated dune profile (FS, DRY, bore-B3)

Figure 5.68 shows simulation result of FS dry condition for B3 bore. The measured profile reveals sediment movement at long distance resulting the thickness of deposition to be thin while simulated profile shows sediment deposition on fore dune foot.

5.9.6 Dune Profile Simulation: Coarse Sand

Figure 5.69 shows CS dry condition for bore B3. The erosion pattern of simulated dune profile exhibit relatively high crest. However, the depositional pattern may be regarded

as satisfactory. Figure 5.70 and Figure 5.71 show dry and wet dune, respectively, for bore B2. The simulated profile for wet is better than that of dry.

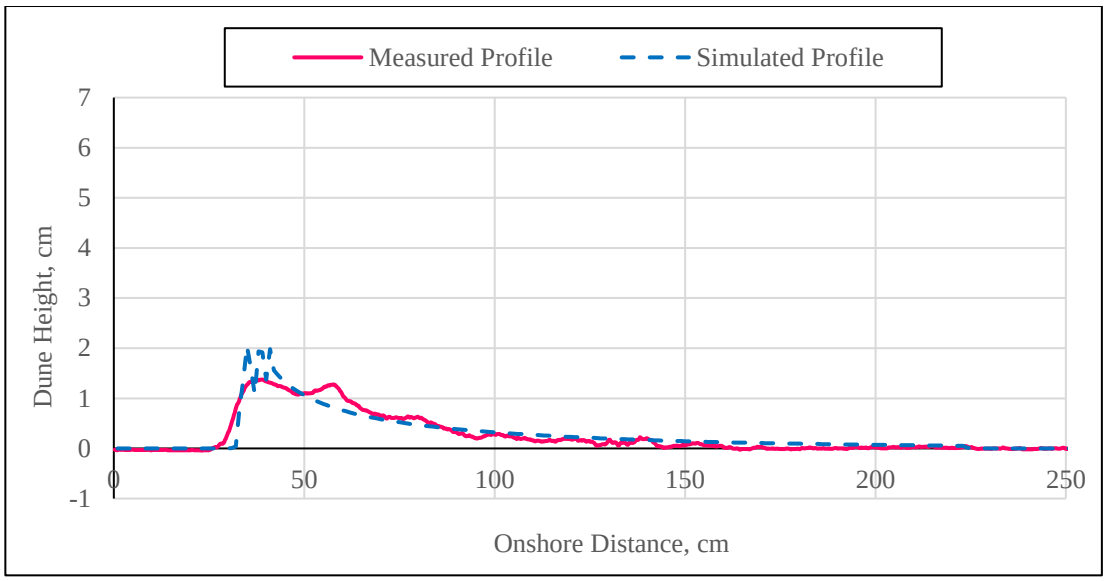

Figure 5.69 Comparison of measured simulated dune profile (CS, DRY, bore-B3)

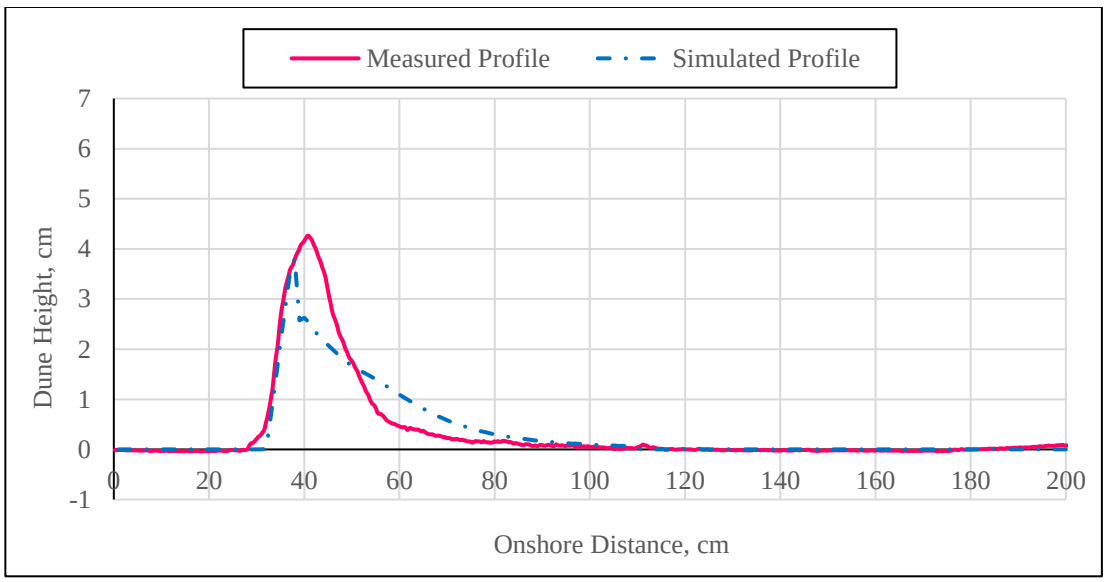

Figure 5.70 Comparison of measured simulated dune profile (CS, DRY, bore-B2)

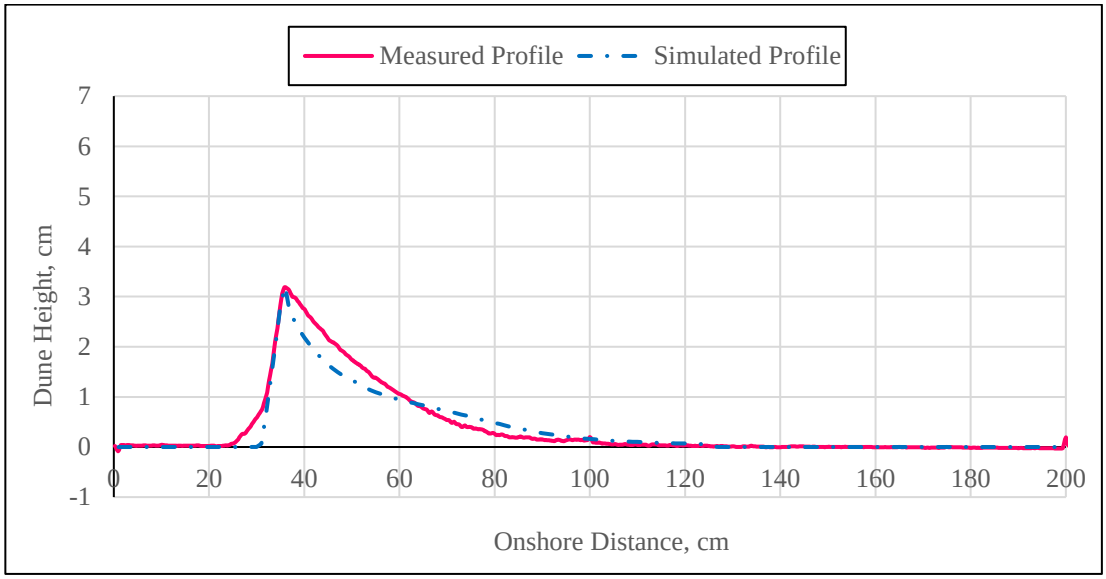

Figure 5.71 Comparison of measured simulated dune profile (CS, WET, bore-B2)

5.9.7 Dune Profile Simulation: Medium Sand

Figure 5.72 shows wet medium sand for bore b3 profile. Increased crest is observed in simulated profile. Figure 5.73 and Figure 5.74 show dry and wet dune, respectively, for bore B2. The simulated profile is found to be satisfactory.

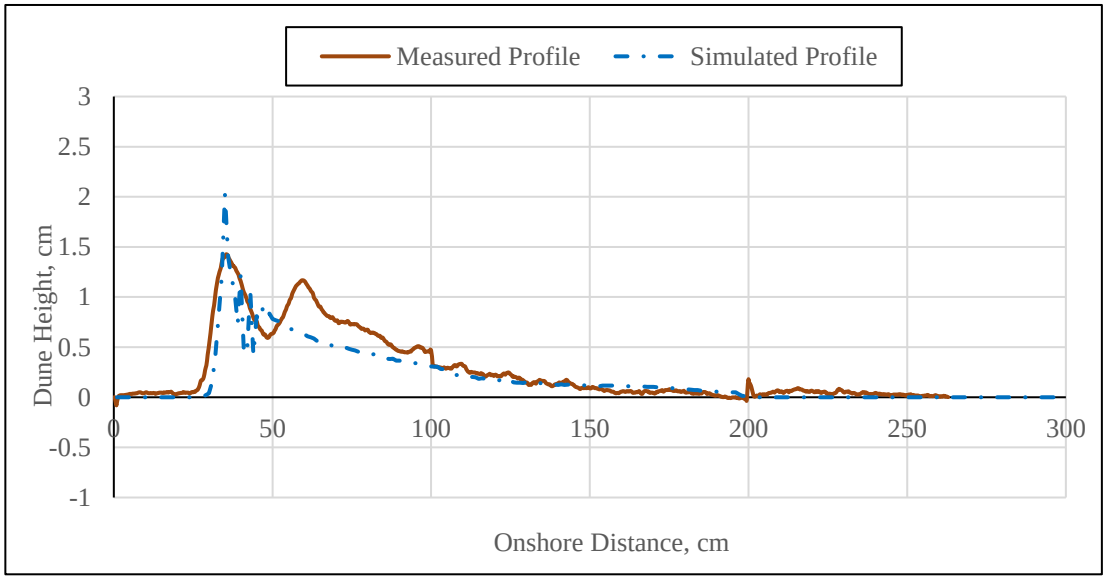

Figure 5.72 Comparison of measured simulated dune profile (MS, WET, bore-B3)

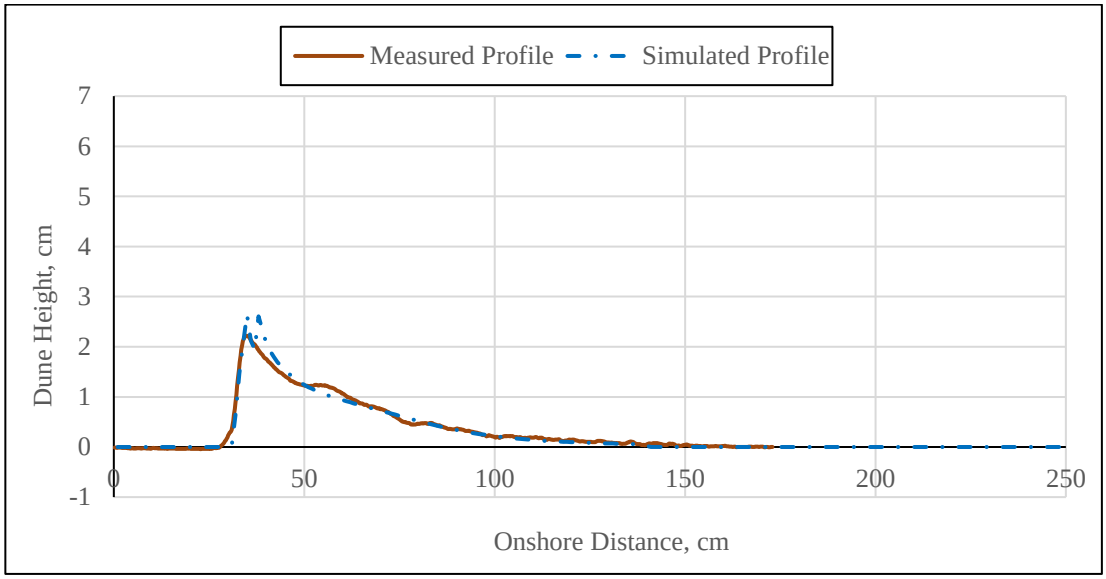

Figure 5.73 Comparison of measured simulated dune profile (MS, DRY, bore-B2)

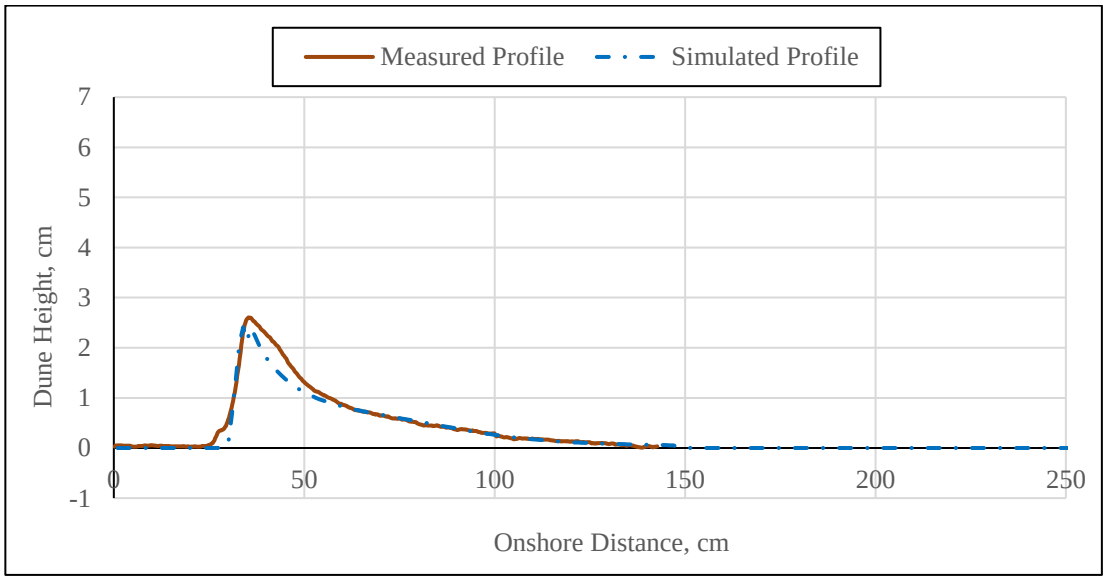

Figure 5.74 Comparison of measured simulated dune profile (MS, WET, bore-B2)

The above figures represents the ability of the existing model to simulate the sand dune erosion during overwash. Although, the process of sediment transport is very complex, the model is expected to perform better by adjusting few parameter and redefining few relationship which play very much pivoting role in sediment transport. Such matters are identified from the numerical analysis and their scopes are briefly discussed in the following subsection.

5.9.8 Comparison of Dune Sediment and River Sediment Transport

i. It is obvious that the dune sediment is generally located in the subaerial part of the coast. To describe the onset of sediment movement, Shields parameter or modified Shields parameter is commonly used. This parameter naturally considers the submerged sediment condition. But for a sediment on the land area necessitates parameter(s) to be incorporated to account for this difference.

ii. The marine sediment transport has the bed load and suspended load component. The flow depth is usually higher than what have been observed during dune overwash experiments. It is evident from this laboratory study that bed load is highly dominated with very easy initial movement of dune sediment (perhaps due to the thrust or slamming force applied on the fore dune part), at very low depth of flow, usually not commonly occurred in open channel or coastal sediment transport. Therefore, a relatively very high sediment concentration just above the bed may encounter this difference.

iii. High erosion is obvious due to the dune overflow of clear water. Naturally, the water in the river has sediment laden flow which is usually considered in the formulation of sediment transport model.

iv. Sediment fall velocity is influenced by the sediment concentration as well. It appears that the existing formulae that gives effective (hindered) fall velocity, is not sufficient enough to account for the very high sediment concentration at relatively low flow depth.

v. Mostly the incipient sediment movement considers that sediment is resting on a horizontal surface, as can be seen in the Shields parameter expression and also, there are literature that includes the bed angle. However, in the present study, dune is a triangular shaped formation with steep slope that requires a parameter to be included for the formulation of incipient condition of sediment movement.

5.10 Remarks

Experimental results have been presented along with the relevant discussion. Numerical simulation is performed and it is found that the model can predict the final

dune profile, considering different parameters. Conclusions are drawn on the basis of these results as well as few scopes of future research in this area have been.

CHAPTER SIX

CONCLUSIONS AND RECOMMENDATIONS

6.1 Introduction

Laboratory experiments were conducted to investigate dune erosion due to overwash considering initially wet and initially dry condition on steep bed slope and mild bed slope using three different types of sand as dune. The essential parameters and distinguishable phenomenon involved in the overwash process are identified. Sediment transport rate and volume is also investigated taking into account of the over flow water rate and volume. Finally, numerical simulation is performed to investigate the influential parameters and phenomena found in the laboratory study which is expected to guide quantitative estimation of dune sediment erosion features like rate of transportation, spatial extent of landward sand movement along with the deposition thickness and in general dune design.

6.2 Conclusions

This study completely focused on the overwash erosion mechanism of subaerial sediments that constitute dune. Up to the author's knowledge, for the first time this is the study that considers wet/dry condition of dune sand. Referring to the very complex phenomena involved in the process, the following conclusions can be drawn based on dune geometry, sediment property, hydrodynamics; and lastly numerical modeling that includes these factors.

Dune Geometry and Sediment Property

1. Dune size, shape and principal bore parameters are essential factors in this transport process and simple analytical approach is capable to represent this relationship. Consequently some empirical relationship are developed which are applicable to median grain sizes ranging from 0.15 mm to 0.90 mm for initially wet and dry condition to estimate sediment transport rate.
2. The difference in sediment transport between DD and WD diminishes as the overwash duration becomes longer (complete inundation). But at low duration,

the presence of air in dune (dry condition) as well as porosity, affects sediment transport.

3. Waterfront spreading time through dry dune mainly depends on hydraulic conductivity and hydrodynamic condition while overflowing. This time required for coarse and medium sand is much less than that of fine sand.

Sediment Property

4. Initially wet fine sand has the highest erosion resistant capacity against overwash due to inter-granular attraction or suction and longest time scale.
5. The mechanism of in/exfiltration plays a significant role mainly for coarse sand in initially wet condition. Angle of repose is found to be an influential parameter to differentiate sediment transport between dry and wet condition. Repose angle is also important in sediment deposition that shapes dune profile evolution.
6. Sediment transport for initially wet dune, seems to be inconsistent with the Shields parameter, perhaps due to active suction. However, for initially dry dune, the sediment transport is more or less consistent with the Shields parameter, especially when the inundation period is longer, i.e. dune becomes completely submerged.

Hydrodynamics

7. Steep bed slope has high sediment transport rate, especially in DD case than the mild bed slope. This may be due to the short overwash duration but a faster overflow of water resulted more sediment to move landward. On the other hand, mild bed slope case is reverse in nature- longer overwash duration and low overflow velocity.
8. However, mild slope resulted more sediment volume transport than steep slope, almost for all types of sand and bore sizes. This is due to the longer duration of overflowing water in mild bed slope experiments. The overflowing water carried more sediment. Numerical model simulated this result particularly for fine sand during large bore.

Modeling

9. Numerical modelling of hydrodynamics and dune morphology is performed based on the shallow water equations and sand transport models. The model can simulate dune sediment transport for fine sand reasonably for wet and dry condition.
10. The reasons and scopes of the model improvement based on detailed observation during laboratory study are mentioned below:
    i. It is natural that the dune sediment is generally located in the subaerial part of the coast. To describe the onset of sediment movement, Shields parameter or modified Shields parameter is commonly used. This parameter usually considers the submerged sediment condition. But for a sediment on the land area necessitates parameter to be incorporated to account for this difference. High erosion is obvious due to the dune overflow of clear water. Naturally, the water in the river or sea has sediment laden flow which is usually considered in the formulation of sediment transport model. This is achieved in the model by an increase of the sediment erosion capacity by introducing coefficient of erosion (c_e) of magnitude 2.0~2.4.
    ii. The marine sediment transport has the bed load and suspended load component. The flow depth is usually higher than what have been observed during dune overwash experiments. It is evident from this laboratory study that bed load is highly dominated with very easy initial movement of dune sediment (perhaps due to the thrust or slamming force applied on the fore dune part), at very low depth of flow, usually not commonly occurred in open channel or coastal sediment transport. Therefore, a relatively very high sediment concentration just above the bed encountered this difference. The adaptation coefficient (α_o) is introduced with a range of 10~20.
    iii. Sediment fall velocity is influenced by the sediment concentration as well as imposed flow velocity. It appears that the existing formulae that gives effective (hindered) fall velocity, is not sufficient enough to account for the very high sediment concentration at relatively low flow depth with

high velocity. Therefore, a modified sediment deposition model is expected to show better morphological evolution. Hence, coefficient of deposition (c_d) in introduced with a range of 1.5~3.0.

iv. Mostly the incipient sediment movement considers that sediment is resting on a horizontal surface. However, in the present study, dune is a triangular shaped formation with steep slope that requires consideration of gravitational force to influence onset of sediment movement. Apart from that, sensitivity analysis reveals that a sediment condition coefficient/multiplying factor (ε) ranging 1.3~23 (or $\tau_c\varepsilon$ ranging 0.2~8.0) can differentiate initially dry and wet sediment transport.

11. Hence, it is obvious that improved correlation for sediment erosion and deposition is a must to explain the dune sediment transport process during tsunami overwash. The coefficients proposed in this study are significant in describing the nature and mechanism of wet and dry dune sediment transport in subaerial part as well as to simulate this process by numerical modeling.

6.3 Recommendations

(a) The study may be extended to two dimensional condition by conducting experiments in the wave basin for regular and irregular wave overwash or tsunami overwash.

(b) Influence of degree of saturation on sediment transport can be investigated.

(c) Sediment transport response for variation of dune sand density can be analyzed.

(d) The above mentioned study can be combined with different dune geometry.

REFERENCES

Ahrens, P. A. (2003). "Simple equations to calculate fall velocity and sediment scale parameter." *J. Waterway, Port, Coastal, Ocean Eng.*, ASCE, 129 (3), 146-150.

Armanini, A., and Di Silvio, G. 1988. "A one-dimensional model for the transport of a sediment mixture in nonequilibrium conditions." *Journal of Hydraulic Research*, 263, 275–292. (Source: Wu and Wang, 2007)

Ayat, B., and Kobayashi, N. (2015). "Vertical cylinder density and toppling effects on dune erosion and overwash." *Journal of Waterway, Port, Coastal and Ocean Engineering*, 141(1), 04014026.

Balmforth, N. J., Hardenberg, J. von, Provenzale, A., and Zammett, R. (2008). "Dam breaking by wave-induced erosional incision." *J. Geophys. Res.*, 113, F01020, doi: 10.1029/2007JF000756.

Bradbur, A. P., and Powell, K. A. (1992). "The short term profile response of shingle spits to storm wave action." *Proceedings of the 23rd International Conference on Coastal Engineering*, pp. 2694-2707.

Brahms, A. (1753). Anfangsgründe der deich-und. Wasserbaukunst, Aurich (Source: Van Rijn, 1993).

Cao, Z., Pender, G., Wallis, S. and Carling, P.A. (2004). "Computational dam-break hydraulics over erodible sediment bed," *Journal of Hydraulic Engineering*, 130 (7), 689-703.

Cao, Z. (1999). "Equilibrium near-bed concentration of suspended sediment." *Journal of Hydraulic Engineering*, 125 (12), 1270-1278.

Chang, H. H. (1992). "Fluvial processes in river engineering", Krieger Publishing Co., Malabar, Florida.

Donnelly, C., Larson, M., and Hanson, H. (2009). "A numerical model of coastal overwash." *Proceedings of the Institution of Civil Engineers - Maritime Engineering*, 2009, 162, No. 3, 105-114.

Donnelly, C., Kraus, N., and Larson, M. (2006). "State of knowledge on measurement and modeling of coastal overwash." *Journal of Coastal Research,* 22(4), 965-991.

Engelund, F., and Fredsoe, J. (1982). "Sediment ripples and dunes." *Ann. Rev. Fluid Mech*., Vol. 14, 13-37.

Engelund, F., and Hansen, E. (1967). "Comparison between similarity theory and regime formulae." *Basic Research-Progress Report 13,* Hydraulic Laboratory, Technical University of Denmark.

Figlus, J., Kobayashi, N., and Gralher, C. (2012). "Onshore migration of emerged ridge and ponded runnel." *Journal of Waterway, Port, Coastal and Ocean Engineering,* 138(5), 331-338.

Figlus, J., Kobayashi, N., Gralher, C., and Iranzo, V. (2011). "Wave overtopping and overwash of dunes." *Journal of Waterway, Port, Coastal and Ocean Engineering,* 137 (1), 26-33.

Fuchs, H.; and Hager, W. H. (2015). "Solitary impulse wave transformation to overland flow." *Journal of Waterway, Port, Coastal and Ocean Engineering,* 141 (5): 04015004.

Gralher, C., Kobayashi, N., and Do, K. (2012). "Wave overwash of vegetated dunes." *Proceedings of the 33rd International Conference on Coastal Engineering.*

Hancock, M. W., and Kobayashi, N. (1994). "Wave overtopping and sediment transport over dunes." *Proceedings of the 24th International Conference on Coastal Engineering,* pp. 2028-2042.

Harleman, D. R. F., and Melhorn, P. F. (1963). "Dispersion-permeability correlation in porous media." *Journal of the Hydraulics Division, Proceedings of the ASCE, vol. 89(HY2),* 67-85.

Herminghaus, S. (2005). "Dynamics of wet granular matter." *Advances in Physics,* 55 (3), pp. 221-261.

Kobayashi, N., Gralher, C., and Do, K. (2013). “Effects of woody plants on dune erosion and overwash.” *Journal of Waterway, Port, Coastal and Ocean Engineering*, 139 (6), 466-472.

Kobayashi, N., Farhadzadeh, A., Melby, J., Johnson, B., and Gravens, M. (2010). “Wave overtopping of levees and overwash of dunes.” *Journal of Coastal Research*, 26 (5), 888–900.

Kobayashi, N., Buck, M., Payo, A., and Johnson, B. D. (2009). “Berm and dune erosion during a storm.” *Journal of Waterway, Port, Coastal and Ocean Engineering*, 135 (1), 1-10.

Kobayashi, N. and Lawrence, A. R. (2004). “Cross-shore sediment transport under breaking solitary waves,” *Journal of Geophysical Research*, 109, C03047.

Kobayashi, N., Tega, Y., and Hancock, M. W. (1996). “Wave reflection and overwash of dunes.” *Journal of Waterway, Port, Coastal and Ocean Engineering*, 122(3), 150-153.

Komura, S. (1963). “Discussion of ‘Sediment transportation mechanics: Introduction and properties of sediment.’” *Journal of Hydraulic Division*, ASCE, 89 (1), 263-266.

Kraus, N. C., and Wise, R. A. (1993). “Simulation of January 4, 1992 storm erosion at ocean city, Maryland*.” Shore and Beach,* 61(1), 34-41.

Lambe, T., W., and Whitman, R., V. (1979). *Soil Mechanics, SI Version.* John Wiley and Sons, Inc.

Larson, M., Donnelly, C., Jimenez, J. A., and Hanson, H. (2009). “Analytical model of beach erosion and overwash during storms.” *Proceedings of the Institution of Civil Engineers - Maritime Engineering*, 2009, 162, No. 3, 115-125.

Larson, M., and Kraus, N. C. (1989). “SBEACH. Numerical model for simulating storm-induced beach change; Report 1. Empirical foundation and model development.” *Technical Report, CERC 89-9,* Vicksburg, Mississippi: U.S. Army Waterways Experiment Station, Coastal Engineering Research Center, 267p.

Larson, M., Kubota, S., and Erikson, L. (2001). “Modeling sediment transport and profile evolution in the swash zone.” *Proceedings of the Coastal Dynamics ’01,* ASCE, 908-917.

Larson, M., Kubota, S., and Erikson, L. (2004). “Swash-zone sediment transport and foreshore evolution: field experiments and mathematical modeling.” *Marine Geology,* 212, 61-79.

Larson, M., Wise, R. A., and Kraus, N. C. (2004). “Coastal overwash. Part 2: Upgrade to SBEACH.” *Regional Sediment Demonstration Technical Note, EDRC/RSM-TN-15.* Vicksburg, Mississippi: U.S. Army Engineering Research and Development Center.

Larson, M., Wise, R. A., and Kraus, N. C. (2004). “Modeling dune response by overwash transport.” *Proceedings of the 29th International Conference on Coastal Engineering*, pp. 2133-2145.

Leatherman, S. P., Williams, A. T., and Fisher, J. S. (1977). “Overwash sedimentation associated with a large-scale northeaster.” *Marine Geology,* 24, 109-121.

Lin, B. 1984. “Current study of unsteady transport of sediment in China.” *Proc., Japan–China Bilateral Seminar on River Hydraulics and Engineering Experiences,* Tokyo–Kyoto–Saporo, Japan, 337–342. (Source: Wu and Wang, 2007)

Loof, H. de, Steetzel, H J., and Kraak, A. W. (1996). “Breach-growth: experiments and modelling.” *Proceedings of the 25th International Conference on Coastal Engineering*, pp. 2746-2755.

Mehta, A., and Barker, G. C. (1994). "The dynamics of sand." *Reports on Progress in Physics*. 57 (4), pp. 383-416.

Mitarai, N., and Nori, F. (2006). “Wet granular material.” *Advances in Physics*, 55 (1-2), pp. 1-45.

Mitchell, J. K., and Soga, K. (2005). *Fundamentals of soil behavior*. 3rd Edition, John Wiley and Sons, Inc., NJ, USA.

Nielsen, P. (1992). *Coastal Bottom Boundary Layers and Sediment Transport.* World Scientific, 324 p.

Raju, K. M. A. H., and Sato, S. (2015). "An experimental investigation on influence of air void in sand dune sediment transport due to overwash." *Proceedings of the Coastal Sediments 2015,* 11-15 May, San Diego, CA, USA. (CD-ROM).

Ruby, W. W. (1933). "Settling velocities of gravel, sand and silt particles." *Am. J. Sci.,* 25 (148), 325-338. (Source: Ahrens, 2003).

Santamarina, J. C., and Cho, G. C. (2004). "Soil behaviour: The role of particle shape." *Skempton Conf.: Advances in Geotechnical Engineering*, R. J. Jardine, D. M. Potts, and K. G. Higgins, eds., Vol. 1, Thomas Telford, London, 604–617.

Shimozono, T., Sato, S., and Tajima, Y. (2007). "Numerical study of tsunami run-up over erodible sand dunes." *Proceedings of the Coastal Sediments,* pp. 1089-1102.

Sleath, J. F. A. (1984). *Sea bed mechanics.* John Wiley and Sons, Inc.

Srinivas, R., and Dean, R. A. (1996). "Cross-shore hydrodynamics and profile response modeling." *Coastal Engineering,* 27, 195-221.

Stauble, D. K. (1979). "The interaction of swash and sediment on the backshore in the presence and absence of barriers." *PhD dissertation,* Department of Environmental Sciences, University of Virginia, 127p. (Source: Donnelly et al. 2006)

Steetzel, H. J., Vroeg, H. de, Rijn, L. C. van, and Stam, J. M (1998). "Morphological modeling using a modified multi-layer approach." *Proceedings of the 26th International Conference on Coastal Engineering,* pp. 2368-2381.

Steetzel, H. J., and Visser, P. J. (1992). "Profile development of dunes due to overflow." *Proceedings of the 23rd International Conference on Coastal Engineering,* pp. 2669-2679.

Steetzel, H. J. (1990) "Cross-shore transport during storm surges." *Proceedings of the 22nd International Conference on Coastal Engineering,* pp. 1922-1934.

Sternberg, H. (1875). “Untersuchungen über das Längen und querprofil geschiebeführender”. *Flüse Zeitschrift Bauwesen,* vol. 25 (Source: Van Rijn, 1993).

Sweby, P. K. (1985). “High resolution TVD schemes using flux limiters”. *Lecture Note in Applied Mathematics,* 22, 289-309.

Tanaka, H., Suntoyo, and Nagasawa, T. (2002). “Sediment intrusion into gamo lagoon by wave overtopping.” *Proceedings of the 28th International Conference on Coastal Engineering,* pp. 823-835.

Tinh, N. X., Donnelley, C., Tanaka, H., and Larson, M. (2008). “A new empirical formula for coastal washover sediment volume.” *Proceedings of the 31st International Conference on Coastal Engineering,* pp. 1736-1748.

Toro, E. F. (2001). *Shock capturing methods for free surface shallow flows*, Wiley, Chichester, England.

Vanoni, V. A., ed. (1975). *Sedimentation Engineering,* Manual no. 54, ASCE.

Van Rijn, L.C. (1993). *Principles of Sediment Transport in Rivers, Estuaries and Coastal Seas*, Amsterdam, Aqua Publications.

Vincent, S., and Bonneton, P. (2001). “Numerical modeling of bore run-up on sloping beaches using a Maccormack TVD-Scheme.” *Journal of Hydraulic Research* 39(1), 41-49.

Visser, P. J. (1994). “A model for breach growth in sand-dikes.” *Proceedings of the 24th International Conference on Coastal Engineering,* pp. 2755-2769.

Visser, P. J., Vrijling, J. K., and Verhagen, H. J. (1990). “A field experiment on breach growth in sand-dikes.” *Proceedings of the 22nd International Conference on Coastal Engineering,* pp. 2087-2100.

Visser, P. J. (1988). “A model for breach growth in a dike-burst.” *Proceedings of the 21st International Conference on Coastal Engineering,* pp. 1897-1910.

Wadell, H. (1932). “Volume, Shape, and Roundness of Rock Particles.” *The Journal of Geology,* 40 (5), 443-451. (Source: Mitchell and Soga, 2005)

Webster, A. G. (1919). “On the angle of repose of wet sand.” *Proceedings of the National Academy of Sciences of the United States of America*. Vol. 5, No. 7 (Jul. 15, 1919), pp. 263-265.

Williams, P. J. (1978). “Laboratory development of a predictive relationship for washover volume on barrier island coastlines.” *Master’s thesis,* Department of Civil Engineering, University of Delaware, 141p. (Source: Donnelly et al. 2006).

Wu, W. (2004). “Depth-averaged 2-D numerical modeling of unsteady flow and non-uniform sediment transport in open channels.” *Journal of Hydraulic Engineering*, 130 (10), 1013-1024.

Wu, W. (2008). *Computational River Dynamics.* Taylor and Francis, London, UK.

Wu, W.; and Wang, S. S. Y. (2006). “Formulas for sediment porosity and settling velocity.” *Journal of Hydraulic Engineering*, 132 (8), 858-862.

Wu, W., Wang, S. S.Y., Jia, Y., and Robinson, K. M. (1999). “Numerical simulation of two-dimensional head cut migration,” *Proc. 1999 International Water Resources Engineering Conference*, Seattle, USA. (CD-ROM).

Zhang, R. J.; Xie, J. H.; Wang, M F.; and Huang, J. T. (1989). *Dynamics of river sedimentation*, Water and Power Press, Beijing, China (in Chinese). (Source: Wu, 2008).

Zhou, J., and Lin, B. 1998. “One-dimensional mathematical model for suspended sediment by lateral integration.” *Journal of Hydraulic Engineering*, 1247, 712–717.

Appendix-A

Table A-1: Sediment Transport Data for Figure 5.3

Distance (cm)	DRY Sand wt. (gm)	WET Sand wt. (gm)
2	51.101	174
4	55.687	93.516
6	53.578	93.988
8	46.834	91.641
10	34.824	76.287
12	31.187	74.875
14	26.733	51.102
16	23.679	54.21
18	19.299	44.452
20	16.572	38.907
22	16.671	33.041
24	15.458	27.785
26	15.235	27.242
28	13.403	23.138
30	12.686	20.489
32	10.569	21.42
34	10.407	17.381
36	8.863	10.765
38	9.479	13.159
40	7.812	12.377
42	9.143	10.911
44	5.754	13.247
46	6.343	11.947
48	5.97	10.143
50	4.809	11.24
50-60	14.762	22.492
60-70	11.261	22.54
70-80	9.896	16.372
80-90	17.73	13.773
90-100	6.16	7.927
100-110	5.302	8.203
110-120	3.808	8.123
120-130	4.536	2.674
130-140	3.78	5.098
140-150	4.037	3.79
150-250	11.44	4.692

Table A-2: Sediment Transport Data for Figure A-1 (Trial Run-6)

Distance (cm)	DRY Sand wt (gm)	WET Sand wt (gm)
2	21.871	46.986
4	18.928	31.107
6	20.754	24.282
8	19.44	16.117
10	17.446	11.528
12	14.18	8.681
14	12.4	6.902
16	10.026	4.613
18	8.217	3.467
20	6.081	2.795
22	5.62	2.011
24	4.211	1.327
26	3.637	1.022
28	2.903	0.824
30	2.674	0.662
32	2.274	0.262
34	1.994	0.22
36	1.606	0.087
38	1.813	0.069
40	1.38	0.022
42	1.31	
44	1.432	
46	1.448	
48	0.421	
50	0.236	

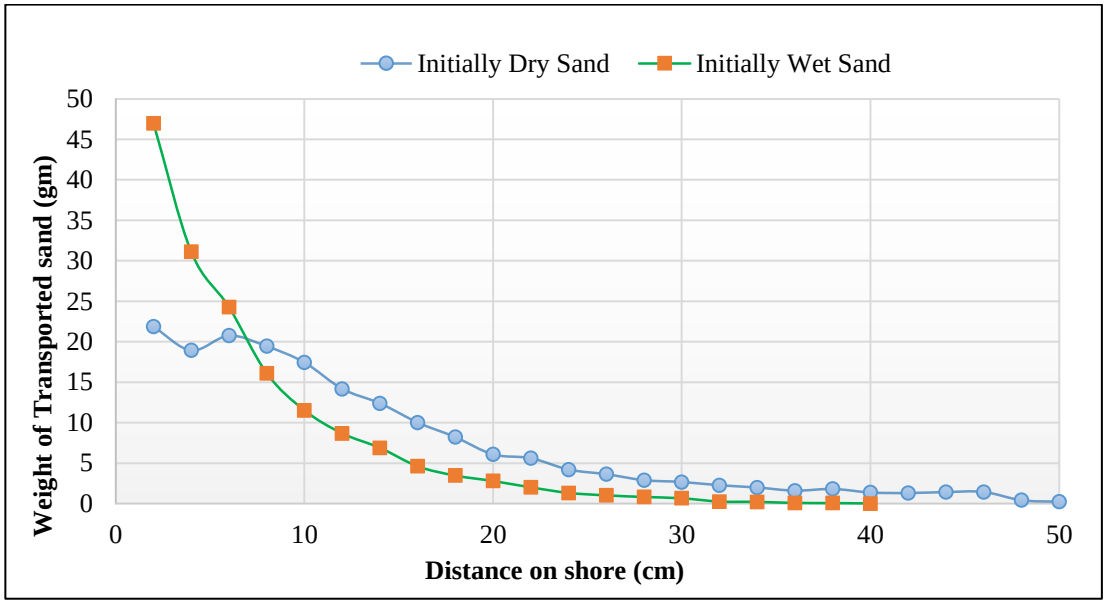

Figure A-1 Plot of initially dry and initially wet dune (Trial Run-6: coarse sand, h1=30 cm, h2=37 cm, ΔH=7 cm, steep slope)